ARCHIVES OF ACOUSTICS
10, 1, 3-16 (1985)

ACOUSTIC PRESSURE OF A SYSTEM OF CONCENTRIC ANNULAR SOURCES IN A PARALLEL-PIPED LAYER OF A GASEOUS MEDIUM*

WITOLD RDZANEK

Department of Theoretical Physics, Higher Pedagogical School
(65–069 Zielona Góra, Pl. Słowiański 6)

In this paper, an expression was derived for the acoustic pressure distribution in the near and far fields, radiated by a system of planar concentric annular sources. The propagation of the pressure wave was considered for a parallel-piped layer, bounded by rigid baffles, filled with a lossless gaseous medium. It was assumed that the system of sources, with known axially-symmetric vibration velocity distribution, was on one of the planar and rigid baffles. Linear phenomena dependent sinusoidally on time were analysed.

By solving the Neumann boundary problem by means of the method of Hankel transforms of the zeroth order, an integral expression was obtained for the acoustic pressure distribution in a parallel-piped layer. The pressure, expressed by an integral in the complex variable plane, was represented in the form of a series of residua at the poles of the subintegral function, giving a formula, convenient for practical calculations and easy to interpret, in the form of a series of normal waves. The theoretical analysis of the acoustic pressure distribution was supported by numerical examples, for which curves of acoustic pressure were plotted as a function of the distance from the source.

1. Introduction

This paper is concerned with investigations of the acoustic properties of a system of concentric annular sources, consisting in the determination of the acoustic field distribution in a parallel-piped layer.

Most of the previous studies on the wave generation and propagation were concerned with analyses of the acoustic pressure distribution in the far field for the whole space or for a half-space. In the latter case, it was assumed that the source of the acoustic wave was in a planar and rigid baffle.

* This investigation was carried out within the problem MR.I.24

Considering these problems, McLACHLAN [4] carried out a detailed analysis of the problem of the directional characteristic of a planar annular piston with uniform vibration velocity distribution.

A similar expression for the directional characteristic of a single circular ring was given by THOMPSON [7].

A detailed analysis of the pressure distribution in the far field, radiated by a membrane or a circular plate, excited to axially-symmetric or axially-nonsymmetric self vibration, was carried out in paper [6]. This analysis was an attempt to determine the way in which the field distribution is affected by the individual elements of the vibrating surface of the membrane or plate, i.e. a system of planar concentric annular sources.

More complex acoustic phenomena occur for generation of acoustic waves in a layered medium, and in the simplest case-in a parallel-piped layer.

Within this range of problems, deep theoretical research was carried out by BREKHOVSKIKH [1], by analysing both electromagnetic waves and acoustic waves generated by point sources.

The present paper refers to papers [6] and [1]. The object of the analysis carried out in this theoretical study is the investigation of the pressure distribution in the near and far field, radiated by a system of planar concentric annular sources. The wave propagation was considered for a parallel-piped layer, filled with a lossless gaseous medium, bounded by rigid baffles. Linear phenomena dependent sinusoidally on time were analysed on the assumption that the system of sources was on one of the planar and rigid baffles.

Assuming knowledge of the vibration velocity distribution on the surface of the system of sources, the Neumann boundary problem was solved and an integral expression obtained for the acoustic pressure distribution in the parallel-piped layer. In view of the axially-symmetric vibration velocity distribution assumed here, the general method of Hankel transforms of the zeroth order was used. The pressure, expressed by an integral in the complex variable plane, was represented in the form of a series of residua at the poles of the subintegral function, giving a formula, convenient for practical calculations and easy to interpret, for the acoustic pressure in the form of a series of the so-called normal waves.

In the numerical example, calculations were made for the acoustic pressure radiated by a circular membrane, excited to axially-symmetric vibration, i.e. by a system of planar concentric annular sources. The surface of the membrane was divided in such a way that the annular surfaces were bounded by nodal circles for the respective vibration modes. In view of the axially-symmetric vibration assumed here, all the points on the surface of any of the rings vibrate in phase, whereas those of the adjacent rings vibrate in antiphase.

The theoretical analysis carried out in this paper for the acoustic field radiated by a planar system of annular sources in a parallel-piped layer was supported by numerical examples, for which curves of pressure were plotted as a function of the distance from the source.

2. Expression for the acoustic pressure in integral form

We consider the problem of acoustic wave propagation in a parallel-piped layer of a homogeneous gaseous medium with the rest density ϱ_0 and the sound wave velocity c_0. The parallel-piped layer of the medium is bounded by planar, rigid baffles spaced at the distance h. The sound source is a vibrating system of a finite number of concentrically situated planar circular rings, placed on the plane $z = 0$, which is the rigid baffle.

We consider linear phenomena dependent sinusoidally on time. It is assumed that the vibration velocity distributions on the surface of the rings are axially-symmetric, assumed to be known. Thus, the value of the normal component of the vibration velocity is known, $\boldsymbol{nv} = -v$, where $\boldsymbol{n}$ is a unitary vector normal to the surface of the source, directed in a direction opposite from that of the velocity vector $\boldsymbol{v}$. The vibrating surface of the sth circular ring, arbitrarily chosen from the system of sources, is bounded by circles with the radii r_s and r_{s-1}, with $r_{s-1} < r_s$.

Within the parallel-piped layer, filled by a gaseous medium with the density ϱ_0, for the acoustic potential $\Phi_s(r, z)\exp(i\omega t)$, whose source is the sth vibrating circular ring, the Helmholtz equation

$$\Delta\Phi_s(r, z) + k^2\Phi_s(r, z) = 0 \tag{1}$$

is valid. The quantity $k = \omega/c_0$ is the wave number, ω is the angular frequency. One should find such a solution of equation (1) for the region $\{0 \leqslant z \leqslant h, 0 \leqslant r < \infty\}$, which satisfies the inhomogeneous Neumann boundary condition

$$\left.\frac{\partial\Phi_s(r, z)}{\partial z}\right|_{z=0} = \begin{cases} -v_s(r) & \text{for the sth ring} \\ 0 & \text{beyond the ring,} \end{cases} \tag{2}$$

and the homogeneous Neumann boundary condition

$$\left.\frac{\partial\Phi_s(r, z)}{\partial z}\right|_{z=h} = 0, \tag{3}$$

where $v_s(r)$ is the vibration velocity distribution function assumed to be known.

Following the general method of Hankel transforms of the zeroth order, the solution is sought in the form

$$\Phi_s(r, z) = \int_0^\infty g(\tau, z)J_0(\tau r)\tau d\tau, \tag{4}$$

where

$$g(\tau, z) = \int_0^\infty \Phi_s(r, z)J_0(\tau r)rdr, \tag{5}$$

J_0 is a Bessel function of the zeroth order, while the complex parameter τ is a propagation constant in the radial direction. Equation (1) can become

$$\frac{d^2 g(\tau, z)}{dz^2} + (k^2 - \tau^2) g(\tau, z) = 0, \tag{6}$$

with the following solution:

$$g(\tau, z) = A \exp(-i\gamma z) + B \exp(i\gamma z), \tag{7}$$

where A and B are integration constants, γ is a propagation constant towards the axis z and $k^2 = \gamma^2 + \tau^2$.

Relation (2) is replaced by

$$\left.\frac{dg(\tau, z)}{dz}\right|_{\substack{z=0 \\ r_{s-1} \leqslant r \leqslant r_s}} = -W_s(\tau), \tag{8}$$

where

$$W_s(\tau) = \int_{r_{s-1}}^{r_s} v_s(r_0) J_0(\tau r_0) r_0 dr_0 \tag{9}$$

is a characteristic function of the sth ring, which is the set of points $\{r_{s-1} \leqslant r \leqslant r_s, 0 \leqslant \varphi \leqslant 2\pi\}$.

The integration constants A and B can be determined from relations (3) and (8). This gives

$$g(\tau, z) = -W_s(\tau) \frac{\cos\gamma(h-z)}{\gamma \sin\gamma h}. \tag{10}$$

The use of inverse Hankel transformation from formula (4) and consideration that for phenomena sinusoidally dependent on time the dependence of pressure on the potential is linear: $p(r) = ik\varrho_0 c_0 \Phi(r)$ give the sought solution in integral form for the acoustic pressure generated by the sth ring, in the form

$$p(r, z) = -ik\varrho_0 c_0 \int_0^{\infty} \frac{\cos\gamma(h-z)}{\gamma \sin\gamma h} W_s(\tau) J_0(\tau r) \tau d\tau. \tag{11}$$

3. Expression for the acoustic pressure in the form of a series of normal waves

When the distance at which a point of the field is, is much larger than the linear dimensions of the source and than the length of the acoustic wave radiated, it is convenient to transform formula (11) to a form in which the integral is calculated within the limits $(-\infty, +\infty)$. The following dependence can be

used [8]:

$$J_0(u) = \frac{1}{2}\left[H_0^{(2)}(u) - H_0^{(2)}(-u)\right], \tag{12}$$

where $H_0^{(2)}$ is a cylindrical Hankel function of the zeroth order, of the second kind, satisfying the radiation condition of the time dependence exp ($i\omega t$). The substitution of (12) in (11) and the taking advantage of the evenness property of the characteristic function $W_s(\tau)$ with respect to the variable τ (see definition (9)) give

$$p(r, z) = \varrho_0 c_0 \frac{-ik}{2} \int_{-\infty}^{+\infty} \frac{\cos\gamma(h-z)}{\gamma \sin\gamma h} W_s(\tau) H_0^{(2)}(\tau r)\tau d\tau. \tag{13}$$

Integration will be carried out over the real axis, where the singular point $\tau = 0$, in integrating for the transition from negative real values to positive ones, is bypassed along a small half-circle underneath, since $H_0^{(2)}(\tau r)$ has a logarithmic singularity at the point $\tau = 0$.

Expression (13) can be represented in the form of a series of residua at the poles of the subintegral function. To achieve this, it is possible to use Jordan's lemma and Cauchy's residua theorem [2], closing the integration path in the lower halfplane of the complex variable τ (Fig. 1).

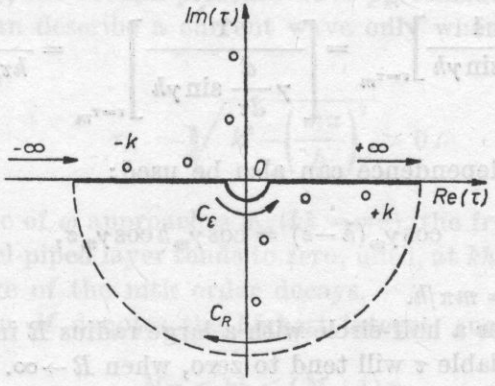

Fig. 1. Integration path including poles of the subintegral function (13) in the lower halfplane of the complex variable

The poles of the subintegral function (13) are at the points defined by the roots of the equation $\sin\gamma h = 0$, whose solutions are $\gamma h = m\pi$; $m = 0, \pm 1, \pm 2, \ldots$ In the neighbourhood of the points, defined by a root corresponding to $m = 0$,

$$\frac{1}{\gamma \sin\gamma h} \simeq \frac{1}{h(k^2 - \tau^2)}. \tag{14}$$

Expression (14) has poles of the first order at the points $\tau_0 = k$, $\tau_0 = -k$. In general, when $m = 0, \pm 1, \pm 2, \ldots$, from the expression $\gamma h = m\pi$, for the poles $\tau_m = \pm\sqrt{k^2-(m\pi/h)^2}$.

It will be easier to analyse integral (13) when it is considered that in real conditions in a gaseous medium there is the phenomenon of absorption of propagating waves. In view of this, it is assumed initially that the wave number k has a low negative value of the imaginary component $k = k_0 - i\delta$; k_0, $\delta > 0$.

The integration will thus include the poles in the lower half-plane of the complex variable τ, i.e. those for which $\tau_0 = k$, $\tau_m = \sqrt{k^2-(m\pi/h)^2}$. The integration gives as a result a final expression in which it will be possible, in the limits, to pass from the value of δ to zero.

The residuum of the subintegral function (13) can be calculated, i.e.

$$\operatorname{Res}[F(\tau)]_{\tau=\tau_m} = \tau_m \cos\gamma_m(h-z) W_s(\tau_m) H_0^{(2)}(\tau_m r) \operatorname{Res}\left[\frac{1}{\gamma \sin\gamma h}\right]_{\tau=\tau_m}. \tag{15}$$

For the pole $m = 0$, considering relation (14),

$$\operatorname{Res}\left[\frac{1}{\gamma\sin\gamma h}\right]_{\tau=k} = \operatorname{Res}\left[\frac{1}{k(h-\tau)(k+\tau)}\right]_{\tau=k} = -\frac{1}{2kh}. \tag{16}$$

For the poles $m = 1, 2, \ldots$

$$\operatorname{Res}\left[\frac{1}{\gamma\sin\gamma h}\right]_{\tau=\tau_m} = \left[\frac{1}{\gamma\dfrac{d}{d\tau}\sin\gamma h}\right]_{\tau=\tau_m} = \frac{-1}{h\tau_m\cos\gamma_m h}. \tag{17}$$

The following dependence can also be used:

$$\cos\gamma_m(h-z) = \cos\gamma_m h \cos\gamma_m z, \tag{18}$$

where $\gamma = 0$, $\gamma_m = m\pi/h$.

The integral over a half-circle with a large radius R in the lower half-plane of the complex variable τ will tend to zero, when $R \to \infty$. For very large R the function $H_0^{(2)}(\tau r)$ will tend to zero, when $r \neq 0$. The value of the integral over the half-circle C_ε with a small radius ε in the limits for $\varepsilon \to 0$ will also tend to zero.

The use of Cauchy's residua theorem indicates that integral (13) is equal to the sum of the remainders of the subintegral function at the poles, multiplied by the factor $-2\pi i$. There emerges the following expression for the acoustic pressure, in the form of a series of normal waves:

$$p(r, z) = p_0(r) + \sum_{m=1}^{\infty} p_m(r, z), \tag{19}$$

where

$$p_0(r) = \varrho_0 c_0 \frac{\pi k}{2h} W_s(k) H_0^{(2)}(kr), \tag{20}$$

$$p_m(r, z) = \varrho_0 c_0 \frac{\pi k}{h} \cos \frac{m\pi z}{h} W_s(\tau_m) H_0^{(2)}(r\tau_m). \tag{21}$$

Each of the components $p_m(r, z)$ in expression (21) is suitable to describe the pressure wave, propagating towards the increasing values of the radial variable r and the standing wave towards the variable z.

When τ_m tends to zero, the amplitude of the mth normal wave tends to infinity, in view of the infinite value of the Hankel function. This specific case corresponds to a resonance at which the pressure value is in theory infinitely large. This follows from the analysis carried out for the acoustic wave propagation in a lossless medium. The parameter $\gamma_m = m(\pi/h)$ is called the critical wave number (the cut-off wave number), since it determines the wave frequency ω_m at which free propagation of a normal wave of the mth order decays, i.e. the frequency at which τ_m takes a zero value. This occurs when $\gamma_m = k$, i.e. when $kh = m\pi$.

For such frequencies ω (the wave frequencies in a free space) at which $\omega > \omega_m(k = m\pi/h)$, the normal pressure wave p_m considered propagates freely. Expression (21) can describe a current wave only when τ_m is a real, positive quantity, i.e.

$$\tau_m = \sqrt{k^2 - \left(\frac{m\pi}{h}\right)^2} > 0. \tag{22}$$

When the value of ω approaches $\omega_m(kh \to m\pi)$, the frequency of the normal wave in the parallel-piped layer tends to zero, until, at $kh = m\pi$, the free propagation of the wave of the mth order decays.

In a case when M denotes the highest integer, such for which

$$M\pi < kh \leqslant (M+1)\pi, \tag{23}$$

then M will define the order of the highest normal pressure wave, p_m, which can propagate in the parallel-piped layer with a prescribed value of the interference parameter kh.

For $\omega < \omega_m(kh < m\pi)$ the normal pressure wave p_m considered is damped along the propagation direction. In this case $m > M$, whereas the phase of the square root is assumed to be $-\pi/2$, i.e.

$$\tau_m = -i|\tau_m|, \tag{24}$$

where

$$|\tau_m| = \sqrt{\left(\frac{m\pi}{h}\right)^2 - k^2} > 0. \tag{24a}$$

The characteristic function $W(\tau_m)$, defined by formula (9), is even with respect to the parameter τ_m, which takes real values for $m < M$ and purely imaginary ones for $m > M$. It is thus a real function, i.e. $W(\tau_m) = W^*(\tau_m)$. For real τ_m $(m < M)$ [8]

$$H_0^{(2)}(r\tau_m) = J_0(r\tau_m) - iN_0(r\tau_m), \tag{25}$$

while for purely imaginary $\tau_m (m > M)$

$$H_0^{(2)}(-ir|\tau_m|) = \frac{2i}{\pi} K_0(r|\tau_m|), \tag{26}$$

where N_0 is a Neumann function of the zeroth order and K is a MacDonald function of the zeroth order.

After separating the real component $p' = Re(p)$ and the imaginary one $p'' = \mathrm{Im}(p)$, the acoustic pressure (19) can be written in the following way:

$$p = p' + ip'', \tag{27}$$

where

$$p'(r, z) = \varrho_0 c_0 \frac{\pi k}{2h} \sum_{m=0}^{M} \varepsilon_m \cos\left(\frac{m\pi z}{hW}\right) W_s(\tau_m) J_0(r\tau_m), \tag{28}$$

$$p''(r, z) = \varrho_0 c_0 \frac{\pi k}{2h} \left\{ - \sum_{m=0}^{M} \varepsilon_m \cos\left(\frac{m\pi z}{h}\right) W_s(\tau_m) N_0(r\tau_m) + \right.$$

$$\left. + \frac{2}{\pi} \sum_{m=M+1}^{\infty} \varepsilon_m \cos\left(\frac{m\pi z}{h}\right) W_s(-i|\tau_m|) K_0(r|\tau_m|) \right\}, \tag{29}$$

$$\varepsilon_m = 1 \text{ for } m = 0 \quad \text{and} \quad \varepsilon_m = 2 \text{ for } m \geqslant 1.$$

In expression (29) the infinite series $(M+1 \leqslant m < \infty)$ can be replaced in specific numerical calculations by a finite number of terms $M' - (M+1)$. Summation is then carried out over the index m from $m = M+1$ to the value $m = M'$, dependent on the magnitude of the parameters ka, kh and kr.

4. Acoustic pressure for much larger distances with respect to the length of the wave radiated

In a specific case, when the distance r of a point of the field is much large than the length of the wave radiated, λ, and when $\tau_m \neq 0$, the Bessel, Neumann and MacDonald functions in expressions (28) and (29) can be replaced by their asymptotic representations:

$$J_0(r\tau_m) \simeq \sqrt{\frac{2}{\pi r\tau_m}} \cos\left(r\tau_m - \frac{\pi}{4}\right),$$

$$N_0(r\tau_m) \simeq \sqrt{\frac{2}{\pi r\tau_m}} \sin\left(r\tau_m - \frac{\pi}{4}\right),$$

$$K_0(r|\tau_m|) \simeq \sqrt{\frac{\pi}{2r|\tau_m|}} \exp(-r|\tau_m|). \tag{30}$$

From the practical point of view, it is very important to be able to predict the pressure distribution about the source, when the distance r of a point of the pressure studied is larger than the linear dimensions of the source. When, in addition, in series (28) and (29) $r \geqslant h$, then in practical calculations only the finite number of M terms can be considered, for which $m\lambda < 2h (m\pi < kh)$. Consideration of dependencies (30), (28) and (29) gives then

$$p(r, z) = \varrho_0 c_0 \frac{k}{h} \sqrt{\frac{\pi}{2r}} \exp\left(i\frac{\pi}{4}\right) \sum_{m=0}^{M} \varepsilon_m \cos\left(\frac{m\pi z}{h}\right) W_s(\tau_m) \frac{\exp(-ir\tau_m)}{\sqrt{\tau_m}}.$$

5. Characteristic function

Bearing in mind the practical applications, the surface vibration velocity distribution can be assumed to be the same as that which occurs in the case of a circular membrane excited to axially-symmetric vibration. Such dimensions of the individual annular surfaces are assumed that they are bounded by circles corresponding to nodal circles for the (0, n) mode of the vibrating circular membrane. Since the object of the analysis is axially-symmetric vibration, then all the points on the surface of any of the rings vibrate in phase, while all the two adjacent annular surfaces vibrate in antiphase.

For phenomena harmonic in time, the distribution of self vibration velocity for the (0, n) axially-symmetric mode is expressed by the formula [3]

$$v_n(r) = v_{0n} J_0\left(\frac{r}{a} q_n\right), \tag{32}$$

where $q_n = a(\omega_n/c_M)$ is a root of the equation $J_0(q_n) = 0$, ω_n is the angular frequency of self vibration, c_M is the wave propagation velocity on the membrane, v_{0n} is the maximum vibration velocity. The radii r_s of the nodal circles for the $(0, n)$ mode of vibration, as found from the equation

$$J_0\left(\frac{r_s}{a}\right) q_n = 0, \tag{33}$$

are $r_s = a(q_s/q_n)$, $s = 1, 2, \ldots, n-1$; with, for $s = n$, $r_n = a$ being the radius of the membrane, i.e. of the external nodal circle (see [5]).

The characteristic function (9)

$$W_s(\tau) = v_{0n} \int_{aq_{s-1}/q_n}^{aq_s/q_n} J_0\left(\frac{r_0}{a} q_n\right) J_0(\tau r_0) r_0 dr_0 \tag{34}$$

for the sth ring, being the set of points $\{a(q_{s-1}/q_n) \leqslant r \leqslant a(q_s/q_n),\ 0 \leqslant \varphi \leqslant 2\pi$, after considering the integral property [8]

$$\int_0^u w J_0(hw) J_0(lw)\, dw = \frac{u}{h^2 - l^2} \{h J_1(hu) J_0(lu) - l J_0(hu) J_1(lu)\}, \tag{35}$$

is

$$W_s(\tau) = \frac{v_{0n} a^2}{q_n^2 - (a\tau)^2} \left\{ q_s J_1(q_s) J_0\left(\frac{q_s}{q_n} a\tau\right) - q_{s-1} J_1(q_{s-1}) J_0\left(\frac{q_{s-1}}{q_n} a\tau\right), \right. \tag{36}$$

where $J_0(q_s) = J_0(q_{s-1}) = 0$.

When in turn the source of the acoustic field is a system of concentric circular pistons, i.e. when the vibration velocity distribution on the surface of the sth annular piston is uniform, $v_s = v_{0s} = \text{const.}$, then the characteristic function

$$W_s(\tau) = v_{0s} \int_{r_{s-1}}^{r_s} J_0(\tau r_0) r_0 dr_0, \tag{37}$$

after considering the integral property (35) for $l = 0$, is

$$W_s(\tau) = \frac{v_{0s}}{\tau} [r_s J_1(\tau r_s) - r_{s-1} J_1(\tau r_{s-1})]. \tag{38}$$

In calculating the characteristic function from formulae (36) and (38), the quantity τ should be replaced by τ_m, as defined by relation (22) or (24), depending on whether $m\pi < kh$ or $m\pi > kh$.

6. Numerical example with analysis of results

In analysing the acoustic pressure radiated by a circular membrane for the axially-symmetric vibration mode (0, 2), two vibrating surface elements, separated by the nodal circle $a(q_1/q_2)$, where $a = 2$ cm, $q_1 = 2.4048\ldots$, and $q_2 = 5.5201\ldots$, were distinguished. The central element of the membrane is a circular source, being the set of points $\{0 \leqslant r \leqslant a(q_1/q_2),\ 0 \leqslant \varphi \leqslant 2\pi\}$, the external element is an annular source, being the set of points $\{a(q_1/q_2) \leqslant r \leqslant a,\ 0 \leqslant \varphi \leqslant 2\pi\}$.

In the numerical example the value of the acoustic pressure p radiated by a surface source was referred to the pressure $p_p = \varrho_0 c_0 v_0$. The relative pressure value p/p_0 was represented graphically depending on the dimensionless parameter r/h,

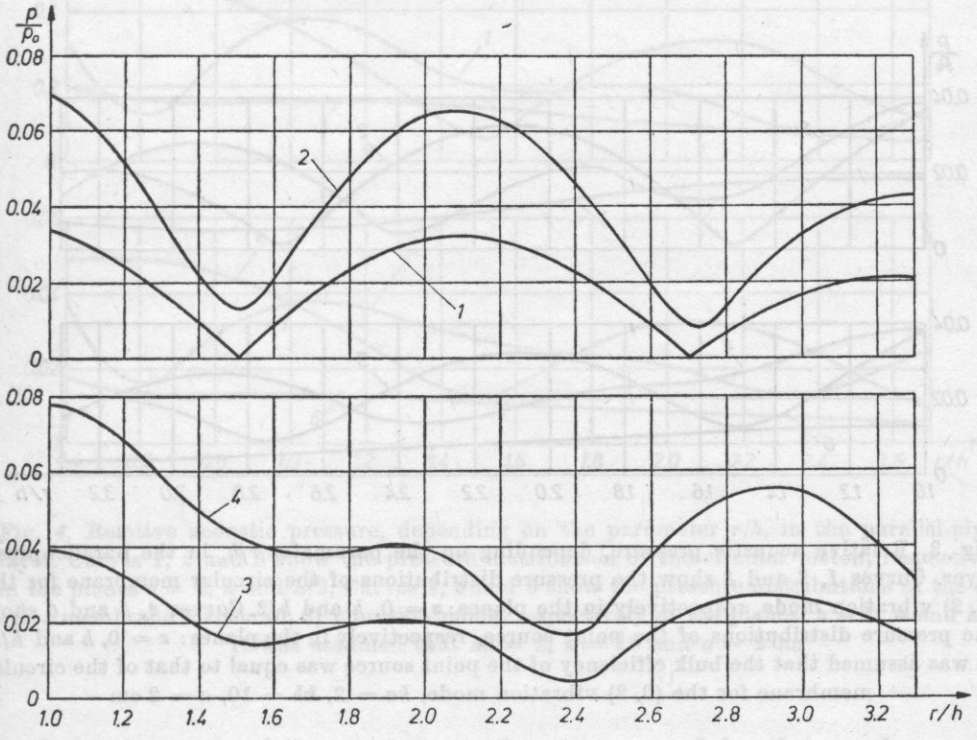

Fig. 2. Relative acoustic pressure p/p_0 of the sources separated on the circular membrane for the (0, 2) vibration mode, depending on the parameter r/h in the parallel-piped layer. It was assumed that $a = 2$ cm, $ka = 2$, $kh = 10$. Pressure distribution in the plane $z = h = 10$ cm: *1* — circular (central) source, curve *2* — annular (external) source. Pressure distribution in the plane of the source ($z = 0$): curve *3* — circular source, curve *4* — annular source

or r/a, with a fixed distance between the baffles, $h = 10$ cm, and the radius $a = 2$ cm.

The curves of the relative acoustic pressure, depending on the parameter r/h, for a separate central element and the external element of the circular membrane are shown in Fig. 2. These curves show that in the variation interval of the parameter r/h under analysis the relative acoustic pressure of the external source exceeds that of the central circular one. This property is satisfied both on the surface of the baffle in which the source is and also on the surface of the baffle at the distance h from the plane of the source. On the baffle at the distance h from the plane of the source there are circles in which the value of the pressure drops to zero (see curve 1 in Fig. 2).

Fig. 3 shows the curves of the relative acoustic pressure, depending on the parameter r/h, radiated by the circular membrane for the (0, 2) vibration mode. This vibrating membrane is a system of two sources: the central circular and

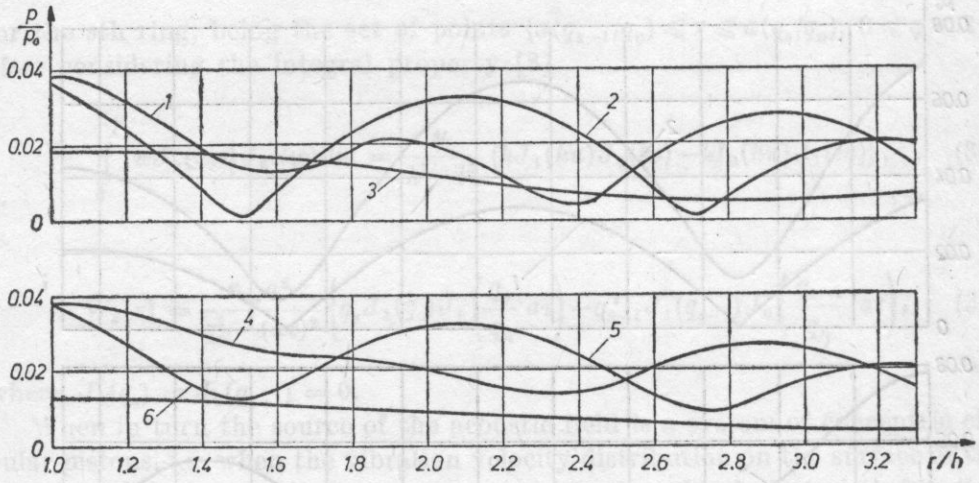

Fig. 3. Relative acoustic pressure, depending on the parameter r/h, in the parallel-piped layer. Curves *1*, *2* and *3* show the pressure distributions of the circular membrane for the (0, 2) vibration mode, respectively in the planes: $z = 0$, h and $h/2$. Curves *4*, *5* and *6* show the pressure distributions of the point source, respectively in the planes: $z = 0$, h and $h/2$. It was assumed that the bulk efficiency of the point source was equal to that of the circular membrane for the (0, 2) vibration mode, $ka = 2$, $kh = 10$, $a = 2$ cm

the external annular ones, separated by a nodal circle with the radius $a(q_1/q_2)$. This figure also shows analogous curves for the point source whose bulk efficiency $Q = 2\pi a^2 v_0 [J_1(q_2)/q_2]$ is the same as that of the circular membrane analysed for the (0,2) vibration mode. For the membrane and the point source separate acoustic pressure curves were plotted depending on the parameter r/h in three planes: in the plane of the source, in a plane at a distance $h/2$ from the plane of

the source and in the plane of the baffle situated at the distance h from the plane of the source. These curves show that larger pressure fluctuations occur on the surfaces of the baffles in the case of the point source. The almost monotonous decrease in the acoustic pressure occurs in the plane $z = h/2$ with increasing parameter r/h, both for the point source and the circular membrane (see curves *3* and *6* in Fig. 3).

As in Fig. 3, acoustic pressure curves, depending on the parameter r/h, were also plotted for the circular membrane in Fig. 4. Curves are also shown for the pressure radiated by a circular piston with the radius $a = 2$ cm. Different

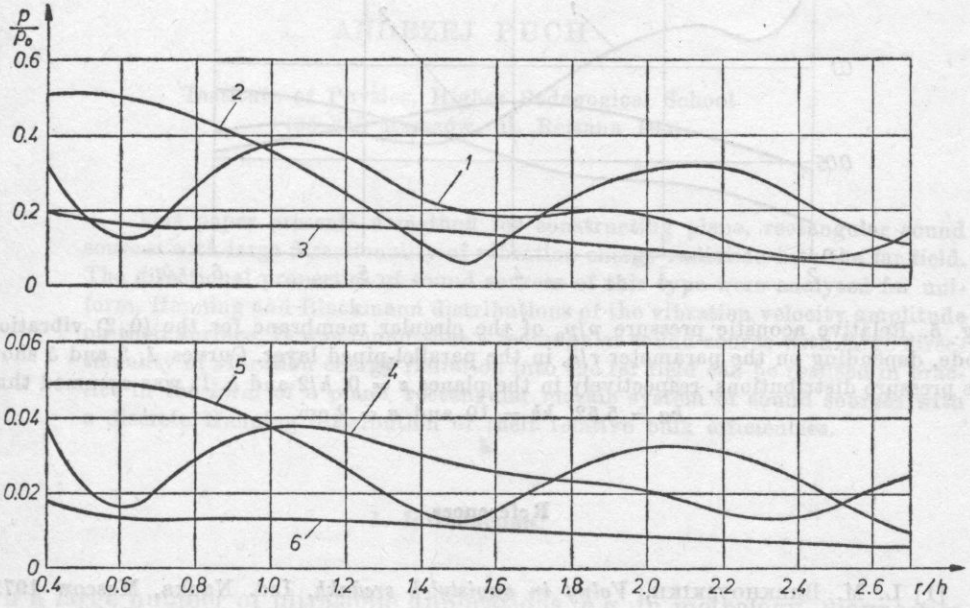

Fig. 4. Relative acoustic pressure, depending on the parameter r/h, in the parallel-piped layer. Curves *1*, *2* and 3 show the pressure distribution of the circular piston, respectively in the planes $z = 0$, h and $h/2$. Curves *4*, *5* and 6 show the pressure distributions of the circular membrane for the (0, 2) vibration mode, respectively in the planes: $z = 0$, h and $h/2$. It was assumed that $ka = 2$, $k = 10$ and $a = 2$ cm

variation intervals of the parameter r/h were assumed for the membrane and the piston (see curves 4,5 and 6 in Figs. 3 and 4). Analysis of the curves (Fig. 4) shows distinct differences among the values of the pressures generated by the membrane and the circular piston for given values of the parameters r/h. It can be assumed with approximation that the value of the pressure from the circular piston is higher by an order of magnitude from that from the circular membrane with a given value of the parameter r/h.

The curves in Figs. 2, 3 and 4 were plotted from calculations for $ka = 2$. Curves of the relative pressure, depending on the parameter r/a, for the circular membrane are shown in Fig. 5. It was assumed that $ka = 5.52$, which corresponds to the resonance vibration frequency.

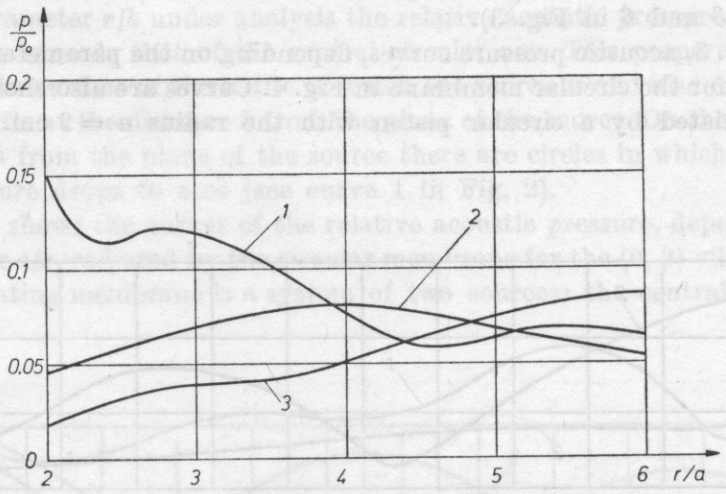

Fig. 5. Relative acoustic pressure p/p_0 of the circular membrane for the (0, 2) vibration mode, depending on the parameter r/a, in the parallel-piped layer. Curves *1*, *2* and *3* show the pressure distributions, respectively in the planes $z = 0$, $h/2$ and h. It was assumed that $ka = 5.52$, $kh = 10$ and $a = 2$ cm

References

[1] L. M. Brekhovskikh, *Volny in swoistyleh sredakh*, Izd. Nauka, Moscow 1973.

[2] J. W. Dettman, *Applied complex variables*, Mc Millan, New York – London 1965.

[3] I. Malecki, *Theory of acoustic waves and systems* (in Polish), PWN, Warsaw 1964.

[4] N. W. McLachlan, *Loudspeakers*, Dower Publications, New York 1960.

[5] W. Rdzanek, *Mutual acoustic interactions in a system of concentric annular sources* (in Polish), Higher Pedagogical University, Zielona Góra 1983.

[6] W. Rdzanek, *Acoustic field distribution from a planar system of annular sources* (in Polish), Scientific Reports, Higher Pedagogical School, 1984, Physics II (in press).

[7] W. Thompson, Jr., *The computation of self-and mutual radiation impedances for annular and elliptical pistons using Bouwkamp's integral*, J. Sound Vib., 17, 2, 221–233 (1971).

[8] G. N. Watson, *Theory of Bassel functions*, 2nd ed., University Press, Cambridge 1966.

Received on November 23, 1983; revised version on December 11, 1984.

ARCHIVES OF ACOUSTICS
10, 1, 17-35 (1985)

RECTANGULAR SOURCES AND SYSTEMS OF SOUND SOURCES WITH LARGE DIRECTIONALITY

ANDRZEJ PUCH

Institute of Physics, Higher Pedagogical School
(35–310 Rzeszów, ul. Rejtana 16a)

This paper presents a method for constructing plane, rectangular sound sources with large directionality of vibration energy radiation into the far field. The directional properties of sound sources of this type were analysed for uniform, Hanning and Blackmann distributions of the vibration velocity amplitude on their surface. It was found that a rectangular sound source with large directionality of vibration energy radiation into the far field can be realised in practice in the form of a plane, rectangular mosaic system of sound sources with a discrete Hanning distribution of their relative bulk efficiencies.

1. Introduction

In a large number of ultrasonic applications, e.g. in metrology, diagnostics or ultrasonic technology, there is the need for using sound sources with large directionality of vibration energy radiation into the far field, in order to obtain the appropriate shape of and ultrasonic wave beam or the required energy concentration in some region of a medium.

The construction and study of the properties of sound sources with large directionality of vibration energy radiation have to date been the subjects of a large number of theoretical and experimental investigations (e.g. [2], [3], [10], [12], [13]). The authors of these papers paid most attention to the selection of an appropriate vibration velocity amplitude distribution on the surface of a planar or spherical sound source with given shape, most often a circular one. In the 1970's much interest was enjoyed by the properties of a sound source with a Gaussian vibration velocity amplitude distribution on its surface [2], [3], [10] and [13]. Recently, intensive research has been carried out on the properties of systems of sound sources (e.g. [5], [7] and [8]).

This paper presents a method for constructing rectangular mosaic system of sound sources with large directionality of vibration energy radiation into the far field.

2. Radiation directionality of a planar sound source

Let us assume that in the plane $z = 0$ (Fig. 1), which is an ideal rigid baffle S_0, there is a planar sound source σ_0 which vibrates harmonically at the frequency f_0. Let it radiate vibration energy into the half-space $z > 0$, filled with a lossless and homogeneous liquid medium with density ϱ, in which the sound wave propagates at the velocity c. Let us assume that, as a result of the vibration

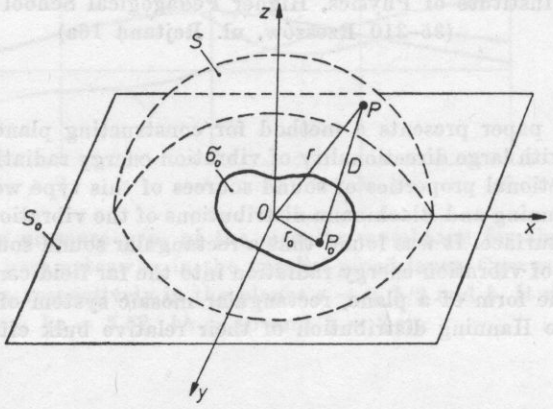

Fig. 1. The sound source σ_0 placed in the baffle S_0 and radiating vibration energy into the medium filling the half-space over the baffle

of the sound source σ_0, the distribution of the normal component of the vibration velocity in the plane of the baffle S_0 is defined as

$$v(S_0, t) = \varkappa(S_0)\exp(-j2\pi f_0 t), \tag{1}$$

where

$$\varkappa(S_0) \neq 0 \quad \text{for the surface of the source } \sigma_0, \tag{2}$$

$$\varkappa(S_0) \neq 0 \text{ for the other part of the baffle } S_0;$$

is a function determining the vibration velocity amplitude distribution on the plane S_0.

In the half-space $z > 0$, let us consider the surface of the hemisphere S with the radius

$$r \gg r_g = \pi f_0 r_{0m}^2/c, \tag{3}$$

surrounding the sound source σ_0 in its far field [4], [9], where r_{0m} is the longest of the distances between points of the contour of the sound source σ_0 and the origin of the coordinate system. The acoustic pressure distribution generated by the sound source σ_0 on the surface of the hemisphere S can be expressed by the formula [4], [9]

$$p(S, t) = P(S)\exp(-j2\pi f_0 t), \tag{4}$$

where

$$P(S) = -j\frac{f_0\varrho}{r}\exp(j2\pi r f_0/c)\int_{S_0}\varkappa(S_0)\exp[-j2\pi f_0 r_0\cos(r_0, r)/c]dS_0 \tag{5}$$

is a function determining the acoustic pressure amplitude distribution on the surface of the hemisphere S. Since the function [4], [9]

$$P_0(S) = -j\frac{f_0\varrho}{r}\exp(j2\pi r f_0/c) \tag{6}$$

defines the acoustic pressure amplitude distribution generated on the surface of the hemisphere S by a point sound source with unit efficiency, placed in the baffle S_0 instead of the planar sound source ϱ_0, expression (5) can then be represented as

$$P(S) = P_0(S)R(S), \tag{7}$$

where

$$R(S) = \int_{S_0}\varkappa(S_0)\exp[-j2\pi f_0 r_0\cos(r_0, r)/c]dS_0 \tag{8}$$

is a function defining the relative acoustic pressure amplitude distribution on the surface of the hemisphere S. It can be noted that the function $R(S)$ does not depend on the radius r. In view of this, this function determines the relative acoustic pressure amplitude distribution on the surface of the hemisphere S with any radius r which satisfies condition (3). Since at a given vibration frequency f_0 of the sound source δ_0 the function $R(S)$ depends only on the angle between the radius r and the axis $0z$, the function $R(S)$ can then be used in evaluating the sound source σ_0 in terms of directionality of acoustic pressure wave radiation in the far field. In comparing sound sources with respect to one another, it is more convenient to use the normalised function $\bar{R}(S)$, i.e. the function $\bar{R}(S)$ satisfying the condition

$$\bar{R}(S) = 1 \quad \text{for the angle } (r, r_0) = \pi/2. \tag{9}$$

It follows from dependence (8) that for the angle $(r, r_0) = \pi/2$ the function $R(S)$ takes the value

$$V_0 = \int_{S_0}\varkappa(S_0)dS_0, \tag{10}$$

equal to the bulk efficiency of the sound source σ_0 placed in the baffle S_0. In view of this and from (8),

$$\bar{R}(S) = R(S)V_0, \tag{11}$$

The function $\bar{R}(S)$ is called the directional characteristic of the sound source σ_0 [4].

3. The spatial spectrum of the vibration velocity amplitude distribution function

Let us represent expression (8) in a rectangular coordinate system. Let $\nu = f_0/c$ denote the spatial frequency of a sound wave radiated by the sound source σ_0 into the medium filling the half-space $z > 0$. Since [4], [9]

$$\nu r_0 \cos(r_0, r) = \nu r_0 [\cos(r_0, x)\cos(x, r) + \cos(r_0, y)\cos(y, r)], \tag{12}$$

then, when

$$x = r_0 \cos(r_0, x), \tag{13}$$

$$y = r_0 \cos(r_0, y) \tag{14}$$

are the coordinates of points of the baffle S_0, and

$$\nu_x = \nu \cos(x, r), \tag{15}$$

$$\nu_y = \nu \cos(y, r) \tag{16}$$

are the components of the spatial frequencies of partial planar waves whose spatial superposition represents the wave radiated by the sound source σ_0 into the medium filling the half-space $z > 0$ [1], [15], the function $R(S)$ can be given in the form

$$R(\nu_x, \nu_y) = \int_{-\infty}^{+\infty} \int_{-\infty}^{+\infty} \varkappa(x, y) \exp[-j2\pi(x\nu_x + y\nu_y)]\, dx\, dy. \tag{17}$$

It follows from dependencies (15) and (16) that in the half-space $z \geqslant 0$ the spatial frequencies ν_x and ν_y can take values from an interval defined by the inequality

$$\sqrt{\nu_x^2, \nu_y^2} \leqslant \nu^2. \tag{18}$$

It can be noted that expression (17) has a form analogous to a simple, two-dimensional Fourier transform [1], [15]. Let us consider the spatial spectrum of the distribution function $\varkappa(x, y)$ of the vibration velocity amplitude in the plane of the baffle S_0, defined by the expression

$$K(\nu_x, \nu_y) = \int_{-\infty}^{+\infty} \int_{-\infty}^{+\infty} \varkappa(x, y) \exp[-j2\pi(x\nu_x + y\nu_y)]\, dx\, dy, \tag{19}$$

where $-\infty < \nu_x, \nu_y < +\infty$. It follows from dependencies (17) and (19) that the distribution $R(\nu_x, \nu_y)$ of the relative acoustic pressure amplitude on the surface of the hemisphere S can be determined from the spatial spectrum $K(\nu_x, \nu_y)$ of the distribution function $\varkappa(x, y)$ of the vibration velocity amplitude in the plane of the baffle S_0. Namely,

$$R(\nu_x, \nu_y) = K(\nu_x, \nu_y) H_\nu(\nu_x, \nu_y), \tag{20}$$

where

$$H_\nu(\nu_x, \nu_y) = 1 \quad \text{for } \sqrt{\nu_x^2, \nu_y^2} \leqslant \nu^2, \tag{21}$$

$$H_\nu(\nu_x, \nu_y) = 0 \quad \text{for the other } \nu_x, \nu_y,$$

with $-\infty < \nu_x, \nu_y < +\infty$. It follows from dependencies (20) and (21) that the baffle S_0 plays the role of a low-pass spatial filter [1] with the spatial transmittance $H_\nu(\nu_x, \nu_y)$, causing restriction of the spatial spectrum $K(\nu_x, \nu_y)$ of the distribution $\varkappa(x, y)$ to the region of spatial frequencies defined by expression (18).

It can be noted in turn ((10) and (19)) that the bulk efficiency of the sound source σ_0 is given by the expression

$$V_0 = \int_{-\infty}^{+\infty} \int_{-\infty}^{+\infty} \varkappa(x, y)\, dx\, dy = K(0, 0), \tag{22}$$

where K (0, 0) is a component of the spatial spectrum $K(\nu_x, \nu_y)$ of the distribution function $\varkappa(x, y)$ for the spatial frequencies $\nu_x = \nu_x = 0$. In view of this and from (11) and (20), the directional characteristic of the sound source σ_0 can be determined in the following way:

$$\bar{R}(\nu_x, \nu_y) = K(\nu_x, \nu_y) H_\nu(\nu_x, \nu_y) / K(0, 0). \tag{23}$$

It follows hence that the directional characteristic of the sound source σ_0, for a given spatial frequency ν, can be determined from the spatial spectrum $K(\nu_x, \nu_y)$ of the function $\varkappa(x, y)$ defining the vibration velocity amplitude distribution in the plane of the baffle S_0, which contains the sound source σ_0.

4. The effect on the directional characteristic of the sound source of its shape and that of the vibration velocity amplitude distribution on its surface

The function $\varkappa(x, y)$, defining the vibration velocity amplitude distribution in the plane of the baffle S_0, can be represented as the product of the function $f(x, y)$, which was used to define the shape of the vibration velocity amplitude distribution on the surface of the sound source σ_0, and the distribution $z(x, y)$, defining the shape of this source. Namely,

$$\varkappa(x, y) = f(x, y) z(x, y), \tag{24}$$

where

$$z(x, y) = 1 \quad \text{for the surface of the source } \sigma_0, \tag{25}$$

$$z(x, y) = 0 \quad \text{for the other part of the baffle } S_0.$$

Let us determine the spatial spectrum of the distribution function (24). The use of the theorem on the Fourier transform of the product of the function and the distribution [1] gives

$$K(\nu_x, \nu_y) = \int_{-\infty}^{+\infty} \int_{-\infty}^{+\infty} F(\mu_x, \mu_y) Z(\nu_x - \mu_x, \nu_y - \mu_y) d\mu_x d\mu_y$$

$$= F(\nu_x, \nu_y) * Z(\nu_x, \nu_y). \tag{26}$$

Hence, it follows that the spatial spectrum $K(\nu_x, \nu_y)$ of the distribution function $\varkappa(x, y)$ of the vibration velocity amplitude in the plane of the baffle S_0, containing the planar sound source σ_0, is a convolution of the spatial spectrum $F(\nu_x, \nu_y)$ of the function $f(x, y)$, which was used to define the shape of the vibration velocity amplitude distribution on the surface of the source σ_0, with the spatial spectrum $Z(\nu_x, \nu_y)$ of the distribution $z(x, y)$, defining the shape of this source. In view of this and from (11) and (23), the directional characteristic of the sound source σ_0 can be determined by the expression

$$\bar{R}(\nu_x, \nu_y) = [F(\nu_x, \nu_y) * Z(\nu_x, \nu_y)] H_v(\nu_x, \nu_y) V_0. \tag{27}$$

The authors of previous papers [2], [3], [13] and [14], on the study of the properties of sound sources with large directionality of vibration energy radiation into the far field, did not go beyond the analysis of the effect of chosen functions of the shape of the distribution $f(x, y)$ on the directional characteristic of the sound source, neglecting the effect on this characteristic, of the distribution $z(x, y)$ defining the shape of the source. Further considerations here will propose a method for constructing sound sources with large directionality of vibration energy radiation, consisting in selection of an appropriate function defining the shape of the vibration velocity amplitude distribution on the surface of a source with prescribed form.

5. Sound sources with large directionality of vibration energy radiation

The absolutely directional sound source will be understood here to be a source radiating vibration energy only towards the axis $0z$. Accordingly, the spatial spectrum of the vibration velocity amplitude distribution function in the plane of the baffle S_0, containing such a source, can be determined in the fol-

lowing way:

$$K(\nu_x, \nu_y) = \varkappa_0 \delta(\nu_x, \nu_y), \tag{28}$$

where $\delta(\nu_x, \nu_y)$ is a Dirac distribution.

Let us determine the vibration velocity amplitude distribution in the plane of the baffle S_0, containing the absolutely directional sound source. The use of the theorem of the inverse Fourier transform of the Dirac distribution [1] gives

$$\varkappa(x, y) = \varkappa_0, \tag{29}$$

Hence, it follows that the absolute directional sound source is a source with infinitely large size and uniform vibration velocity amplitude distribution on its surface. Using this idealized model, unrealizable practically, of the sound source, it is possible to determine the method for constructing sound source with large directionality of vibration energy radiation. Since the distribution $\delta(\nu_x, \nu_y)$ can be defined as the limit of the function series $K(\nu_x, \nu_y; A, B)$ satisfying the conditions [11]:

$$\lim_{\substack{A\to 0 \\ B\to 0}} K(\nu_x, \nu_y; A, B) = 0 \quad \text{for } \nu_x, \nu_y \neq 0, \tag{30}$$

and

$$\int_{-\infty}^{+\infty} \int_{-\infty}^{+\infty} K(\nu_x, \nu_y; A, B) d\nu_x d\nu_y = 1 \quad \text{for all } A, B > 0, \tag{31}$$

the distribution function $\varkappa(x, y)$ of the vibration velocity amplitude in the plane of the baffle S_0, containing a sound source with large directionality of vibration energy radiation into the far field, should be chosen in such a way that the function series $K(\nu_x, \nu_y; A, B)$, derived from the Fourier transform $K(\nu_x, \nu_y)$ of the distribution function $\varkappa(x, y)$ would satisfy the conditions given above. Accordingly, it can be shown that the sound source with a Gaussian vibration velocity amplitude distribution analysed in papers [2], [3], [10] and [13] is a sound source with large directionality of vibration energy radiation in the sense defined above, since the function series $K(\nu_x, \nu_y; A, B)$, derived from the spatial spectrum $K(\nu_x, \nu_y)$ of the distribution function $\varkappa(x, y)$ of the vibration velocity amplitude in the plane of the baffle S_0, containing this source, which has the following form in a rectangular coordinate system [13]:

$$K(\nu_x, \nu_y; A, B) = K(\nu_x; A) K(\nu_y; B), \tag{32}$$

where

$$K(\nu_x; A) = \frac{1}{A} \exp(-\pi \nu_x^2 / A^2), \tag{33}$$

whereas

$$K(\nu_y;\ B) = \frac{1}{B}\exp(-\pi\nu_y^2/B^2), \tag{34}$$

satisfies [10] conditions (30) and (31). Since a sound source with a Gaussian distribution, as the absolutely directional sound source, is a source with infinitely large size, therefore, strictly speaking, it is realizable in practice realizable only in approximation [2]. Further considerations will show that it is not possible to construct practically realizable sound sources with large directionafity of vibration energy radiation into the far field.

6. Rectangular sound sources with large directionality of vibration energy radiation

Let us now construct a rectangular sound source with the sides a and b showing large directionality of vibration energy radiation into the far field. The following series will be used for that purpose [11]:

$$K(\nu_x,\ \nu_y;\ A,\ B) = K(\nu_x;\ A)K(\nu_y;\ B), \tag{35}$$

where

$$K(\nu_x;\ A) = \frac{1}{A}\operatorname{sinc}(\nu_x/A), \tag{36}$$

whereas

$$K(\nu_y;\ B) = \frac{1}{B}\operatorname{sinc}(\nu_y/B), \tag{37}$$

satisfying conditions (30) and (31), with $A = 1/a$, $B = 1/b$, while

$$\operatorname{sinc}(z) = \frac{\sin(\pi z)}{\pi z}. \tag{38}$$

Let us consider uniform, Hanning and Blackmann distributions. The Fourier transforms of these distributions are functions of the form of (35) [6].

a) Uniform distribution. Let us assume that the vibration velocity amplitude distribution in the plane of the baffle S_0 is defined in the following way (Fig. 2):

$$\varkappa(x,\ y) = \varkappa_0\varkappa(x)\varkappa(y), \tag{39}$$

where

$$\varkappa(x) = 1 \quad \text{for } |x| \leqslant a/2, \tag{40}$$
$$\varkappa(x) = 0 \quad \text{for } |x| > a/2,$$

whereas

$$\varkappa(y) = 1 \quad \text{for } |y| \leqslant b/2, \tag{41}$$

$$\varkappa(y) = 0 \quad \text{for } |y| > b/2,$$

Let us determine the spatial spectrum of the distribution function (39). The use of the theorem on the ourier transform of the product of distribution with separated variables and the theorem on the transform of the distribution $sgn(z)$ [11] gives

$$K(v_x, v_y) = \varkappa_0 K(v_x) K(v_y), \tag{42}$$

where

$$K(v_x) = a\,\mathrm{sinc}(av_x), \tag{43}$$

whereas

$$K(v_y) = b\,\mathrm{sinc}(bv_y). \tag{44}$$

The transform $K(v_x)$ (Fig. 2) of the distribution function (40) is a function having the main maximum for $v_x = 0$ and side extremes decreasing as $|v_x|$ increases, at a rate of 20 dB/decade. The highest of the side extremes are larger by 13 dB than the main one.

b) Hanning distribution. Let us assume that the vibration velocity amplitude distribution in the plane of the baffle S_0 is defined in the following way (Fig. 2):

$$\varkappa(x, y) = \varkappa_0 \varkappa(x) \varkappa(y), \tag{45}$$

where

$$\varkappa(x) = 0.5 + 0.5\cos(2\pi x/a) \quad \text{for } |x| \leqslant a/2, \tag{46}$$

$$\varkappa(x) = 0 \quad \text{for } |x| > a/2,$$

whereas

$$\varkappa(y) = 0.5 + 0.5\cos(2\pi y/b) \quad \text{for } |y| \leqslant b/2,$$

$$\varkappa(y) = 0 \quad \text{for } |y| > b/2. \tag{47}$$

Let us determine the spatial spectrum of the distribution function (45). This gives

$$K(v_x, v_y) = \varkappa_0 K(v_x) K(v_y), \tag{48}$$

where

$$K(v_x) = a\,[0.5\,\mathrm{sinc}(av_x) + 0.25\sin(av_x - 1) + 0.25\,\mathrm{sinc}(av_x + 1)\,], \tag{49}$$

whereas

$$K(v_y) = b\,[0.5\,\mathrm{sinc}(bv_y) + 0.25\,\mathrm{sinc}(bv_y - 1) + 0.25\,\mathrm{sinc}(bv_y + 1)\,]. \tag{50}$$

The transform $K(\nu_x)$ (Fig. 2) of the distribution function (46) is a function having the main maximum for $\nu_x = 0$ and side extremes decreasing as $|\nu_x|$ increases, at a rate of 60 dB/decade. The highest of the side extremes are larger by 32 dB than the main maximum. Compared with the uniform distribution, the transform $K(\nu_x)$ of the distribution function $\varkappa(x)$ for the Hanning distribution has a wider main maximum, but lower and more slowly decreasing side extremes.

c) Blackmann distribution. Let us assume that the vibration velocity amplitude distribution in the plane of the baffle S_0 is defined in the following way (Fig. 2):

$$\varkappa(x, y) = \varkappa_0 \varkappa(x)\varkappa(y), \tag{51}$$

where

$$\varkappa(x) = 0.42 + 0.5\cos(2\pi x/a) + 0.08\cos(4\pi x/a) \quad \text{for } |x| \leqslant a/2,$$
$$\varkappa(x) = 0 \quad \text{for } |x| > a/2, \tag{52}$$

whereas

$$\varkappa(y) = 0.42 + 0.5\cos(2\pi y/b) + 0.08\cos(4\pi y/b) \quad \text{for } |y| \leqslant b/2,$$
$$\varkappa(y) = 0 \quad \text{for } |y| > b/2. \tag{53}$$

Let us determine the spatial spectrum of the distribution function (51) This gives

$$K(\nu_x, \nu_y) = \varkappa_0 K(\nu_x) K(\nu_y), \tag{54}$$

where

$$K(\nu_x) = a[0.42\,\mathrm{sinc}(a\nu_x) + 0.25\,\mathrm{sinc}(a\nu_x - 1) + 0.25\,\mathrm{sinc}(a\nu_x + 1) + 0.04\,\mathrm{sinc}(a\nu_x - 2) + 0.04\,\mathrm{sinc}(a\nu_x + 2)], \tag{55}$$

whereas

$$K(\nu_y) = b[0.42\,\mathrm{sinc}(b\nu_y) + 0.25\,\mathrm{sinc}(b\nu_y - 1) + 0.25\,\mathrm{sinc}(b\nu_y + 1) + 0.04\,\mathrm{sinc}(b\nu_y - 2) + 0.04\,\mathrm{sinc}(b\nu_y + 2)]. \tag{56}$$

The transform $K(\nu_x)$ (Fig. 2) of the distribution function (52) is a function having the main maximum for $\nu_x = 0$ and side extremes decreasing as $|\nu_x|$ increases, at a rate of 34 dB/decade. The highest of the side extremes are larger by 57 dB than the main maximum. Compared with the Hanning distribution, the transform $K(\nu_x)$ of the distribution function $\varkappa(x)$ for the Blackmann distri-

bution has a wider main maximum, but lower and more slowly decreasing side extremes.

It follows from these considerations that each of the distributions: uniform, Hanning's and Blackmann's, can be used to construct a rectangular sound source with large directionality of vibration energy radiation into the far field. To achieve this, for a given frequency f_0 of vibration of the surface of the sound source, appropriately large size of the source, compared with the length of the sound wave in the medium where this source will radiate vibration energy,

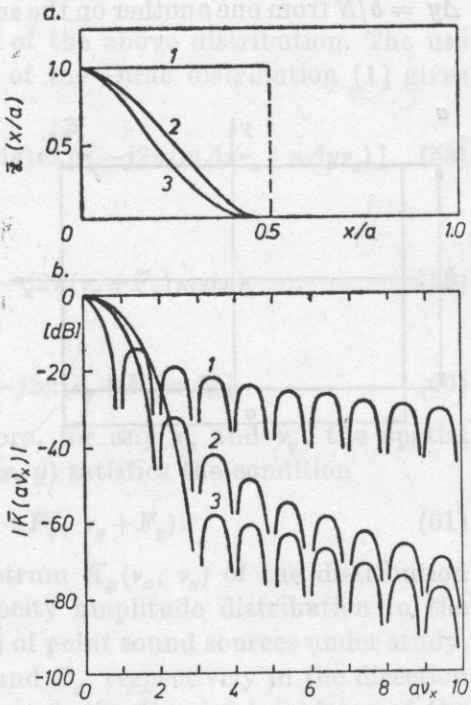

Fig. 2. Vibration velocity amplitude distribution function (a) and their Fourier transforms (b) for uniform (1), Hanning (2) and Blackmann (3) distributions

should be selected. In view of the magnitude of side extremes of the directional characteristic, compared with its main maximum, the Blackmann distribution seems to be most useful for practical application. However, the considerable width of the main maximum of the directional characteristic in this case requires the use of sound sources with appropriately large size, compared with the wavelength, much larger than are necessary in the case of the Hanning distribution. In view of this, a rectangular sound source with the Hanning distribution of the vibration velocity amplitude on its surface seems to be more useful for application as a source with large directionality of vibration energy radiation into the far field than one with uniform or Blackmann distributions.

7. Rectangular systems of sound sources with large directionality of vibration energy radiation

Let us consider a rectangular sound source σ_0 with the sides a and b (Fig. 3) showing large directionality of vibration energy radiation in the far field. Let us assume that the vibration velocity amplitude distribution in the plane of the baffle S_0, containing this source, is defined by the function $\varkappa(x, y)$.

Let us replace the sound source σ_0 by a system consisting of a number of point sound sources σ_{mn}, spaced respectively at intervals $\Delta x = a/M$ and $\Delta y = b/N$ from one another on the surface of the rectangle occupied by the sound

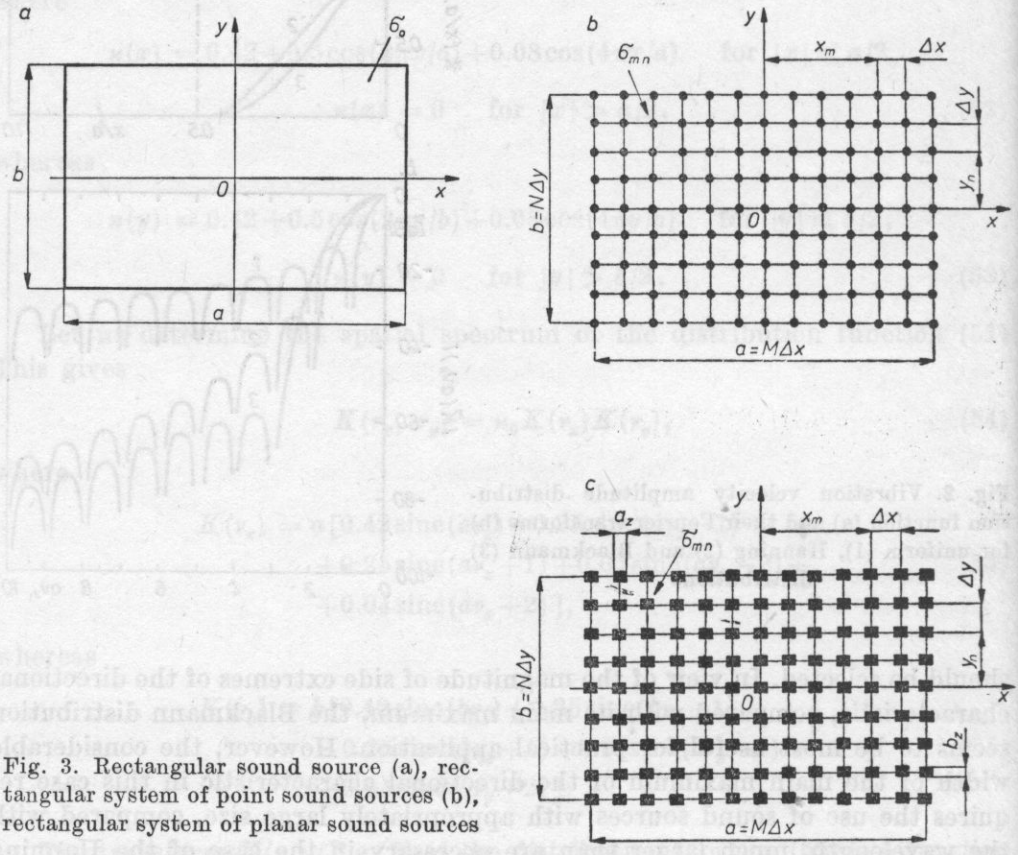

Fig. 3. Rectangular sound source (a), rectangular system of point sound sources (b), rectangular system of planar sound sources

source σ_0 (Fig. 3). Let us assume that the efficiencies of individual sources in the system are equal to the values $\varkappa(m\Delta x, n\Delta y)$ of the distribution function $\varkappa(x, y)$. Accordingly, the vibration velocity amplitude distribution in the plane of the baffle S_0, containing the system of point sound sources under study,

is defined by the expression (Fig. 4)

$$\varkappa_p(x, y) = \varkappa(x, y)\frac{1}{\Delta x\,\Delta y}\,\mathrm{III}(x/\Delta x,\ y/\Delta y)$$

$$= \varkappa(x, y)\sum_{m=-\infty}^{+\infty}\sum_{n=-\infty}^{+\infty}\delta(x-m\Delta x,\ y-n\Delta y) \tag{57}$$

$$= \sum_{m=-M/2}^{M/2}\sum_{n=-N/2}^{N/2}\varkappa(m\Delta x,\ n\Delta y)\,\delta(x-m\Delta x,\ y-n\Delta y).$$

Let us determine the spatial spectrum of the above distribution. The use of the theorem on the Fourier transform of the Dirac distribution [1] gives

$$K_p(\nu_x,\ \nu_y) = \sum_{m=-M/2}^{M/2}\sum_{n=-N/2}^{N/2}\varkappa(m\Delta x,\ n\Delta y)\exp\left[-j2\pi(m\Delta x\nu_x+n\Delta y\nu_y)\right]. \tag{58}$$

Since

$$\exp(-j2\pi\nu_x m\Delta x) = \exp\left[-j2\pi(\nu_x+F_x)m\Delta x\right] \tag{59}$$

and

$$\exp(-j2\pi\nu_y n\Delta y) = \exp\left[-j2\pi(\nu_y+F_y)n\Delta y\right], \tag{60}$$

where $F_x = 1/\Delta x$ and $F_y = 1/\Delta y$, therefore, for any ν_x and ν_y, the spatial spectrum $K_p(\nu_x, \nu_y)$ of the distribution $\varkappa_p(x, y)$ satisfies the condition

$$K_p(\nu_x,\ \nu_y) = K_p(\nu_x+F_x,\ \nu_y+F_y). \tag{61}$$

Hence, it follows that the spatial spectrum $K_p(\nu_x, \nu_y)$ of the distribution $\varkappa_p(x, y)$, which defines the vibration velocity amplitude distribution in the plane of the baffle S_0 containing the system of point sound sources under study, is a periodic function with the periods F_x and F_y, respectively in the direction of the axes $0\nu_x$ and $0\nu_y$. From the theorem on the Fourier transform of the distribution $1/\Delta x\Delta y\ \mathrm{III}(x/\Delta x,\ y/\Delta y)$ [1], the spatial spectrum $K_p(\nu_x, \nu_y)$ of distribution (57) can also be represented in the form

$$K_p(\nu_x,\ \nu_y) = F_xF_y\sum_{k=-\infty}^{+\infty}\sum_{l=-\infty}^{+\infty}K(\nu_x-kF_x,\ \nu_y-lF_y). \tag{62}$$

Hence, it follows that the spectrum $K_p(\nu_x, \nu_y)$ of the distribution $\varkappa_p(x, y)$, defining the vibration velocity amplitude distribution in the plane of the baffle S_0 containing the system of point sound sources under study, is the sum of the spectra $K(\nu_x, \nu_y)$ of the distribution function $\varkappa(x, y)$ of the vibration velocity amplitude in the plane of the baffle S_0, containing the rectangular sound source σ_0 (Fig. 4), multiplied by F_xF_y and displaced by F_x and F_y with respect to each

other, respectively in the direction of the axes $0v_x$ and $0v_y$. In view of this and from (20), the relative acoustic pressure amplitude distribution on the surface of the hemisphere S, surrounding the system of point sources under study in its far field, is defined by the expression

$$R_p(v_x, v_y) = K_p(v_x, v_y) H_v(v_x, v_y). \tag{63}$$

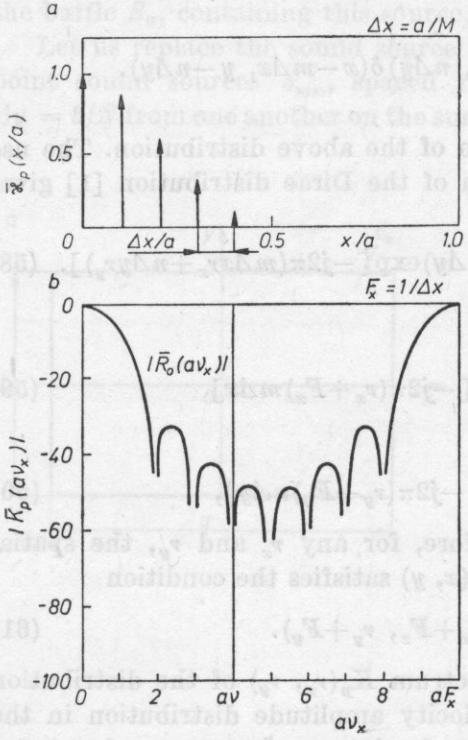

Fig. 4. Vibration velocity amplitude distribution (a) and its Fourier transform (b) for a discrete Hanning distribution

It follows from dependencies (22) and (58) that

$$R_p(0, 0) = \sum_{m=-M/2}^{M/2} \sum_{n=-N/2}^{N/2} \varkappa(m\Delta x, n\Delta y) = V_p, \tag{64}$$

where V_p is the efficiency of the system of point sound sources under study. In view of this and from (23), the directional characteristic of this system of sound sources is given by the expression

$$\bar{R}_p(v_x, v_y) = R_p(v_x, v_y)/V_p. \tag{65}$$

It follows from dependencies (62), (63) and (65) that when $F_x, F_y \geqslant 2\nu$, i.e. when $\Delta x, \Delta y \ll \lambda/2$, where $\lambda = 1/\nu$, then

$$\bar{R}_p(v_x, v_y) \simeq \bar{R}(v_x, v_y). \tag{66}$$

Hence, it follows that when the intervals among the individual sources of a system of point sound sources are sufficiently small compared with half the length of the sound wave radiated, the directional characteristic of this system has a shape close to that of the directional characteristic of the rectangular sound source σ_0 (Fig. 4).

Let us now replace the rectangular sound source σ_0 by a practically realizable system of planar sound sources σ_{mn}, spaced at the respective intervals $\Delta x = a/M$ and $\Delta y = b/N$, on the surface of the rectangle occupied by the sound source σ_0 (Fig. 3). Let us assume that the vibration velocity amplitude distribution in the plane of the baffle S_0, containing the central source σ_{00} of the system, set apart from the other sources, is defined by the function $\varkappa_{00}\varkappa_z(x, y)$. Let us assume that the coefficients $\varkappa_{mn}$ for the individual sources σ_{mn} in the system are equal to the values $\varkappa(m\Delta x, n\Delta y)$ of the distribution function $\varkappa(x, y)$. Accordingly, the vibration velocity amplitude distribution in the plane of the baffle S_0, containing the system of planar sound sources now under study, can be defined in the following way:

$$\varkappa_u(x, y) = \varkappa_z(x, y) * \varkappa_p(x, y), \tag{67}$$

with

$$\varkappa_p(x, y) = \sum_{m=-M/2}^{M/2} \sum_{n=-N/2}^{N/2} \varkappa(m\Delta x, n\Delta y)\,\delta(x - m\Delta x, y - n\Delta y). \tag{68}$$

Let us now determine the spatial spectrum of distribution (67). The use of the theorem on the Fourier transform of the convolution of the function and the distribution [1] gives

$$K_u(\nu_x, \nu_y) = K_z(\nu_x, \nu_y)K_p(\nu_x, \nu_y), \tag{69}$$

where

$$K_p(\nu_x, \nu_y) = \sum_{m=-M/2}^{M/2} \sum_{n=-N/2}^{N/2} \varkappa(m\Delta x, n\Delta y)\exp[-j2\pi(m\Delta x\nu_x + n\Delta y\nu_y)]. \tag{70}$$

In view of this and from (20), the relative acoustic pressure distribution on the surface of the hemisphere S, surrounding the system of planar sound sources under study in its far field, is defined by the expression

$$R_u(\nu_x, \nu_y) = [K_z(\nu_x, \nu_y)K_p(\nu_x, \nu_y)]H_v(\nu_x, \nu_y) = R_z(\nu_x, \nu_y)R_p(\nu_x, \nu_y). \tag{71}$$

In view of this and from (22),

$$R_u(0, 0) = R_z(0, 0)R_p(0, 0) = V_zV_p = V_u, \tag{72}$$

where V_u is the bulk efficiency of the system of sources under study. From

dependencies (64) and (72), it can be written that

$$V_u = \sum_{m=-M/2}^{M/2} \sum_{n=-N/2}^{N/2} V_{mn}, \tag{73}$$

where

$$V_{mn} = V_z \varkappa(m\Delta x,\ n\Delta y) \tag{74}$$

is the bulk efficiency of the source σ_{mn} of the system. Hence, it follows that the series of the values $\varkappa(m\Delta x,\ n\Delta y)$ of the distribution function $\varkappa(x,\ y)$ is defined by a discrete distribution of the relative bulk efficiencies of the sources σ_{mn} in the system, referred to the efficiency V_z of its central source σ_{00}. From (23), (75) and (72), the directional characteristic of the rectangular system of planar sound sources is defined by the expression

$$\bar{R}_u(\nu_x,\ \nu_y) = R_u(\nu_x,\ \nu_y)/V_u = \bar{R}_z(\nu_x,\ \nu_y)\bar{R}_p(\nu_x,\ \nu_y). \tag{75}$$

It follows from the above dependence that the directional characteristic of the system of planar sound sources is the product of the directional characteristic of the central source σ_{00} of this system and the directional characteristic of a system of point sources derived by replacing each of the sources σ_{mn} by a point source. In a case when the dimensions of each of the sources σ_{mn} in the system are small compared with the length $\lambda = 1/\nu$ of the wave radiated, it can be assumed that

$$\bar{R}_z(\nu_x,\ \nu_y) \simeq 1. \tag{76}$$

In this case, expression (75) can be represented as

$$\bar{R}_u(\nu_x,\ \nu_y) \simeq R_p(\nu_x,\ \nu_y). \tag{77}$$

In view of this, in a case when the dimensions of each of the sources σ_{mn} in the system of planar sound sources under study are sufficiently small compared with the length of the wave radiated, the directional characteristic of this system has a shape close to that of the directional characteristic of a rectangular system of point sources derived by replacing each source δ_{mn} in the system of planar sound sources by a point source.

In summary, it follows from the considerations made that the directionality of vibration energy radiation in the far field, close to that showed by a rectangular sound source σ_0 with the vibration velocity amplitude distribution on its surface defined by the function $\varkappa(x, y)$, will occur for a mosaic system of sound sources, composed of planar sound sources with sufficiently small dimensions compared with the length of the wave radiated, spaced on the surface of the rectangle occupied by the source δ_0, at intervals which are also sufficiently short compared with half the wavelength. In addition, the relative bulk efficiencies of the sources in this system must be equal to the values of the distribution

function $\varkappa(x, y)$ at the intervals at which its individual sources are spaced. Fig. 5 shows the directional characteristic of a rectangular mosaic system of sound sources, determined for a discrete Hanning distribution of the relative bulk efficiencies of the sources in this system. It was assumed that $a = b = 4\lambda$,

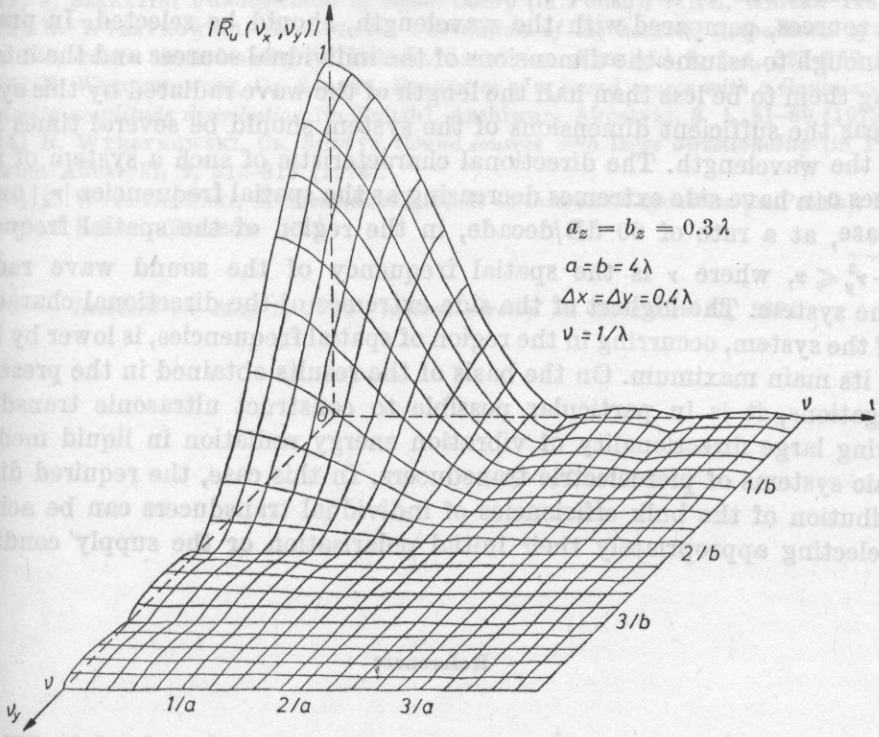

Fig. 5. Directional characteristic of a rectangular mosaic system of planar sound sources with a discrete Hanning distribution of their relative bulk efficiencies

$\Delta x = \Delta y = 0.4\lambda$, $a_z = b_z = 0.3\lambda$ (Fig. 3). This characteristic does not differ practically from that of a rectangular sound source with the same dimensions and Hanning distribution of the vibration velocity amplitude on its surface (Fig. 2).

8. Conclusions

It follows from these considerations that a rectangular sound source with large directionality of vibration energy radiation into the far field can be realized in practice in the form of a rectangular mosaic system of planar sound sources, vibrating in phase, with a discrete Hanning distribution of their bulk ef-

ficiencies. To achieve this, for a given frequency of vibration of the surfaces of the sound sources, it is necessary to select sufficiently large dimensions of the system of sources, compared with the length of the sound wave in the medium in which this system will radiate vibration energy. In addition, as small as possible dimensions of the individual sources in the system and intervals among those sources, compared with the wavelength, should be selected. In practice, it is enough to assume the dimensions of the individual sources and the intervals among them to be less than half the length of the wave radiated by this system, whereas the sufficient dimensions of the system should be several times larger than the wavelength. The directional characteristic of such a system of sound sources can have side extremes decreasing as the spatial frequencies $|\nu_x|$ and $|\nu_y|$ increase, at a rate of 60 dB/decade, in the region of the spatial frequencies $\sqrt{\nu_x^2+\nu_y^2} \leqslant \nu$, where ν is the spatial frequency of the sound wave radiated by the system. The highest of the side extremes of the directional characteristic of the system, occurring in the region of spatial frequencies, is lower by 32 dB than its main maximum. On the basis of the results obtained in the present investigations, it is in particular possible to construct ultrasonic transducers, showing large directionality of vibration energy radiation in liquid media, as mosaic systems of piezoelectric transducers. In this case, the required discrete distribution of the bulk efficiencies of individual transducers can be achieved by selecting appropriately their initial polarisation or the supply conditions.

References

[1] W. T. Cathey, *Optical information processing and holography*, John Wiley and Sons, New York, 1974.

[2] L. Filipczyński, J. Etienne, *Theory and experimental investigations of spherical focussing transducers with Gaussian surface velocity distribution* (in Polish), Archiwum Akustyki, **8**, 4, 341–360 (1973).

[3] K. V. Haselberg, J. Krautkramer, *Ein Ultraschall-Strahler für die Werkstoffprüfung mit verbessertem Nahfeld*, Acustica, **9**, 5, 359–364 (1959).

[4] L. E. Kinsler, A. R. Frey, A. B. Coppens, J. V. Sanders, *Fundamentals of acoustics*, John Wiley and Sons, New York 1982.

[5] T. Kujawska, *Dynamic focusing of an ultrasonic beam by means of a phased array of annular transducers using the impulse technique* (in Polish), Archiwum Akustyki, **18**, 1, 71–83 (1983).

[6] A. V. Oppenheim, R. W. Schaffer, *Digital signal processing*, Prentice-Hall, New Jersey 1975.

[7] W. Rdzanek, *Mutual and total acoustic impendances of a system of sources with variable surface vibration velocity distribution* (in Polish), Higher Pedagogical School, Zielona Góra 1977.

[8] W. Rdzanek, *Mutual acoustic impedance of circular membranes and plates with Bessel axially-symmetrical vibration velocity distributions* (in Polish), Archiwum Akustyki, **15**, 3, 245–258 (1980).

[9] W. RDZANEK, *Acoustic field theory* (in Polish), Higher Pedagogical School, Zielona Góra 1982.

[10] A. SNAKOWSKA, R. WYRZYKOWSKI, K. ZIMA, *The near field on the main axis of a membrane with Gaussian vibration velocity amplitude distribution* (in Polish), Archiwum Akustyki, **10**, 3, 285–295 (1975).

[11] J. SZABATIN, *Fundamentals of signal theory* (in Polish), WKŁ, Warsaw 1982.

[12] R. WYRZYKOWSKI, Cz. SOŁTYS, *Calculation of the acoustic impedance of sound sources with known directionality* (in Polish), Archiwum Akustyki **7**, 3–4, 327–336 (1972).

[13] R. WYRZYKOWSKI, Cz. SOŁTYS, *Properties of a sound source with a Gaussian vibration velocity amplitude distribution* (in Polish), Archiwum Akustyki, **8**, 1, 81–89 (1973).

[14] R. WYRZYKOWSKI, Cz. SOŁTYS, *Sound sources with large directionality* (in Polish), Archiwum Akustyki, **9**, 313–319 (1974).

[15] R. WYRZYKOWSKI, *Mathematical methods in theoretical acoustics* (in Polish), Higher Pedagogical School, Rzeszów 1975.

Received on May 9, 1984; revised version on December 11, 1984.

ARCHIVES OF ACOUSTICS
10, 1, 37-57 (1985)

EVALUATION OF THE PHASE ERROR IN SOUND INTENSITY MEASUREMENT

TERESA KWIEK-WALASIAK

Department of Ergonomy, Adam Mickiewicz University
(61-812 Poznań, ul. Kantaka 2)

This paper presents an analysis of phase dependencies occurring in investigations of sound intensity, in particular those of the effect of the phase error of measurement equipment on the value and direction of the intensity vector measured at some point. Two methods of intensity measurement, based on measurement of the particle velocity from the pressure gradient, were taken into consideration: the direct method (formulae (5), (10), (12), (13)) and the one based on the cross-spectrum of acoustic pressure signals (formulae (6), (23)).

The phase error $\Delta\varphi$ causes changes in the directional characteristic of the system (formula (28), Fig. 7), changes in the values of intensity, measured with changed order of the measurement channels (formula (30), Fig. 6), the ratio of the values of the real part of the cross-spectrum of the pressure processes from the two microphones to that of its imaginary part (Figs. 9–10), and also in the existence of the imaginary part of their cross-spectrum when the two microphones are affected by the same acoustic field (formula (42), Fig. 8).

This paper presents theoretical considerations and specific examples of phase error evaluation in equipment used in investigations (Fig. 1) on the basis of the changes in question, which cause it.

The phase error of equipment causes considerable distortion of results, involving changes in the measured values, direction and also the sign of the intensity vector in some cases (see Fig. 11), therefore it is important to interpret it correctly.

Notation

$E(f)$ – expected value of the function of f
$e_{\Delta x}$ – unity vector in the direction Δx
F_x – Fourier transform of the function of x
F_x^* – conjugate value of F_x
$G_{ik}(j\omega)$ – measured auto ($i = k$) or cross spectral density function

$g_{ik}(j\omega)$ — real spectral density function undistorted by measurement error
$H_i(j\omega)$ — transmittance of the channel i
$|H_i|$ — amplification factor of the channel i
$I(r)$ — intensity vector at the point r
$I(t)$ — intensity as a function of time
$I(\omega)$ — intensity spectrum
$I(\Delta\omega)$ — intensity component measured in the band $\Delta\omega$
k — wave number
T — analysis time
α — angle between the straight line connecting the fronts of the microphones and the wave incidence direction
Δx — spacing of the microphones in the probe
ε — effective error of the measured quantity
τ_i — pulse response of the channel i
Φ — phase shift between the pressure signals from the two microphones
$\Delta\varphi$ — phase error of equipment
$\Phi_{\Delta x}$ — phase shift of pressure behaviour caused by spacing the microphones at the distance Δx
$\psi(r)$ — phase difference between the pressure and velocity signals at the point r

1. Introduction

The value of the sound intensity vector at some point r of the field can be given by the formula

$$I(r) = E[p(r, t)v_n(r, t)], \tag{1}$$

where p is the acoustic pressure of the wave and v_n is the particle velocity of the medium in the direction n.

Assuming in general that the phase shift in sinusoidal waves with frequency ω, between the wave pressure and the particle velocity, as expressed by the formulae

$$\begin{aligned} p &= |p|\cos(\omega t - \psi), \\ v &= |v|\cos\omega t, \end{aligned} \tag{2}$$

is ψ, the sound intensity can be given by the dependence

$$I(r) = \frac{|p|\,|v|}{2T}\left[\frac{1}{2}\int_0^T \cos\psi dt + \frac{1}{2}\int_0^T \cos(2\omega t - \psi)\,dt\right]. \tag{3}$$

The first term of the formula denotes energy propagation and is independent of time. The mean value of the second integral tends to zero when $T \to \infty$.

The value of the phase shift ψ depends on the structure of the field at a given point and determines the impedance of the medium at this point. It is difficult, even for simple sources, to estimate theoretically the value of the angle at any point of the field. In the far field, where all waves can approximately be considered plane, the angle $\psi = \pi/2$.

The practical evaluation of the acoustic intensity is based on the measurement of the particle velocity as the pressure gradient by the two-microphone method:

$$\boldsymbol{I}(r) = \frac{1}{\varrho} E\left[p(r, t) \int_0^t \mathbf{grad}\ p(r, t)\, dt\right]. \tag{4}$$

The direct method requires the measurement of the sum and difference between the pressure signals p_1 and p_2 from the two microphones and that the operations should be carried out according to the dependence [6], [7]

$$\boldsymbol{I}(r, t) = \boldsymbol{e}_{\Delta x} \lim_{T\to\infty}\left\{1/2\varrho\Delta x T \int_0^T \left[(p_1+p_2)\int_0^T (p_2-p_1)\,dt\right]dt\right\}, \tag{5}$$

where T is the measurement time, ϱ is the density of the medium, Δx-the spacing of the microphones, the direction of the vector $\boldsymbol{I}$ is defined by Δx.

In turn, the method of intensity calculation by means of the function of the cross-spectrum is based on the formula [2], [3] [5]

$$\boldsymbol{I}(\omega) = (\boldsymbol{e}_{\Delta x})\,(1/\varrho\Delta x\omega)\,\mathrm{Im}G_{12}(j\omega). \tag{6}$$

The error involved in the velocity evaluation based on the pressure gradient measurement according to the following dependence, which is basic for the two methods,

$$v(r, t) = -(1/\varrho\Delta x)\int_0^t [p_2(t)-p_1(t)]\,dt, \tag{7}$$

is affected by the phase error of equipment $\Delta\varphi(\omega)$, which is the phase difference between two channels, summing up with the physical phase difference between the pressure signals, resulting from the value of the spacing of the microphones, Δx, in the microphone probe, $\Phi_{\Delta x}$,

$$\Phi(\omega) = \Phi_{\Delta x}(\omega) \pm \Delta\varphi(\omega). \tag{8}$$

The behaviour of the acoustic pressure processes registered by the two microphones is thus described by the dependencies

$$p_1 = A\cos\omega t,$$
$$p_2 = B\cos[\omega t + \Phi_{\Delta x}(\omega) \pm \Delta\varphi(\omega)]. \tag{9}$$

2. Effect of the phase error of equipment on the results of the intensity measurement

In spite of all technical operations, there is usually a slight phase difference between channels. Below is presented the effect of the phase error on the results obtained by the direct method of intensity measurement and that of cross-

spectrum. Fig. 1 shows a schematic diagram of the equipment used in the investigations to confirm the considerations.

2. 1. *Effect of the phase error in the direct method*

When between measurement channels there is the phase difference $\Delta\varphi$ and also that in amplification, then, instead of the acoustic pressures $p_1(t)$ and $p_2(t+\Delta x/c)$, the measurement system registers the pressures (Fig. 2) $P_1 =$

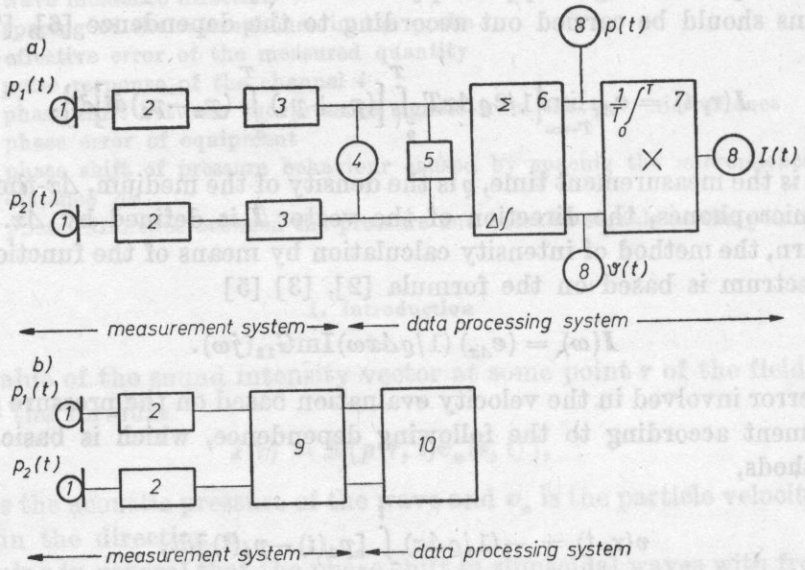

Fig. 1. A general diagram of the equipment used in the intensity investigations. The measurements system is the same for the direct and cross-spectral methods, with different measurement data processing system for each (a) for the direct method, (b) for the cross-spectral method. 1 — MV201 1/2′ microphones, 2 — 00017 RFT amplifiers, 3 — system of 00017 RFT 1/3 octave filters, 4 — SS 4100 Iwatsu two-stream oscilloscope, 5 — BK 2971 phasemeter, 6 — author's own signal summation and differentiation-integration system, 7 — DISA 55 D 75, 52B25 multiplication and integration system, 8 — V 541 digital voltmeter, 9 — magnetic recorder (with different types used (see the text)), 10 — energy spectrum analyser, Universal Digital Analyser Plurimat S, or 3720 and 3721 Hewlett-Packard correlator and integration system

$p_1(t)/\tau_1$ and $P_2 = p_1(t+\Delta x/c)/\tau_2$. Thus, the system measures some intensity value $I(r, t)$, which is different from the real intensity $I(r)$ (formula (5)):

$$\hat{\boldsymbol{I}}(r, t) = \boldsymbol{e}_{\Delta x}(1/2T\Delta x\varrho)\int_0^T \left\{\left[p_1(t)/\tau_1 + p_2\left(t+\frac{\Delta x}{c}\right)/\tau_2\right]\int_0^t \left[p_2\left(t+\frac{\Delta x}{c}\right)/\tau_2 - p_1(t)/\tau_1\right]dt\right\}dt, \tag{10}$$

where τ_i is the pulse response of the channel i.

When using this method the two channels should show as high phase and amplitude agreement as possible, since it is impossible to compensate for the differences in a simple way at the stage of intensity calculations. It is easy to eliminate differences in amplification, but some inevitable left-over phase difference causes error to arise in evaluation, which can be represented for the current sinusoidal wave in the following way.

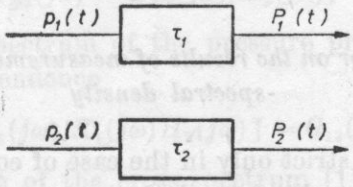

Fig. 2. A schematic diagram of the time transformation of the channels of the measurement system. τ_i denotes the pulse response of the channel i

The pressures registered by the two microphones can be given by the harmonic series

$$p_1(t) = \sum_i A_i \cos[\omega_i t + (k_i \Delta x \pm \Delta\varphi(\omega_i)/2],$$
$$p_2(t) = \sum_i B_i \cos[\omega_i t - (k_i \Delta x \pm \Delta\varphi(\omega_i)/2]. \tag{11}$$

The phase error causes a shift in the pressure phase, and thus at the same time, it affects the value of intensity measured by method represented by formula (5). This is expressed by the following formula, obtained as a result of the substitution of (11) in (5),

$$I(r, t) = (1/2\varrho\Delta x) \sum_i [(A_i B_i/\omega_i) \sin(k_i \Delta x \pm \Delta\varphi(\omega_i)]. \tag{12}$$

A more accurate result of the intensity measurement can be obtained by determining the arithmetic mean from two measurements carried out with changed order of microphones with respect to the wave incidence direction. In one of the measurements, the phase difference between the channels sums up with the phase difference caused by the spacing of the microphones, and it detracts in the other, and thus the mean value calculated for any bands $\Delta\omega$ from two measurements can be expressed by the following dependence:

$$\begin{aligned} I_{av}(r, \Delta\omega) &= (|I(r, \Delta\omega)^{(a)}| + |I(r, \Delta\omega)^{(b)}|)/2 \\ &= I(r, \Delta\omega)\,[\sin(k\Delta x - \Delta\varphi) + \sin(k\Delta x + \Delta\varphi)]/2k\Delta x \\ &= I(r, \Delta\omega) \cos\Delta\varphi \sin k\Delta x/k\Delta x. \end{aligned} \tag{13}$$

The values of k and $\Delta\varphi$ are calculated for the centre frequency of the band $\Delta\omega$.

In the case when the amplification factors of channels, $H_1(\omega)$ and $H_2(\omega)$, are different from unity, they also have to be considered in the intensity measurement:

$$I(r, t) = e_{\Delta x}(1/2H_1H_2\varrho\Delta x)\sum_i (A_iB_i\sin k_i\Delta x/k_i\Delta x). \tag{14}$$

2.2 Effect of the phase error on the results of measurements by the method of cross-spectral density

Formula (6) would be strict only in the case of equipment with ideal transmission, undistorted by amplitude and phase error. In practice, instead of the signals p_1 and p_2, at the output of the measurement equipment there are the signals P_1 and P_2, resulting from the passage through channels with definite pulse responses τ_1 and τ_2, or, in the frequency domain, with the respective

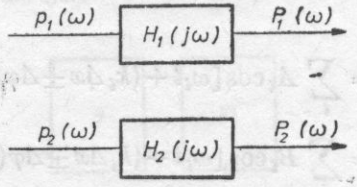

Fig. 3. A schematic diagram of the transfer function of the channels of the measurement system. $H(j\omega)$ denotes the transmittance of the measurement system

transmittances $H_1(j\omega)$ and $H_2(j\omega)$ (Fig. 3). The transmittances $H_1(j\omega)$ and $H_2(j\omega)$ are the complex functions of frequency

$$\begin{aligned} H_1(j\omega) &= |H_1|\exp[-j\varphi_1(\omega)], \\ H_2(j\omega) &= |H_2|\exp[-j\varphi_2(\omega)], \end{aligned} \tag{15}$$

and thus the real cross-spectrum of the signals, $g_{12}(j\omega)$, of the pressures present at points 1 and 2 will in a general case be different from the cross-spectrum of the signals registered by the equipment, $G_{12}(j\omega)$. The real cross-spectrum of the signals p_1 and p_2 is given by the formula

$$g_{12}(j\omega) = E\{F_{p1}(j\omega)F^*_{p2}(j\omega)\}, \tag{16}$$

where E is the mean value.

Since the measured signals P_1 and P_2 are related to the real pressure values

by the dependencies between their transforms:

$$F_{p1}(j\omega)H_1(j\omega) = F_{P1}(j\omega),$$
$$F_{p2}(j\omega)H_2(j\omega) = F_{P2}(j\omega), \tag{17}$$

and hence,

$$F_{p1}(j\omega) = F_{P1}(j\omega)/H_1(j\omega),$$
$$F_{p2}(j\omega) = F_{P2}(j\omega)/H_2(j\omega), \tag{18}$$

herefore, the real cross-spectrum of the pressure processes is related to the measured one by the dependence

$$g_{12}(j\omega) = E[F_{P1}(j\omega)F_{P2}(j\omega)/H_1(j\omega)H_2(j\omega)] = G_{12}(j\omega)/H_1(j\omega)H_2(j\omega), \tag{19}$$

where, from the definition of the cross-spectrum [1],

$$G_{12}(j\omega) = E[F_{P1}(j\omega)F^*_{P2}(j\omega)]. \tag{20}$$

The intensity value calculated from measurements is given by the formula

$$I(j\omega) = e_{\Delta x}\mathrm{Im}\{G_{12}(j\omega)\exp(-j(\varphi_2-\varphi_1))\}/2\pi f\Delta x\varrho|H_1|\,|H_2|$$
$$= e_{\Delta x}\mathrm{Im}\{G_{12}(j\omega)[\cos\Delta\varphi(\omega)\pm j\sin\Delta\varphi(\omega)]\}/2\pi f\varrho\Delta x|H_1|\,|H_2|, \tag{21}$$

where $\Delta\varphi(\omega) = \varphi_2-\varphi_1$ is the phase difference between channels for the frequency ω.

Calculation of the value of the imaginary part of formula (21) gives the dependence

$$\mathrm{Im}\{G_{12}(j\omega)[\cos\Delta\varphi(\omega)\pm j\sin\Delta\varphi(\omega)]\} = \mathrm{Im}G_{12}(\omega)\cos\Delta\varphi(\omega)$$
$$+ R_eG_{12}(\omega)\sin\Delta\varphi(\omega). \tag{22}$$

Substitution of formula (22) into (6) gives the following formula for the intensity value, accounting for the phase error of the equipment,

$$I(j\omega) = [\mathrm{Im}G_{12}(\omega)\cos\Delta\varphi(\omega)\pm\mathrm{Re}G_{12}(\omega)\sin\Delta\varphi(\omega)]/\omega\varrho\Delta x|H_1|\,|H_2|. \tag{23}$$

On the assumption of low phase error, formula (23) becomes the same as (6).

Two measurements, involving changed order of microphones, permits total elimination of the phase error [4], [9] in calculating intensity as the geometric mean of the two imaginary parts of the cross-spectrum.

3. Phase calibration of the measurement system

Irrespective of the further means of signal processing, an intensity measurement system consists of a probe (Fig. 4) — a system of two microphones spaced at Δx, preamplifiers, amplifiers and possibly a magnetic recorder. Despite

careful selection of the elements, it is inevitable for some phase differences to occur between channels; particularly significant sources of phase shift are multi-head tape recorders with different recording and reproducing heads.

In most of the investigations, the author used a two-channel tape recorder which was modified in the laboratory to serve measurement purposes. This

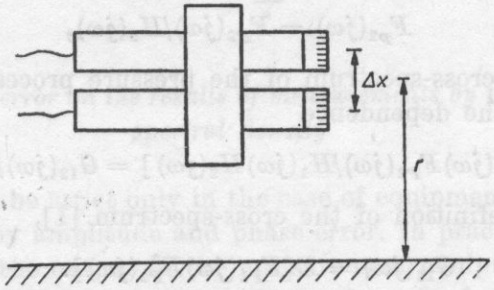

Fig. 4. The microphone probe used in the investigations. 1/2′ microphones spaced at Δx at the distance r from the source

tape recorder with one recording and reproducing head does not cause any phase shift within the resolution capacity of the equipment, 0.5°, in contrast to high-class multi-channel tape recorders with separate recording and reproducing heads, e.g. in the 8–channel Schlumberger tape recorder (where the heads are two four-channel units) only one pair of channels was found to involve low phase shift. Very small inaccuracies in the setting of heads (different for recording and reproducing ones) cause high phase differences. An error of a few thousandths of a millimetre can cause phase error of 90° and 180°, depending on the tape velocity (the error decreases as the velocity increases) and on the frequency (the phase error is lower at higher frequencies), e.g. for 5 kHz at the tape velocity of 190 mm/s the 0.01 mm displacement of the heads causes the phase error $\Delta\varphi = 45°$. In a high-class tape recorder like Schlumberger, under these conditions, error close to 90° was observed, and for a tape velocity of 95 mm/s it was almost 180°. In a Nagra IV *SJ* tape recorder, which was used in some measurements, the phase difference-small at low frequencies: 100 Hz $-1°$, 200 Hz $-2°$ — increases to 40° at 4000 Hz.

The system can be calibrated electrically or acoustically in the plane wave field, e.g. in a tube of standing waves or in the far field.

Measurements of the phase shift between channels for electrical signals supplied from the generator to the inputs of the amplifiers permit; when the first element of system, i.e. the microphone, is neglected; the selection of appropriate elements of the system (e.g. tape recorder tracks) and, in some cases, compensation for the phase differences found.

The microphones themselves are only a slight source of phase error, whereas when they are part of the probe system, they cause some mutual field perturbations [6], [11].

The phase differences between channels can be measured by a phasemeter (or by a two-stream oscilloscope), when the probe is in the plane wave field with varying frequency. The result depends to some extent on the order and the slope (rising or falling) of the release signal, which indicates the purposiveness of averaging of result series. Microphones, together with channels, are changed in position in the course of measurements (positions a and b), which changes their position with respect to the wave front. When the phase measurement process is released by a signal from channel 1 and the measured value of the phase difference between the channels is $\Phi_{2/1}$, the equipment error can be determined rom the dependence

$$\begin{aligned} \Delta\varphi(\omega) &= \Phi_{2/1}^{(a)}(\omega) - \Phi_{\Delta x}(\omega), \\ \Delta\varphi(\omega) &= \Phi_{2/1}^{(b)}(\omega) + \Phi_{\Delta x}(\omega). \end{aligned} \tag{24}$$

When the processes are released by a signal from channel 2, the measured phase difference is $\Phi_{1/2}$ and the equipment error $\Delta\varphi$ results from the equations

$$\begin{aligned} \Delta\varphi(\omega) &= -\Phi_{1/2}^{(a)}(\omega) - \Phi_{\Delta x}(\omega), \\ \Delta\varphi(\omega) &= -\Phi_{12}^{(b)}(\omega) + \Phi_{\Delta x}(\omega). \end{aligned} \tag{25}$$

It is purposeful to carry out a large number of various phase error measuref ments, since phase fluctuations can be observed in the measurement system (a problem signalled in the literature).

4. Evaluation of the phase difference between channels on the basis of the directional responses of the microphone system

The directional responses of the microphone system were made in the far field of a loudspeaker fed from a generator. The microphone system was fixed in the axis of a Drehtisch 02012 *RFT* turntable with remote control programmed for measurements every 15°. The fronts of the microphones described a circle with a radius of 2 cm, which in the far field ensured in this region signals with close values for the two microphones. A few measurements of the responses were carried out, giving good repeatability of the basic structure of the response (the measurements were densified at the characteristic points).

The microphone system shows large directionality at medium and high frequencies (an example for the probe investigated is shown in Fig. 5), permitting the maximum values, and even more distinctly the minimum values, as a function of the angle of the rotation of the probe with respect to the wave

incidence direction, to be found. The maximum values are dozen-odd times as large as the minimum ones, and the difference in their levels is dozen-odd dB.

It is interesting to observe changes in the phase angle between the behaviours p and v for the rotation of the axes of the microphone with respect to the source (Fig. 6) in a free field. When the axes of the microphones are set

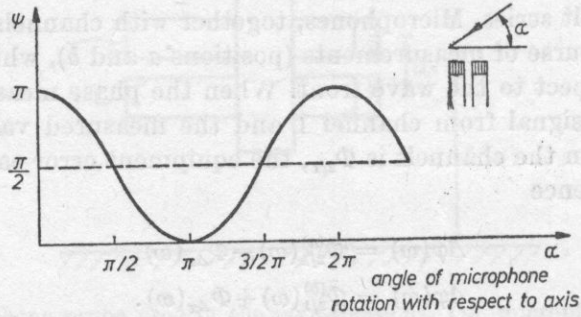

Fig. 5. A change in the angle ψ between the pressure behaviour and the particle velocity as a result of the rotation of the microphones with respect to the axis, relative to the incident wave, observed on the display of a twostream oscilloscope, for the system shown in Fig. 1a

parallel to the direction of the wave ($\alpha = 90°$) it is possible to observe the phase shift $\psi = 90.$ and, as a consequence, zero value of intensity. In turn the angle $\psi = 0°$ and the related intensity maximum can be observed close to the angle $\alpha = 180°$, whereas the value $\psi = 180°$ and the maximum intensity value with the opposite sign occur close to the angle $\alpha = 360°$. A change in the wave incidence angle α with respect to the axes of the microphones is reflected in a change in the value and sign of the intensity vector, according to the cosine function

$$I = e_{\Delta x}|I|\cos\alpha. \tag{26}$$

The behaviour of directional responses obtained for the microphone system used in papers [7–9] (see Fig. 1a) requires interpretation based on theoretical considerations. An ideal directional response would be symmetrical, minimum intensity values would occur for the incidence angles of 90° and 270°. The real responses are not symmetrical and the minima are shifted. This effect, when neglecting some measurement error, results from the existence of the phase error $\Delta\varphi$ in equipment and permits this error to be calculated.

It is seen from formula (12) that the intensity takes a zero value when the argument of the sine function is zero, i.e.

$$k\Delta x\cos\alpha = \Delta\varphi(\omega), \tag{27}$$

or

$$k\Delta x\cos\alpha = \Delta\varphi(\omega)+\pi$$

thus for the following values of the incidence angles α

$$\alpha = \begin{cases} \cos^{-1}(\Delta\varphi(\omega)/k\Delta x), \\ \cos^{-1}[(\pi + \Delta\varphi(\omega)/k\Delta x]. \end{cases} \tag{28}$$

When the angle $\alpha_{\min}$ corresponding to $I_{\min}$ is found from the directional response, it is possible to calculate the phase error for a given frequency from the formula

$$\Delta\varphi(\omega) = k\Delta x \cos\alpha_{\min}. \tag{29}$$

The following values were calculated for the 0.5 kHz directional response shown in Fig. 4:

$$\alpha_{\min} = 115°, \text{ i.e. } \Delta\varphi = 2°; \quad \alpha_{\min} = 285°, \text{ i.e. } \Delta\varphi = 2°.$$

The phase error of equipment is also reflected in the nonsymmetry of the sensitivity of the system, i.e. the different maximum intensity values for $\alpha \cong 0°$ and $\alpha \cong 180°$. A decrease in the sensitivity in one direction is accompanied by its increase in another. The ratio of the maximum amplitudes registered in those cases can be represented by the formula

$$\sin(k\Delta x + \varphi(\omega))/\sin(k\Delta x - \varphi(\omega)) = K, \tag{30}$$

which permits the phase error of equipment to be calculated. The value of the phase error of the example shown in Fig. 5, which was calculated by this method is only $\Delta\varphi = 0.5°$ for $K = 1.2$. When $k\Delta x$ takes the value of $\Delta\Phi$, the directional response changes radically, a double increase in the value measured in one direction is accompanied by a decrease in the intensity value to zero in another, which results from the following dependencies:

$$I_1 = |I|[\sin(k\Delta x + \Delta\varphi)]/k\Delta x = |I|(\sin 2k\Delta x)/k\Delta x,$$

$$I_2 = |I|[\sin(k\Delta x - \Delta\varphi)]/k\Delta x = 0. \tag{31}$$

The intensity change towards the intensity maximum is

$$\varepsilon = I_1/I_{\varphi=0} = 2\cos k\Delta x \simeq 2, \tag{32}$$

corresponding to an increase of $\Delta L = 3$ dB in the measured intensities for low $k\Delta x$. It can be seen in the example of the directional response of the probe discussed, shown in Fig. 6, for the frequency $f = 0.2$ Hz, how strongly the effect of the phase error on the form of the directional response depends on frequency. For one minimum with the angle $\alpha_{\min} = 150°$, the error calculated from formula (29) is only 1.5° which almost causes one of the branches of the response to vanish (a similar effect is cited in ([10]).

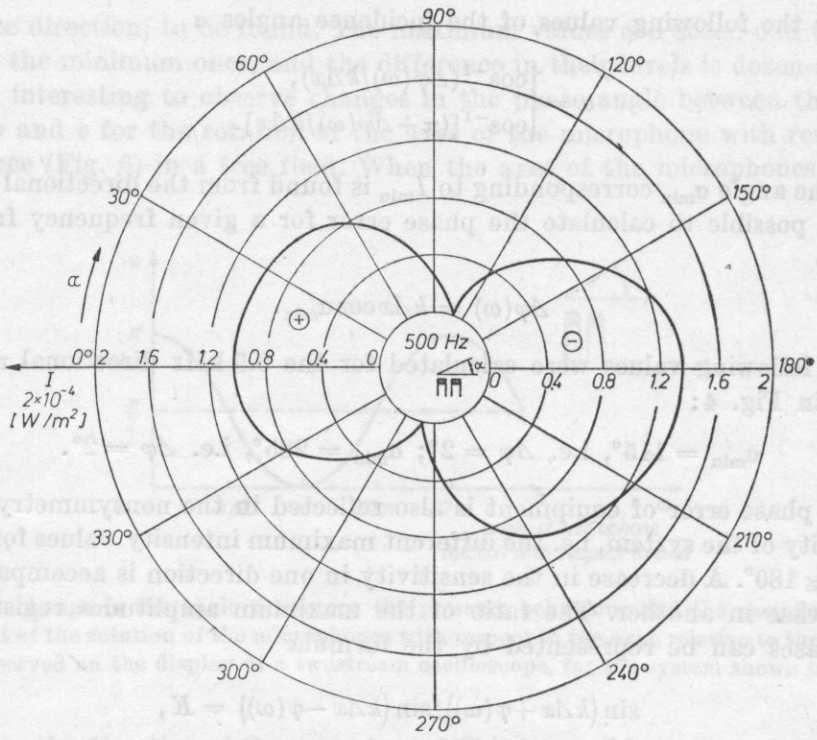

Fig. 6. An example of changes in the value and sign of intensity as a function of the angle α of rotation of the system of 1/2′ microphones for the frequency $f = 0.5$ kHz, with $\Delta x = 0.014$ m. The intensity values on the left branch of the response show a minus sign; those on the right, a plus sign

5. Evaluation of the phase error of a measurement system from the ratio of the real and imaginary parts of the cross-spectral density of the pressure behaviours fro m the two microphones of the probe

The test of the lack or presence of phase shifts between channels over the whole frequency range is the behaviour of the values of the function $\mathrm{Im}G_{12}(j\omega)$ when the input signals are equal for the two channels in terms of amplitude and phase, which results from the following calculations.

When the microphone system is in the sinusoidal wave field, the microphones register processes which can be expressed by formula (9). The auto spectral density functions of the processes are represented by the following definitions [1]:

$$g_{11}(\omega) = 2 \lim_{T\to\infty} E[F_{p1}(j\omega)F^*_{p1}(j\omega)], \tag{33}$$

$$g_{22}(\omega) = 2 \lim_{T\to\infty} E[F_{p2}(j\omega)F^*_{p2}(j\omega)],$$

while the cross-spectral density of the two behaviours is given as

$$g_{12}(j\omega) = 2 \lim_{T\to\infty} E[F_{p1}(j\omega)F^*_{p2}(j\omega)], \tag{34}$$

where F_{p1} and F_{p2} are Fourier transforms of the pressure behaviours p_1 and p_2. In turn, the values of the transforms F_{p1} and F_{p2} are, from the definitions, given by the formulae

$$F_{p1}(j\omega) = (A/2)\int_0^\infty \{[\exp(j\omega_0 t)+\exp(-j\omega_0 t)]\exp(-i\omega t)\}dt = jA\omega/(\omega_0^2-\omega^2), \tag{35}$$

$$F_{p2}(j\omega) = (B/2)\int_0^\infty \{[\exp(j\omega_0 t+\varphi)+\exp[-j(\omega_0 t+\varphi)]]\exp j\omega t\}dt$$

$$= [B/(\omega_0^2-\omega^2)](\omega_0\sin\varphi - j\omega\cos\varphi). \tag{36}$$

Substitution of the expressions of the pressure transforms (35) and (36) in formulae (33) and (34) gives the following dependencies:

$$g_{11}(\omega) = A^2/(\omega_0^2-\omega^2)^2,$$

$$g_{22}(\omega) = [B^2/(\omega_0^2-\omega^2)^2](\omega_0^2\sin^2\varphi+\omega^2\cos^2\varphi) \tag{37}$$

and

$$g_{12}(j\omega) = [AB\omega/(\omega_0^2-\omega^2)](\omega\cos\varphi - j\omega_0\sin\varphi). \tag{38}$$

The modulus of the cross energy density is thus expressed by the formula

$$|g_{12}(\omega)| = [AB\omega/(\omega_0^2-\omega^2)](\omega^2\cos^2\varphi+\omega_0^2\sin^2\varphi)^{1/2}; \tag{39}$$

its real part is

$$\mathrm{Re}\,g_{12}(\omega) = [AB\omega^2/(\omega_0^2-\omega^2)]\cos\varphi \tag{40}$$

and the imaginary part

$$\mathrm{Im}\,g_{12}(\omega) = [jAB\omega\omega_0/(\omega_0^2-\omega^2)]\sin\varphi. \tag{41}$$

There follows the following relationship of the phase difference between signals from the two microphones

$$\tan\varphi(\omega) = \tan[\varphi_{\Delta x}(\omega)\pm\Delta\varphi(\omega)] = \mathrm{Im}G_{12}(\omega)/\mathrm{Re}G_{12}(\omega). \tag{42}$$

With zero phase shift between the process p_1 and p_2, the imaginary part of the cross-spectrum is zero, whereas the real part reaches a maximum value. Fig. 8 shows successively the spectrum of the imaginary part, of the real part and the modulus of the cross-spectrum between the pressure behaviours registered by the measurement system (Fig. 1a) when the microphones in the tube are affected by a signal which is the same in terms of amplitude and phase.

In the case shown in Fig. 8, the value of the phase error $\Delta\varphi$, calculated from the ratio of the real and imaginary parts of the cross-spectrum, is 2° for $f = 0{,}5$ kHz.

An example of the difficulties occurring in the interpretation of results when the phase error of equipment is large with respect to $k\Delta x$, drawn from the author's own investigations, is given below. In some case of excitation of a plate by a tone, with signals being recorded by a Nagra tape recorder, a series of

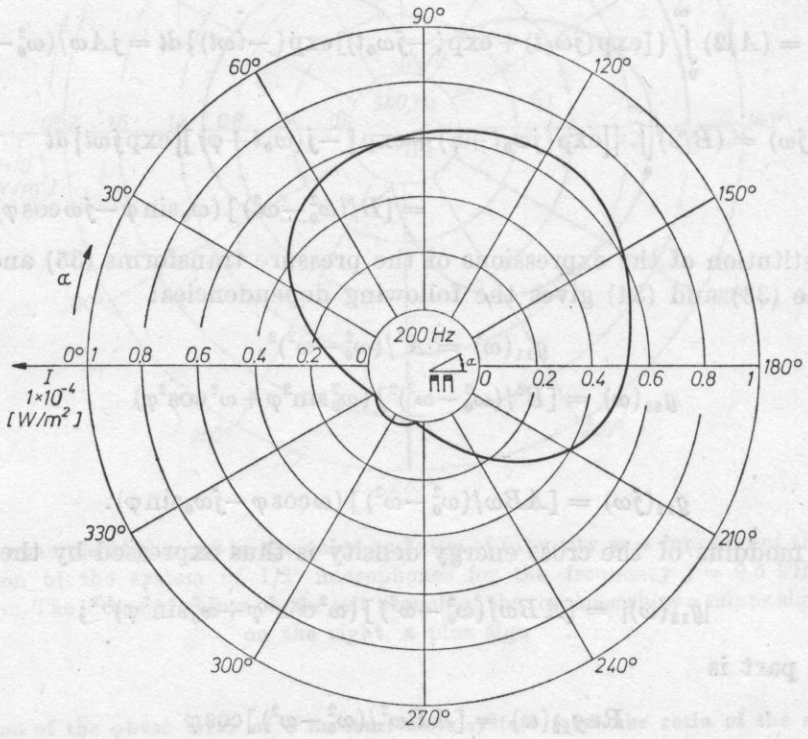

Fig. 7. An example of changes in the directional response of the system of 1/2′ microphones for the frequency $f = 0.2$ kHz as a result of the existence of phase error with the value $\Delta\Phi = 1.5°$ in the system shown in Fig. 1a. The microphones spaced at $\Delta x = 0.014$ m

results was obtained, where the sign of $\mathrm{Im}G_{12}(\omega)$ varied depending on the frequency emitted by the plate, irrespective of the measurement point on the plate (Fig. 8). The measurement for one of the positions of the probe gave probable results and that for the opposite localisation yielded results which it was difficult to interpret. The mean value of the phase error of equipment, $\Delta\varphi(0.5) = 4°$ (with phasemeter measurements indicating 5°), was calculated from the ratio $\mathrm{Re}G_{12}(\omega)/\mathrm{Im}G_{12}(\omega)$ for all the measurement points. In this case (the frequency of the excitation signal $f = 0.5$ kHz, with the resonance frequency of the plate $f = 21$ Hz, the microphone spacing $\Delta x = 0.014$ m, the distance between the probe and the source $r = 0.4$ m) the value of $\Phi_{\Delta x}$ was 7.5°, and

thus the results of the intensity measurements can be represented, in keeping with formula (41), for known values of $\Delta\varphi$ and $\Phi_{\Delta x}$, in the following way:

$$\mathrm{Im}G_{12}^{(a)}(0.5) \sim \text{const. } 0.21, \quad \mathrm{Im}G_{12}^{(b)}(0.5) \sim \text{const. } 0.03.$$

It can be seen from Fig. 9 that in this case it is difficult to compare the calculated and measured values, although, considering the signs of the components, the mean value of intensity in the band is close to zero. (Because of the difficulties in interpretation this method was abandoned in practical applications).

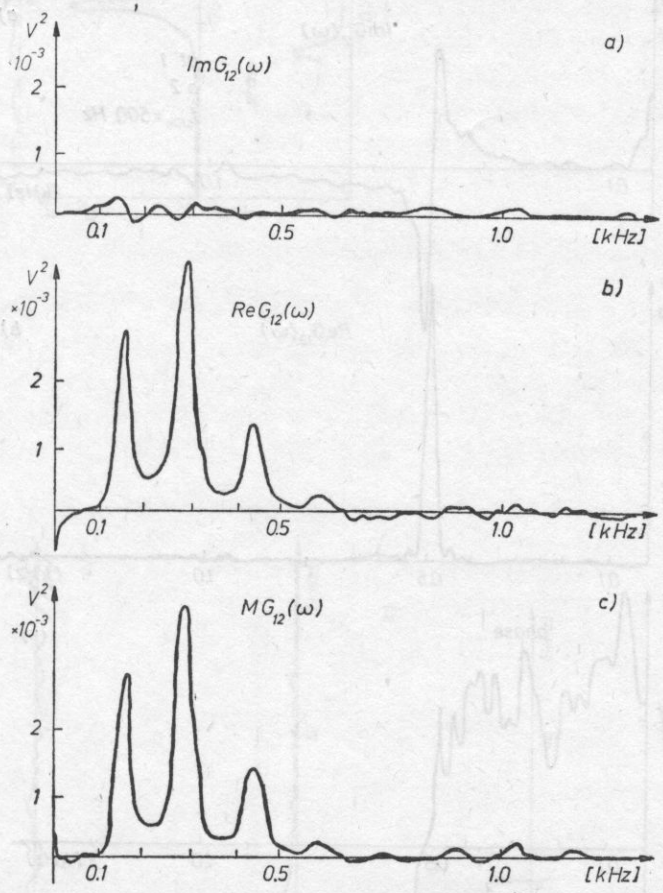

Fig. 8. An example of the behaviour of the cross-spectral density $G_{12}(j\omega)$ of signals from the microphone system placed in the same acoustic field in a tube of standing waves. a) the imaginary part of the spectrum, b) the real part, c) the modulus. The results permit the phase error of equipment to be calculated from formula (42) for any frequency. The signal was white noise, the microphones were spaced at $\Delta x = 0.014$ m. The calculations were carried out on a Hewlett-Packard system (Fig. 1b), with a Nagra tape recorder. The conditions of the calculations: the width of the frequency band analysed B = 15 Hz, the number of countings $N = 128 \times 1024$, summation averaging

The sine function in formula (41) changes its sign for the emitted frequency, there is a phase jump by π. The resultant phase difference, in the case of using a Nagra tape recorder, is too small for correct results to be obtained. The change of the sign of $\mathrm{Im}G_{12}(\omega)$ from + to −, or conversely (Fig. 9), depends, it was found, on the arbitrarily assumed order of signal processing.

It was found that the ratio of the real parts for two positions of the probe $\mathrm{Re}G_{12}^{(a)}(\omega)/\mathrm{Re}G_{12}^{(b)}(\omega) = 1$, which results from calculations (formula (40)) and measurements (Figs. 9–11). However, it was established that when the tone exciting

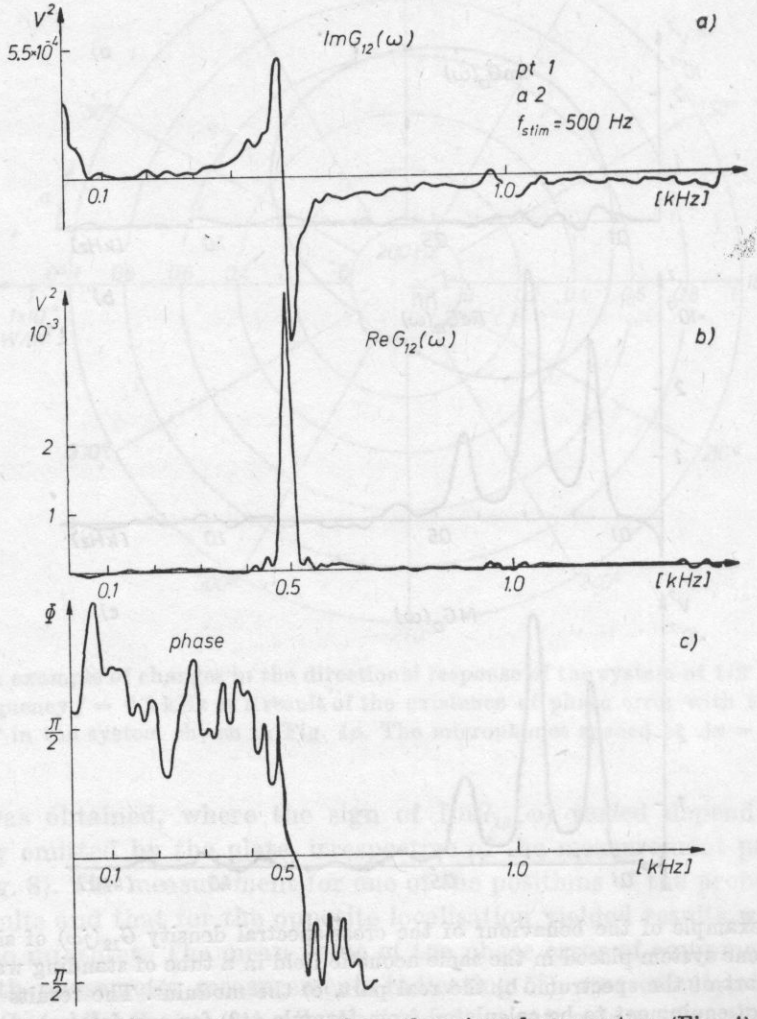

Fig. 9. The cross-spectrum of pressures from the microphone system (Fig. 4), placed over a vibrating plate excited by a tone with the frequency $f = 0.5$ kHz. a) the imaginary part of the spectrum, b) the real part, c) phase. The conditions of the measurements: the microphones spaced at $\Delta x = 0.014$ m, the distance between the probe and the plate $r = 0.04$ m. The conditions of the calculations are the same as in Fig. 8

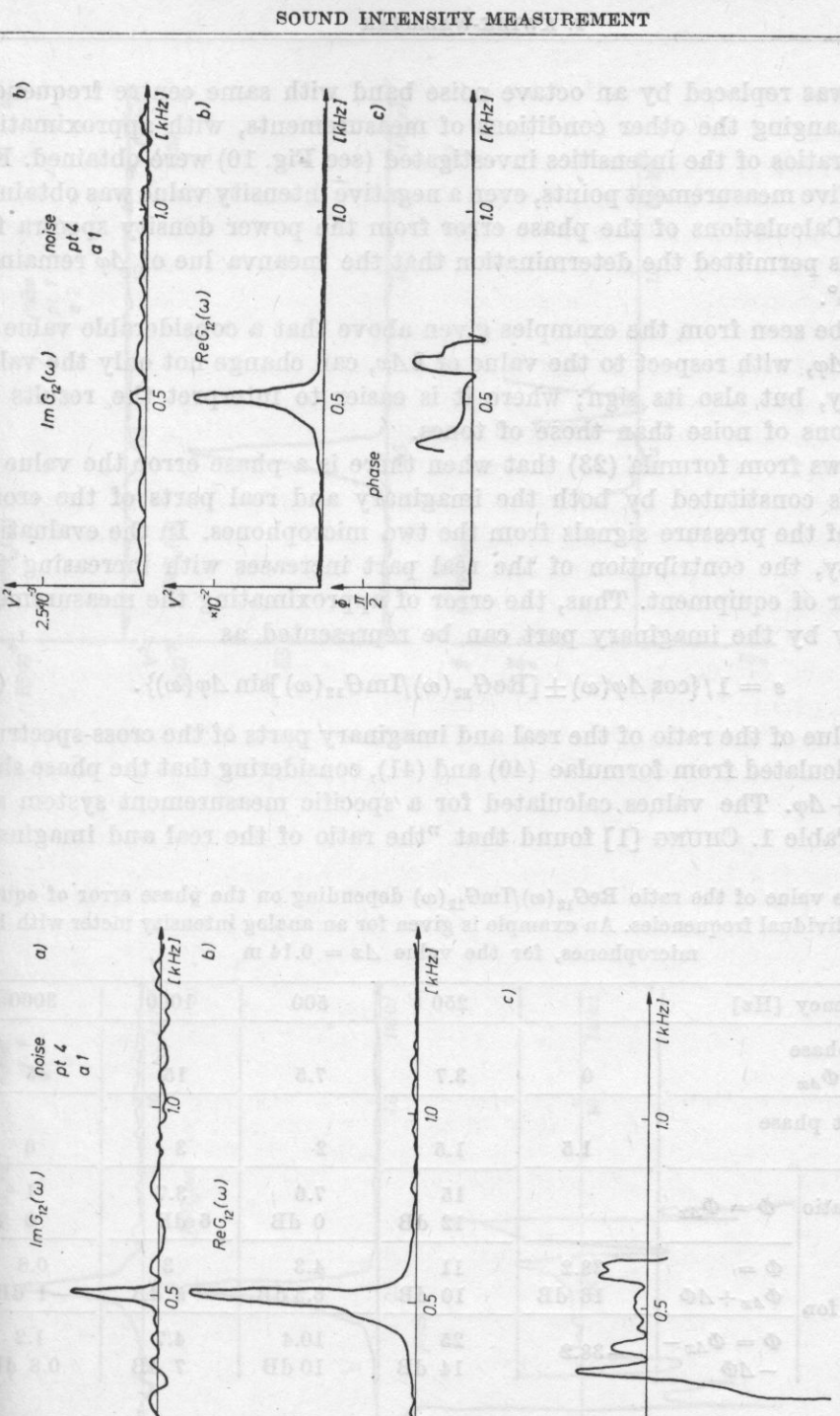

Fig. 10. The cross-spectrum of pressures from the microphone system, placed over a plate excited to vibration by a noise band with the centre frequency $f = 0.5$ kHz. The results were obtained for two positions of the probe (a) and after reversal (b). The other conditions of the measurements and calculations were the same as those in the description of Fig. 9

the plate was replaced by an octave noise band with same centre frequency, without changing the other conditions of measurements, with approximation the above ratios of the intensities investigated (see Fig. 10) were obtained. For one of the five measurement points, even a negative intensity value was obtained (Fig. 11). Calculations of the phase error from the power density spectra for noise bands permitted the determination that the meanva lue of $\Delta\varphi$ remained equal to 4°.

It can be seen from the examples given above that a considerable value of the error $\Delta\varphi$, with respect to the value of $k\Delta x$, can change not only the value of intensity, but also its sign; where it is easier to interpret the results of investigations of noise than those of tones.

It follows from formula (23) that when there is a phase error the value of intensity is constituted by both the imaginary and real parts of the cross-spectrum of the pressure signals from the two microphones. In the evaluation of intensity, the contribution of the real part increases with increasing the phase error of equipment. Thus, the error of approximating the measurement result only by the imaginary part can be represented as

$$\varepsilon = 1/\{\cos\Delta\varphi(\omega) \pm [\mathrm{Re}G_{12}(\omega)/\mathrm{Im}G_{12}(\omega)]\sin\Delta\varphi(\omega)\}. \tag{43}$$

The value of the ratio of the real and imaginary parts of the cross-spectrum can be calculated from formulae (40) and (41), considering that the phase shift $\Phi = k\Delta x + \Delta\varphi$. The values calculated for a specific measurement system are given in Table 1. CHUNG [1] found that "the ratio of the real and imaginary

Table 1. The value of the ratio $\mathrm{Re}G_{12}(\omega)/\mathrm{Im}G_{12}(\omega)$ depending on the phase error of equipment for individual frequencies. An example is given for an analog intensity meter with 1/2′ microphones, for the value $\Delta x = 0.14$ m

Frequency [Hz]			250	500	1000	3000
Physical phase difference $\Phi_{\Delta x}$		0	3.7	7.5	15	45
Equipment phase error $\Delta\Phi$		1.5	1.5	2	3	6
Value of ratio $\frac{\mathrm{Re}G_{12}(\omega)}{\mathrm{Im}G_{12}(\omega)}$ for	$\Phi = \Phi_{\Delta x}$		15 12 dB	7.6 0 dB	3.7 6 dB	1 0
	$\Phi = \Phi_{\Delta x} + \Delta\Phi$	38.2 16 dB	11 10 dB	4.3 6.3 dB	3 5 dB	0.8 −1 dB
	$\Phi = \Phi_{\Delta x} - \Delta\Phi$	−38.2	25 14 dB	10.4 10 dB	4.7 7 dB	1.2 0.8 dB

parts of the cross-spectrum is usually about 15 dB". As can be seen from Table 1, this value varies, depending on the phase difference between behaviours of Φ, taking into account the equipment error, and it is not so large, even when no phase error occurs (see Table 1, case *a*).

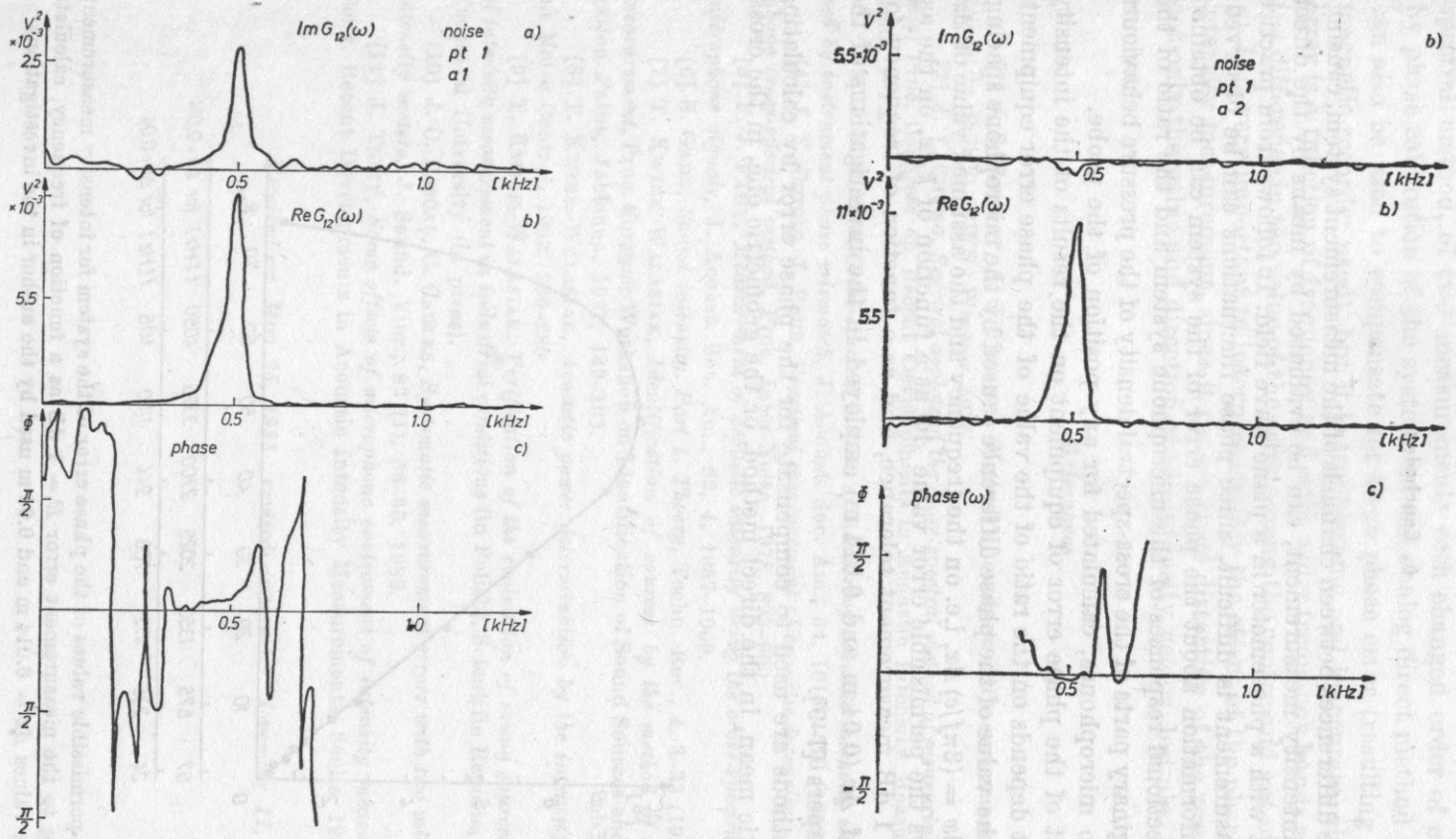

Fig. 11. The results as in Fig. 10, obtained for one of the measurement points, characterized by a change in the sign of the intensity vector after the reversal of the probe (b), as a result of the existence of large-compared with $k\Delta x$ — phase error of the equipment system

6. Conclusion

The phase differences between channels of the measurement system, causing error in the intensity measurement, can be evaluated by means by the direct measurement with a phasemeter in a plane wave field. It follows from practice that the measurement is difficult, since phase fluctuations can be observed. Additional information about the phase error of the system can be obtained from the directional responses of the microphone system and the ratio of the real and imaginary parts of the cross-spectral density of the pressure behaviours from the two microphones, calculated for any position of the probe.

The effect of the phase error of equipment on the results of the intensity measurement depends on the ratio of the value of the phase error equipment, $\Delta\varphi(\omega)$, and the value of the phase difference caused by the microphone spacing, $\Phi_{\Delta x}(\omega) = k\Delta x = (2\pi f/c)\Delta x$, i.e. on the frequency and the assumed value of Δx. Fig. 11 shows the permissible error value $\Delta\Phi$ as a function of $k\Delta x$, on the assumption of 1 dB measurement tolerance, and as a function of frequency for the values of Δx (0.04 m and 0.014 m) employed in the investigations of the author of papers [7–9].

Some methods are used to compensate for the phase error by calculating the arithmetic mean, in the direct method, or the geometric one, in the cross-

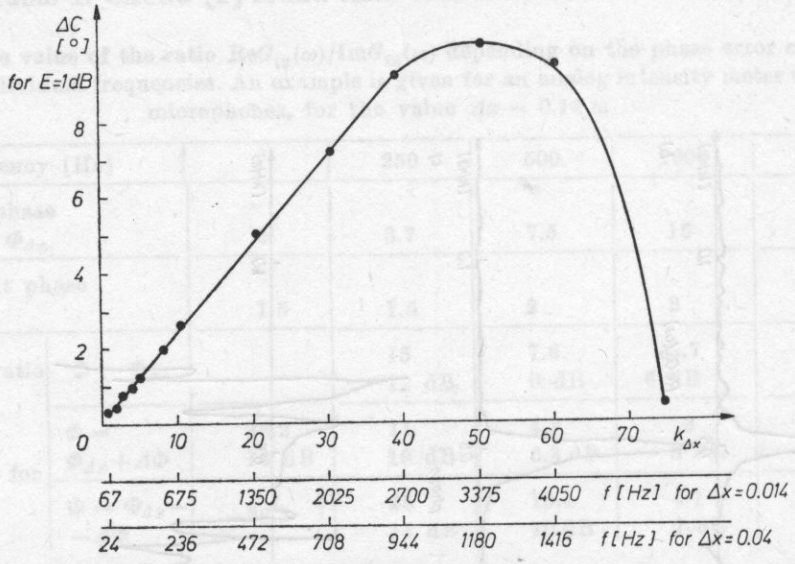

Fig. 12. The permissible values of the phase error of the system for intensity measurements, corresponding to the measurement error $E = 1$ dB as a function of frequency, calculated for the values $\Delta x = 0.014$ m and 0.04 m used by the author in the investigations

spectral method, of two measurements with changed order of circuits [4], or by phase calibration of the system. In the analog direct method phase shifters can also be used to compensate for large phase error (resulting e.g. from the magnetic recorder used), but it is troublesome and inaccurate, since the phase error is a function of frequency and with wider frequency bands analysed there is a difference in the value of the error among the centre and cut-off frequencies.

It is very important to interpret strictly the effect of the phase error on the intensity measurement, since it causes large distortion of the results, changing not only the value and direction of the intensity vector, but also its sign.

References

[1] J. S. Bendat, A. G. Piersol, *Methods of analysis and measurement of random functions* (in Polish), PWN, Warsaw 1976.

[2] J. Y. Chung, *Spectral aspects of the cross-spectral method of measuring acoustic intensity*, Proc. Congress on Recent Developments in Acoustic Intensity Measurement, Senlis, 1981, 1–11.

[3] J. Y. Chung, *Cross-spectral method of measuring acoustic intensity without error caused by instrument phase mismatch*, J. Acoust. Soc. Am., 64, 1613–1616 (1978).

[4] J. Y. Chung, J. Pope, *Practical measurement of acoustic intensity – the two microphone cross-spectral method*, Proc. Inter-Noise, 1978, 893–900.

[5] F. J. Fahy, *Measurement of acoustic intensity using the cross-spectral density of two microphone signals*, J. Acoust. Soc. Am., 62, 4, 1057–1059.

[6] S. Gade, *Sound intensity. Part I. Thoery*, Techn. Rev., 4, 3–33 (1982).

[7] T. Kwiek–Walasiak, *Identification of sources by the method of sound intensity measurement*, Proc. Summer Workshop on Identification of Sound Sources and Sound Propagation Paths, Jabłonna, 1981, 149–163.

[8] T. Kwiek–Walasiak, *Acoustic power determination by the intensity method*, Proc. on Noise Control, 1982, 286–289.

[9] T. Kwiek–Walasiak, *Verification of the evaluation of sound sources by the method of intensity measurement in industrial conditions* (in Polish), Scientific Reports, Świętokrzyska Technical University (in press).

[10] J. C. Pascal, C. Carles, *Systematic measurement errors with two microphone sound intensity meters*, J. Sound. Vibr., 83 (1), 56–65, 1982.

[11] J. Tichy, *Some effects of microphone enviroment of intensity measurements*, Proc. Cong. Recent Developments in Acoustic Intensity Measurements, Senlis, 1981, 25–31.

Received on May 25, 1983; revised version on November 11, 1984.

ARCHIVES OF ACOUSTICS
10, 1, 59-74 (1985)

A FUNDAMENTAL STUDY FOR PREDICTING THE URBAN STREET NOISE BY USE OF THE IMAGE METHOD APPROACH

MITSUO OHTA

Faculty of Engineering, Hiroshima University
(Shitami, Saijo-cho, Higashi-hiroshima city, 724 Japan)

YASUO MITANI

Fukuyama University
(Sanzo, Higashimura-cho, Fukuyama city, 729-02 Japan)

This paper describes a unified statistical method of structural prediction of an arbitrarily fluctuating street noise in the general urban noise environment, especially from a fundamental viewpoint. That is, an analytical expression of the noise propagation characteristics for several cases of typically idealized road traffic models is first derived, in order to express an actual noise environment in the city area, based on the image method approach. Then, by using the newly derived expression of the noise propagation characteristics, two representative evaluation indices of street noise, closely related to the well-known L_{eq} and L_{NP} evaluation indices, can be given in an explicit functional form with several internal mechanisms of the road traffic environments in the city area. Finally the validity of the present theoretical prediction method is experimentally confirmed, especially by use of digital simulation technique for several cases of typically idealized actual road traffic noise environment in the city area.

1. Introduction

In recent years, problems of environmental noise generated by passing transportation vehicles in the city area have become more critical, owing to the hasty popularization of the traffic means in our daily life.

Especially in the city area with complex geometrical structures, such as a single-level intersection, a grade-separated intersection or a multi-lane road etc., the question of analysis of the actual noise environment has not yet been the-

oretically solved in principle because of the arbitrariness of the movement of noise sources and the complicated situation of actual noise propagation paths. Nevertheless, based on the consideration that the environmental random noise phenomena are dominantly caused by the transportation vehicles passing in the city area, a realistic approach to structural evaluation of the effect of the noise generated by these passing vehicles on the resultant environmental noise level, in a functional form with the noise propagation characteristics, is fundamentally important. Before the establishment of new buildings and roads, prediction of this noise effect should be investigated, from the viewpoint of noise control for town planning.

From the above circumstances, in this paper, a fundamental theory of statistical prediction of the general street noise level over a complicated actual city traffic environment is derived, based on the well-known image method approach [1]. More concretely, after expressing the noise propagation characteristic between the noise sources and the observation point over the city area in an explicit functional form by use of the image method approach, a unified statistical method of structural prediction of the arbitrarily fluctuating street noise in several typical cases of the urban noise environment is first derived. Among various evaluation indices of the actual urban noise environment, especially two evaluation indices, closely related to the well-known L_{eq} and L_{NP} [2], can be given in an analytical form with the internal mechanisms of traffic environment.

In view of the complexity of the statistical prediction and the variety of forms of level distribution of urban road traffic noise, the technique of digital simulation seems to be the most powerful and effective way of experimental confirmation. The validity of the prediction method proposed was principally confirmed especially by use of the digital simulation technique for several cases of typically idealized actual road traffic noise environment in the city area, since this kind of study is in an early stage.

2. Explicit expressions of the noise propagation characteristic in the city area

By considering a well-known fact that the urban noise problem is originally caused by a rapid increase in the number of noise sources, such as transportation vehicles, motorcycles etc., and the swift gravitation of the population to the city area, it is necessary to describe first several fundamental models of typical noise environment in the city area, such as a straight road and other different intersections. Then, the actual circumstances in the city area can be analyzed as a complicated composition of these models of typical noise environment.

2. 1. Noise propagation characteristic in the city area with a straight road (Case 1)

Let us consider a straight road with the arbitrary segment $[-L, L]$ and the arbitrary width L_x. It is assumed that an arbitrarily passing vehicle S moves in the middle of the road and an observation point O is placed on the sidewalk by the road, at a distance X from the passing vehicle along the road, as shown in Fig. 1a.

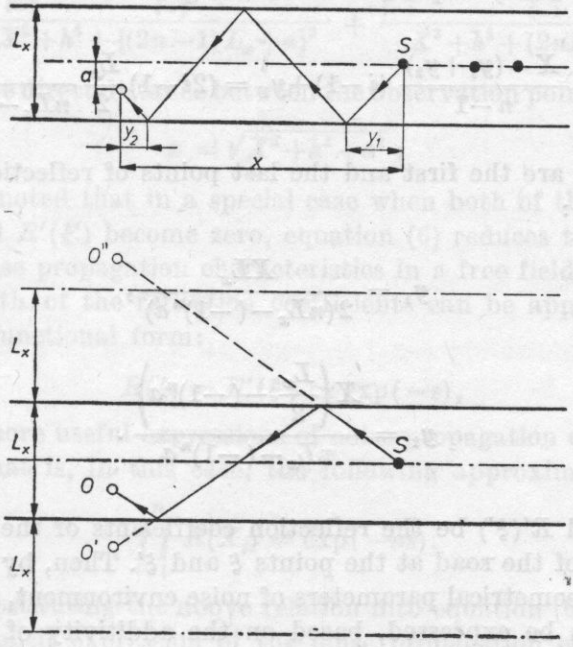

Fig. 1. Analysis of noise propagation characteristics for the straight road model. a) Noise propagation for the straight road, b) Analysis of noise propagation to image observers based on the image method approach

The noise intensity I at the observation point O, generated by the passing vehicle S, is generally expressed by the sum of the direct noise intensity I_1 and the reflected noise intensity I_2:

$$I = I_1 + I_2. \tag{1}$$

Hereupon, by use of the inverse-square law of noise propagation, the direct noise intensity I_1 can be expressed as:

$$I_1 = \frac{QW}{4\pi(X^2+h^2+a^2)}, \tag{2}$$

where h denotes the difference of height between the observation point and the noise source. Moreover, Q is a directivity factor and W is the acoustic power generated by the passing vehicle.

The reflected noise intensity due to the surrounding buildings lined along each side of the road can be evaluated by regularly assuming image observers at a place perpendicular to the road, as shown in Fig. 1b, on the basis of the image method approach. In the case when the noise wave reflects n times from the surrounding buildings, the distance X_i between the ith reflection point and the noise is easily expressed from the geometrical analysis $(1 < i < n)$:

$$X_i \triangleq \Delta \frac{X-(y_1+y_2)}{n-1}(i-1)+y_1 = (2i-1)\frac{L_x}{2}\frac{X}{nL_x-(-1)^n a}, \tag{3}$$

where y_1 and y_2 are the first and the last points of reflection from the noise source, given as:

$$y_1 = \frac{XL_x}{2(nL_x-(-1)^n a)}, \qquad y_2 = \frac{X\left(\frac{L_x}{2}-(-1)^n a\right)}{nL_x-(-1)^n a}. \tag{4}$$

Let $R(\xi)$ and $R'(\xi')$ be the reflection coefficients of the building surfaces along each side of the road at the points ξ and ξ'. Then, by considering these acoustical and geometrical parameters of noise environment, the received noise intensity L_2 can be expressed, based on the additivity of energy quantity:

$$I_2 = \frac{QW}{4\pi}\sum_{n=1}^{\infty}\left[\frac{\prod_{i=1}^{n-1}R(X_{2i})\prod_{i=1}^{n}R'(X_{2i-1})}{X^2+h^2+\{(2n-1)L_x-a\}^2}+\frac{\prod_{i=1}^{n}R(X_{2i})\prod_{i=1}^{n}R'(X_{2i-1})}{X^2+h^2+(2nL_x+a)^2}+\right.$$
$$\left.+\frac{\prod_{i=1}^{n-1}R'(X_{2i})\prod_{i=1}^{n}R(X_{2i-1})}{X^2+h^2+\{(2n-1)L_x+a\}^2}+\frac{\prod_{i=1}^{n}R'(X_{2i})\prod_{i=1}^{n}R(X_{2i-1})}{X^2+h^2+(2nL_x-a)^2}\right]. \tag{5}$$

Substituting equations (2) and (5) into equation (1), one can easily obtain the following expression of the noise propagation characteristics between the observation point O and the arbitrarily passing vehicle S:

$$f(x) = f\left(\sqrt{X^2+h^2+a^2}\right) = \frac{1}{4\pi(X^2+h^2+a^2)} +$$

$$+ \frac{1}{4\pi}\sum_{n=1}^{\infty}\left[\frac{\prod_{i=1}^{n-1} R(X_{2i})\prod_{i=1}^{n} R'(X_{2i-1})}{X^2+h^2+\{(2n-1)L_x-a\}^2} + \frac{\prod_{i=1}^{n} R(X_{2i})\prod_{i=1}^{n} R'(X_{2i-1})}{X^2+h^2+(2nL_x+a)^2} + \right.$$

$$\left. + \frac{\prod_{i=1}^{n-1} R'(X_{2i})\prod_{i=1}^{n} R(X_{2i-1})}{X^2+h^2+\{(2n-1)L_x+a\}^2} + \frac{\prod_{i=1}^{n} R'(X_{2i})\prod_{i=1}^{n} R(X_{2i-1})}{X^2+h^2+(2nL_x-a)^2}\right], \quad (6)$$

where x means the direct distance between the observation point and the vehicle:

$$x = \sqrt{X^2+h^2+a^2}\,. \quad (7)$$

It should be noted that in a special case when both of the reflection coefficients $R(\xi)$ and $R'(\xi')$ become zero, equation (6) reduces to the well-known expression of noise propagation characteristics in a free field of sound. In addition, when both of the reflection coefficients can be approximated in the following same functional form:

$$R(\xi) = R'(\xi') \simeq \exp(-\varepsilon), \quad (8)$$

one can obtain more useful expressions of noise propagation characteristics for practical use. That is, in this case, the following approximation is derived:

$$\prod_{i=1}^{n} R(X_i) = \exp(-n\varepsilon). \quad (9)$$

Therefore, substituting the above relation into equation (6), one can obtain the following explicit expression of the noise propagation characteristics:

$$f(x) = \frac{1}{4\pi(X^2+h^2+a^2)} + \frac{1}{4\pi}\sum_{n=1}^{\infty}\left[\frac{\exp(-n\varepsilon)}{X^2+h^2+\{nL_x+(-1)^n a\}^2} + \right.$$

$$\left. + \frac{\exp(-n\varepsilon)}{X^2+h^2+\{nL_x-(-1)^n a\}^2}\right] \triangleq f_0(x). \quad (10)$$

From the practical point of view, equation (10) can be more simplified in the following two actual cases, in a compact form of expression.

a) Approximate expression of the noise propagation characteristics with a high reflection coefficient of the building surfaces

In a case when the surrounding buildings have high reflection coefficients of sound (i.e., their reflection coefficients become nearly equal to one), an approximate explicit expression of the noise propagation characteristics in the

city area with a straight road can be expressed as:

$$f(x) \simeq \frac{1-\exp(-\varepsilon)}{4\pi(X^2+h^2+a^2)} + \frac{\exp(-\varepsilon)}{8L_x}\left[\frac{\sinh\left(\frac{\pi}{L_x}\sqrt{X^2+h^2}\right)}{\sqrt{X^2+h^2}\left\{\cosh\left(\frac{\pi}{L_x}\sqrt{X^2+h^2}\right)-\cos\left(\frac{\pi a}{L_x}\right)\right\}} + \frac{\sinh\left(\frac{\pi}{L_x}\sqrt{X^2+h^2}\right)}{\sqrt{X^2+h^2}\left\{\cosh\frac{\pi}{L_x}\sqrt{X^2+h^2}-\cos\left(\frac{\pi(L_x+a)}{L_x}\right)\right\}}\right] \triangleq f_1(x). \quad (11)$$

b) Approximate expression of the noise propagation characteristics with a low reflection coefficient of the building surfaces

In the case when the surrounding buildings have low relection coefficients of sound (i.e., they have highly absorptive surfaces, so that their reflection coefficients become nearly equal to zero), an approximate explicit expression for this case can be expressed as:

$$f(x) \simeq \frac{1}{4\pi(X^2+h^2+a^2)} + \frac{\sum_{n=1}^{\infty}\exp(-n\varepsilon)}{4\pi}\left[\frac{1}{X^2+h^2+(L_x+a)^2} + \frac{1}{X^2+h^2+(L_x-a)^2}\right] = \frac{1}{4\pi(X^2+h^2+a^2)} + \frac{1}{4\pi}\frac{\exp}{1-\exp}\times \times\left[\frac{1}{X^2+h^2+(L_x+a)^2} + \frac{1}{X^2+h^2+(L_x-a)^2}\right] \triangleq f_2(x). \quad (12)$$

2.2. Noise propagation characteristics in the city area with a T-type intersection (Case 2)

Now, let us consider the noise propagation characteristics in a case when the passing vehicle is located within the intersection, as shown in Fig. 2. In this case, the geometrical condition for noise reflections is given under the restriction that the sound wave should be reflected first at the corner of the intersection, i.e.;

$$y_1 > X - X_0, \quad (13)$$

where X_0 is the distance between the observation point and the corner. Furthermore, y_1 is the distance between the passing vehicle S and the first reflection point, as shown in Fig. 2.

Therefore, the noise propagation characteristics of the T-type intersection can be expressed as follows:

$$f(x) = \frac{1}{4\pi(X^2+h^2+a^2)} + \frac{1}{4\pi}\sum_{n=1}^{n_1} \frac{\exp(-n\varepsilon)}{X^2+h^2+\{nL_x+(-1)^n a\}^2} + \\ + \frac{1}{4\pi}\sum_{n=1}^{n_2} \frac{\exp(-n\varepsilon)}{X^2+h^2+\{nL_x-(-1)^n a\}^2}. \tag{14}$$

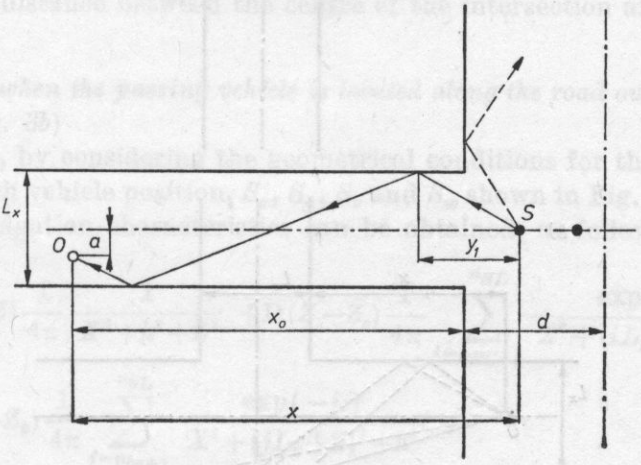

Fig. 2. Analysis of noise propagation characteristics for the T-type intersection

In equation (14), the maximum numbers, n_1 and n_2, of the repeated reflections are limited, due to the finite length of the building rows along the street. That is, the two numbers, n_1 and n_2, in equation (14) can be evaluated as:

$$n_1 \triangleq \max\left\{2\left[\frac{1}{2}\left(\frac{X}{2(X-X_0)} - \frac{a}{L_x}\right)\right],\ 2\left[\frac{1}{2}\left(\frac{X}{2(X-X_0)} + \frac{a}{L_x}\right)-1\right]+1\right\}, \\ n_2 \triangleq \max\left\{2\left[\frac{1}{2}\left(\frac{X}{2(X-X_0)} + \frac{a}{L_x}\right)\right],\ 2\left[\frac{1}{2}\left(\frac{X}{2(X-X_0)} - \frac{a}{L_x}\right)-1\right]+1\right\}. \tag{15}$$

with Gauss' symbol [.]. In the case when the passing vehicle is located along the building rows, it is needless to say that the explicit expression of the noise propagation characteristics is given by equation (6).

2.3. *Noise propagation characteristics in the city area with a crossroads (Case 3)*

In a case when a passing vehicle is located within the intersection as shown in Fig. 3, one can consequently obtain the explicit expression of the noise propagation characteristics, based on the same analysis method as that described in the previous section.

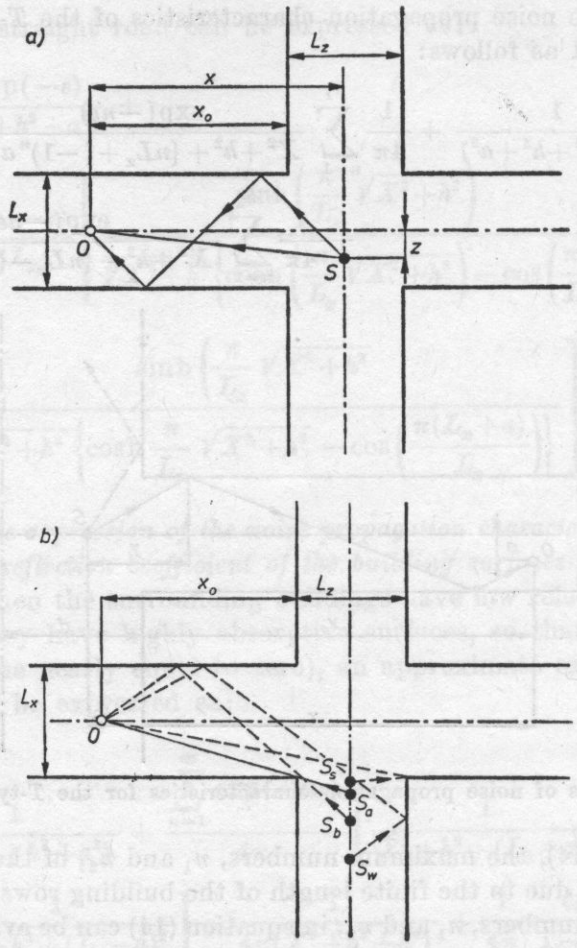

Fig. 3. Analysis of noise propagation characteristics for the crossroads. a) Source inside the crossroads, b) Source outside the crossroads

a) The case when the passing vehicle is located within the intersection (see Fig. 3a)

In view of the fact that this case corresponds to the case when the passing vehicle is located within a T-type intersection, the explicit expression of the noise propagation characteristics is expressed as follows:

$$f(x) = \frac{1}{4\pi(X^2+Z^2+h^2)} + \frac{1}{4\pi}\sum_{n=1}^{n_1}\frac{\exp(-n\varepsilon)}{X^2+(nL_x-Z)^2+h^2} + \frac{1}{4\pi}\sum_{n=1}^{n_2}\frac{\exp(-n\varepsilon)}{X^2+(nL_x+Z)^2+h^2}, \tag{16}$$

with

$$n_1 \triangleq \max\left\{2\left[\frac{1}{2}\left(\frac{X}{2(X-X_0)}-\frac{Z}{L_x}\right)\right],\ 2\left[\frac{1}{2}\left(\frac{X}{2(X-X_0)}+\frac{Z}{L_x}\right)-1\right]+1\right\},$$

and (17)

$$n_2 \triangleq \max\left\{2\left[\frac{1}{2}\left(\frac{X}{2(X-X_0)}+\frac{Z}{L_x}\right)\right],\ 2\left[\frac{1}{2}\left(\frac{X}{2(X-X_0)}-\frac{Z}{L_x}\right)-1\right]+1\right\}.$$

where Z is the distance between the centre of the intersection and the vehicle position.

b) The case when the passing vehicle is located along the road outside the intersection (see Fig. 3b)

In this case, by considering the geometrical conditions for the noise reflections due to each vehicle position, S_s, S_a, S_b and S_w shown in Fig. 3b, the objective noise propagation characteristics can be obtained, as follows:

$$f(x) = D(Z_d-Z)\frac{1}{4\pi}\frac{1}{X^2+h^2+Z^2} + D(Z-Z_s)\frac{1}{4\pi}\sum_{i=n_{SS}+1}^{n_{SL}}\frac{\exp(-i\varepsilon)}{Z^2+(iL_Z+X)^2+h^2} +$$

$$+D(Z-Z_b)\frac{1}{4\pi}\sum_{j=n_{bs}+1}^{n_{bL}}\frac{\exp(-j\varepsilon)}{X^2+(jL_x+Z)^2+h^2} +$$

$$+D(Z-Z_{WB})\sum_{n=1}^{\infty}\left\{\frac{1}{4\pi}\sum_{t=h_{WC}+1}^{n_{WB}}\frac{\exp[-(n+t)\varepsilon]}{(X+tL_z)^2+(nL_x+Z)^2+h^2}\right. +$$

$$+D(Z-Z_{WA})\sum_{n=1}^{\infty}\left\{\frac{1}{4\pi}\sum_{t=h_{WC}+2}^{n_{WA}}\frac{\exp[-(n+t)\varepsilon]}{(X+tL_z)^2+(nL_x+Z)^2+h^2}\right., \quad (18)$$

where each symbol is given by:

(19)

$$Z_d = \frac{L_x}{2}\left(1+\frac{L_z}{2X_0}\right),\quad Z_s = \frac{L_x}{2}\left(\frac{L_z}{2(L_z+X_0)}+1\right),\quad Z_b = \frac{L_x}{2}\left(\frac{L_z}{2X^0}-1\right),$$

$$Z_{WA} = \frac{L_x}{2}\left(\frac{3(2n-1)L_z}{2X_0}-\frac{1}{2}\right),\quad Z_{WB} = \frac{L_x}{2}\left(\frac{(2n+1)L_z}{2(X_0+L_z)}+\frac{1}{2}\right),\quad n_{SL}$$

$$=\left[\frac{X_0(2Z-L_x)}{L_xL_Z}-\frac{1}{2}\right],\quad n_{SS} = \left[\frac{X_0(2Z-L_x)}{L_xL_Z}+\frac{2Z}{L_x}-\frac{1}{2}\right],\quad n_{bS}$$

$$=\left[\frac{X_0(2Z-L_x)}{L_xL_Z}-\frac{1}{2}\right],\quad n_{bL} = \left[\frac{X_0 2(Z+L_x)}{L_xL_Z}-\frac{1}{2}\right],\quad n_{WA}$$

$$= \left[\frac{X_0(2Z+L_x)}{(2n-1)L_xL_Z} - \frac{1}{2} \right], \quad n_{WB} = \left[\frac{(X_0+L_z)(2Z-L_x)}{(2n+1)L_xL_Z} + \frac{1}{2} \right], \quad n_{WC} = \left[\frac{X_0(2Z-L_x)}{(2n+1)L_xL_Z} - \frac{1}{2} \right].$$

In the above expression, $D(.)$ denotes the truncation function defined as

$$D(\xi) = \begin{cases} 0 & (\xi) \leqslant 0), \\ 1 & (\xi) > 0). \end{cases} \tag{20}$$

3. Establishment of the model of the road traffic noise in the city area

As a noise environment model, a main road in the city area having a complex structure with building rows on the both sides is generally considered in this section.

From the additivity of noise energy, the noise intensity I at an observation point along the road is generally expressed as follows:

$$I = \sum_{j=1}^{J} \sum_{i=1}^{n_j} QW_{ij} f(X_{ij}) + v, \tag{21}$$

where J denotes the number of different vehicle-types and n_j is the number of the jth vehicle-type. Also, X_{ij} is the distance between the ith vehicle and the observation point, W_{ij} is the acoustic power generated by the ith vehicle and Q is a directivity factor. Moreover, v denotes the intensity of the background noise.

Let us introduce the following assumptions based on the actual situation of traffic flow:

1) The total number of vehicles passing through the road segment under consideration is governed by the following well-known Poisson distribution [3]:

$$P(n) = \frac{1}{n!} \exp(-N_0) N_0^n. \tag{22}$$

Hereupon, N_0 denotes the mean value of the total vehicle number.

2) The probability distribution function of the number of each vehicle-type is given by the following multi-nomial distribution [4]:

$$P(n_1, n_2, \ldots, n_J | n) = \frac{n!}{n_1!\, n_2! \ldots n_J!} \theta_1^{n_1} \theta_2^{n_2} \ldots \theta_J^{n_J}. \tag{23}$$

In the above expression, $\theta_j (j = 1, 2, \ldots, J)$ denotes the intermixture ratio of the jth vehicle-type.

3) The position of each vehicle occupies independently, X_{ij}, and its probability distribution function is a well-known uniform distribution.

Based on these assumptios made with respect to the traffic flow and the previously derived explicit expressions of the noise propagation characteristics in the city area, let us consider two important representative evaluation indices L_1 and L_2, related to L_{eq} and L_{NP}, among several evaluation indices of the environmental noise. Since it is well-known that L_{eq} is closely related to the averaged noise intensity λ_1, the first evaluation index is adopted as follows:

$$L_1 = 10\log_{10}(\lambda_1/W_0), \tag{24}$$

where W_0 is equal to $10^{-12}W/m$.

On the other hand, in relation to the fact that the widely used evaluation index L_{NP} is defined as $L_{NP} = L_{eq} + 2.56\sigma$ (σ^2 being the variance of the noise level fluctuation), the second evaluation index is adopted as follows:

$$L_2 = 10\log_{10}(\lambda_2/W_0^2), \tag{25}$$

where λ_2 is the variance of the noise intensity fluctuation.

Hereupon, it must be noticed that there is no redundancy of information between λ_1 and λ_2, in constant to the relation between L_{eq} and σ in the definition of L_{NP}.

Accordingly, in order to derive the unified expressions of the above two indices L_1 and L_2, the nth order cumulant of noise intensity fluctuation should first be found in an analytical form. Thus, the moment generating function $g(s)$ of the noise intensity fluctuation I can be derived under the above three assumptions made on the traffic flow and the concrete information on the noi se propagation characteristics, as follows:

$$g(s) \triangleq \langle \exp(sI) \rangle_I = \left\langle \left\langle \left\langle \exp\left(s \sum_{j=1}^{J} \sum_{i=1}^{n_j} Q W_{ij} f(X_{ij}) + sv \right) \right\rangle_{W_{ij}, X_{ij} v | n_j, n} \right\rangle_{n_j | n} \right\rangle_n, \tag{26}$$

where $\langle \cdot \rangle_*$ denotes an expectation operation with respect to the random variable $*$. Hereupon, paying one's attention to the property of statistical independency between the background noise and the road traffic noise, and a multinomial distribution on the number of each vehicle-type, equation (26) can be rewritten, as follows:

$$g(s) = \left\langle \sum_{n_1+n_2+\ldots+n_J=n} \frac{n!}{n_1!\, n_2! \ldots n_J!} \prod_{j=1}^{J} \{Q_j\}^{n_j} \times \right.$$

$$\left. \times \langle \exp[s_1 Q W_{ij} f(X_{ij}) n_j] \rangle_{W_{ij}, X_{ij}} \right\rangle_n \langle \exp(sv) \rangle_v$$

$$= \left\langle \left\{ \sum_{j=1}^{J} \theta_j \langle \exp[sQ W_{ij} f(X_{ij})] \rangle_{W_{ij}, X_{ij}} \right\}^n \right\rangle_n \langle \exp(sv) \rangle_v. \tag{27}$$

Furthermore, from the property of Poisson distribution on the total number of vehicle, the moment generating function can be finally expressed as follows:

$$g(s) = \sum_{n=0}^{\infty} \frac{1}{n!} \exp(-N_0) \{N_0\}^n \left\{ \sum_{j=1}^{J} \theta_j \langle \exp[sQW_{ij} f(X_{ij})] \times \rangle_{W_{ij}, X_{ij}} \right\}^n \langle \exp(sv) \rangle_v$$

$$= \exp\left[N_0 \sum_{n=1}^{\infty} \frac{s^n}{n!} \sum_{j=1}^{J} \theta_j \langle (QW_{ij})^n \rangle_{W_{ij}} \langle f^n(X_{ij}) \rangle_{X_{ij}} \right] \times \langle \exp(sv) \rangle_v. \quad (28)$$

Thus, the nth order cumulant λ_n of the noise intensity fluctuation I can be generally derived as follows:

$$\lambda_n = N_0 \sum_{j=1}^{J} \theta_j \langle (QW_{ij})^n \rangle_{W_{ij}} K_{fn} + \psi_n, \quad (29)$$

where ψ_n denotes the nth order cumulant of only the background noise intensity and K_{fn} denotes the following nth order moment related to the noise propagation characteristics $f(X_{ij})$:

$$K_{fn} \triangleq \langle f^n(X_{ij}) \rangle_{X_{ij}} = \int_{-L}^{L} f^n(X_{ij}) P(X_{ij}) dX_{ij}. \quad (30)$$

Substituting equation (29) into the definition of the two adopted evaluation indices L_1 and L_2, one can as a result obtain the explicit expressions of the two objective indices, as follows:

$$L_1 = 10 \log_{10} \left(\frac{1}{W_0} \left\{ N_0 \sum_{j=1}^{J} \theta_j \langle QW_{ij} \rangle_{W_{ij}} \langle f(X_{ij}) \rangle_{X_{ij}} + \psi_1 \right\} \right), \quad (31)$$

$$L_2 = 10 \log_{10} \left(\frac{1}{W_0^2} \left\{ N_0 \sum_{j=1}^{J} \theta_j \langle Q^2 W_{ij}^2 \rangle_{W_{ij}} \langle f^2(X_{ij}) \rangle_{X_{ij}} + \psi_2 \right\} \right). \quad (32)$$

From the analytical expressions shown in equations (31) and (32), and the explicit expressions of noise propagation characteristics, one can evaluate an actual noise environment in the city area by using information on the traffic flow and the geometrical and acoustical parameters of the circumstances.

4. Experimental considerations

In this section, paying special attention to the urban noise environment with a straight road, the validity of the proposed theoretical results was confirmed experimentally by use of the digital simulation technique, in view of the arbi-

trariness of the fluctuating patterns and the complicated situation of the noise phenomena. Let us consider a straight road with building rows along each side of the road, as shown in Fig. 4. The observation point is placed on the sidewalk at the distance $a (0 < a < L_x/2)$. The passing vehicles in the segment $[-L, L]$ of the road are considered, under the following assumptions:

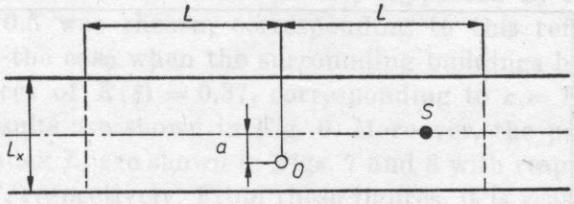

Fig. 4. Straight road model

1) Vehicles passing in the road are composed of two vehicle-types, a light vehicle-type and a heavy vehicle-type, with $J = 2$. The number n_j of passing vehicles of the jth vehicle-type is generated by use of random numbers of a multinomial distribution with the intermixture ratios of the jth vehicle-type: $\theta_1 = 0.8$ and $\theta_2 = 0.2$.

2) Each vehicle in the same vehicle-type generates a constant acoustic power. As is well-known, the ratio of two acoustic powers generated by a heavy vehicle-type and a light vehicle-type is ten to one, according to an empirical value recommended by the Acoustical Society of Japan.

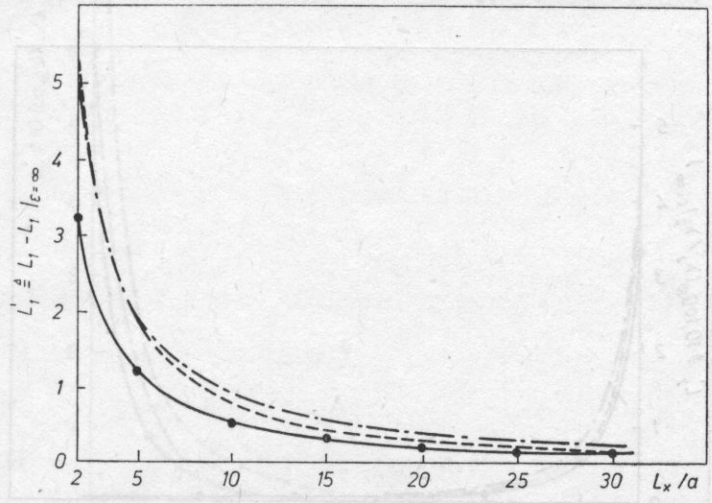

Fig. 5. A comparison between theoretical curves and simulation experiments with respect to L_1, in the case of $R(\xi) = 0.61$. The experimentally sampled points are marked by ·, and the theoretically predicted curves are respectively shown as —— (result by use of $f_0(x)$); – – – – – (result by use of $f_1(x)$); —— – —— (result by use of $f_2(x)$)

In order to show the difference between an urban noise environment and a rural noise one, the difference between the characteristic indices in these two typical environments was considered. Also, for the purpose of unifying the experimental situation between the road width L_x and the distance a, the ratio L_x/a was employed for the horizontal axis in each figure.

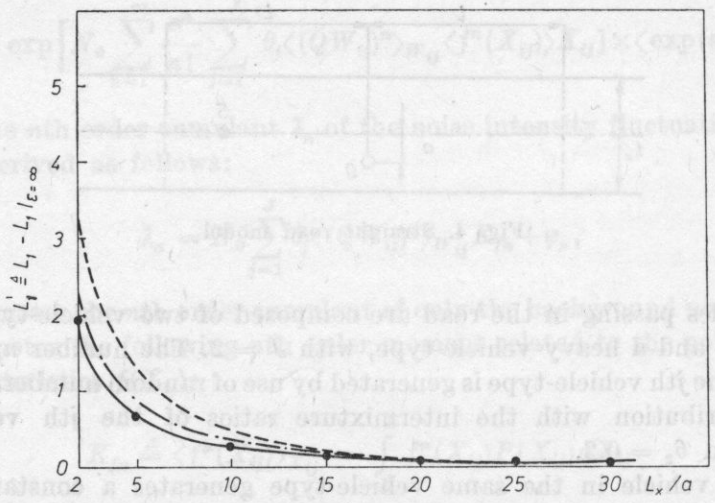

Fig. 6. A comparison between theoretical curves and simulation experiments with respect to L_1, in the case of $R(\xi) = 0.37$. The experimentally sampled points are marked by · , and the theoretically predicted curves are respectively shown as —— (result by use of $f_0(x)$); — — — — — (result by use of $f_1(x)$); —— — —— (result by use of $f_2(x)$)

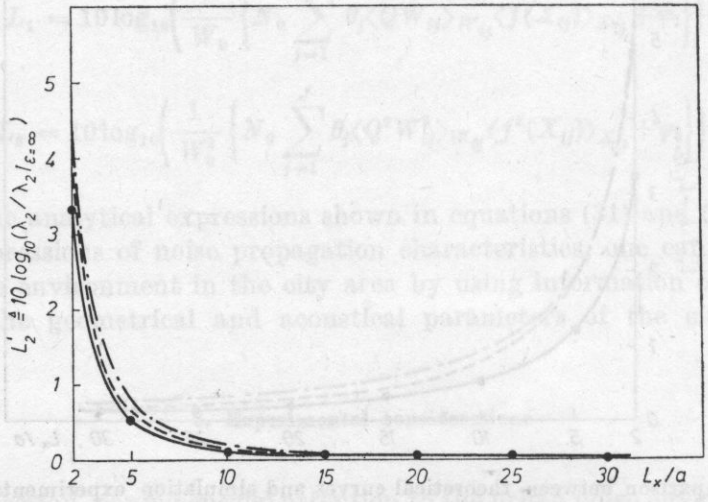

Fig. 7. A comparison between theoretical curves and simulation experiments with respect to L_2, in the case of $R(\xi) = 0.61$. The experimentally sampled points are marked by · , and the theoretically predicted curves are respectively shown as —— (result by use of $f_0(x)$); — — — — — (result by use of $f_1(x)$); —— — —— (result by use of $f_2(x)$)

Fig. 5 shows a comparison between the experimental points sampled by the digital simulation technique and three different theoretical curves for L_1, calculated by using the most precise expression of the propagation characteristics, equation (10), and other approximate expressions of them, equations (11) and (12). In Fig. 5, since the averaged value of reflection coefficients in the urban area is considered as about 0.6–0.7, supported by its empirical value, a value of $\varepsilon = 0.5$ was chosen, corresponding to this reflection coefficient, $R(\xi) = 0.61$. In the case when the surrounding buildings have relatively high absorptive surfaces of $R(\xi) = 0.37$, corresponding to $\varepsilon = 1.0$ in equation (8), the predicted results are shown in Fig. 6. Moreover, the predicted results for the evaluation index L_2 are shown in Figs. 7 and 8 with respect to $R(\xi) = 0.61$ and $R(\xi) = 0.37$, respectively. From these figures, it is reasonable to say that the values predicted by use of the most precise expression $f_0(x)$ of the noise

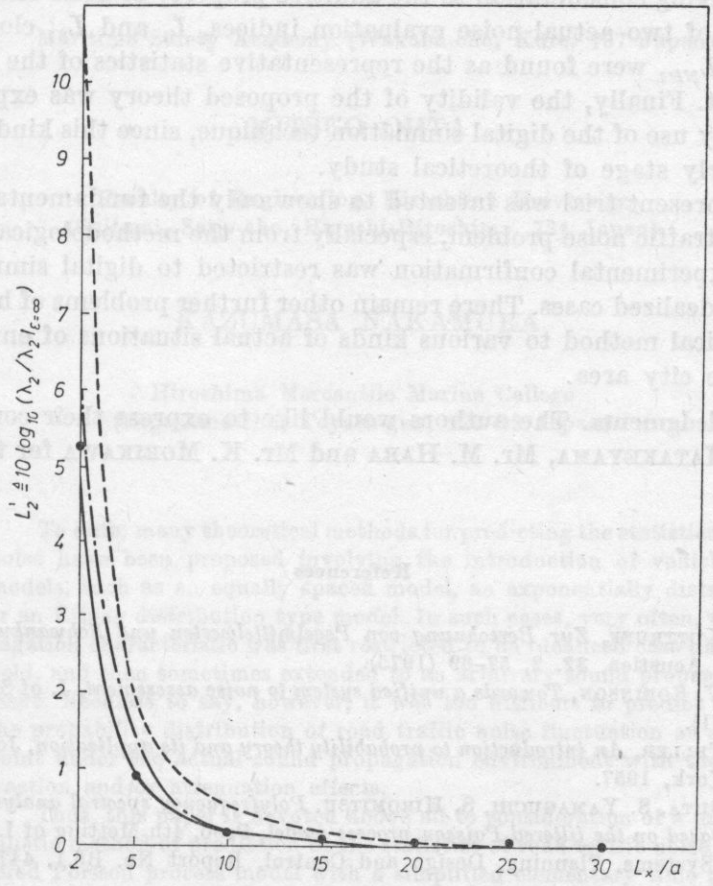

Fig. 8. A comparison between theoretical curves and simulation experiments with respect to L_2, in the case of $R(\xi) = 0.37$. The experimentally sampled points are marked by ·, and the theoretically predicted curves are respectively shown as —— (result by use of $f_0(x)$); – – – – – (result by use of $f_1(x)$); —— – —— (result by use of $f_2(x)$)

propagation characteristics were always in good agreement with the experimentally sampled points. Furthermore, if the approximate expressions $f_1(x)$ and $f_2(x)$ for practical use are suitably used, according to the actual situation of building surfaces, these expressions show good performance in evaluating the noise propagation characteristics in the city area.

5. Conclusion

In this paper, a fundamental prediction theory of the environmental noise in the city area was derived by use of the image method approach. That is, by using two factors of the spatial attenuation of noise waves and the acoustical absorption property of building surfaces, analytical expressions of the noise propagation characteristics for the typical urban noise environment were derived Next, giving consideration to the additive property of noise energy, unified expressions of two actual noise evaluation indices, L_1 and L_2, closely related to L_{eq} and L_{NP}, were found as the representative statistics of the street noise environment. Finally, the validity of the proposed theory was experimentally confirmed by use of the digital simulation technique, since this kind of research is at an early stage of theoretical study.

As this present trial was intented to show only the fundamental treatment of the road traffic noise problem, especially from the methodological viewpoint, then our experimental confirmation was restricted to digital simulation only for several idealized cases. There remain other further problems of how to apply this theoretical method to various kinds of actual situations of environmental noise in the city area.

Acknowledgments. The authors would like to express their cordial thanks to Dr. K. HATAKEYAMA, Mr. M. HARA and Mr. K. MORIKAWA for their helpful assistance.

References

[1] H. KUTTRUFF, *Zur Berechnung von Pegelmittelwerten und Schwankungsgrössen bei Strassenlärm*, Acustica, **32**, 2, 57–69 (1975).

[2] D. W. ROBINSON, *Towards a unified system to noise assessment*, J. of Sound Vib., 14, 279–298 (1971).

[3] W. FELLER, *An introduction to probability theory and its application*, John Wiley and Sons, New York, 1957.

[4] M. OHTA, S. YAMAGUCHI, S. HIROMITSU, *Polyfrequency spectral analysis for the road traffic noise based on the filtered Poisson process model*, Proc. 4th Metting of I.F.A.C. on Environmental Systems, Planning, Design and Control, Report No. B6.1, 447–484 (1977).

Received on September 11, 1984.

ARCHIVES OF ACOUSTICS
10, 1, 75–91 (1985)

A PRACTICAL PROBABILISTIC PREDICTION OF ROAD TRAFFIC NOISE FROM A FILTERED POISSON PROCESS MODEL WITH A SIMPLIFIED ELEMENTARY TIME PATTERN OF TRIANGULAR TYPE

SHIZUMA YAMAGUCHI

Maritime Safety Academy (Wakaba-cho, Kure, 737 Japan)

MITSUO OHTA

Faculty of Engineering, Hiroshima University
(Shitami, Saijo-cho, Higashi-Hiroshima, 724 Japan)

KAZUMASA NAKAMURA

Hiroshima Mercantile Marine College
(Higashino-cho, Toyota-gun, 725–02 Japan)

To date, many theoretical methods for predicting the statistics of road traffic noise have been proposed involving the introduction of vehicle distribution models, such as an equally spaced model, an exponentially distributed model, or an Erlang distribution type model. In such cases, very often, the sound propagation characteristic was first restricted to an idealized case like a free sound field, and then sometimes extended to an arbitrary sound propagation environment. Needless to say, however, it was too difficult to predict systematically the probability distribution of road traffic noise fluctuation at an observation point under the actual sound propagation environment with the complex diffraction and/or attenuation effects.

Thus, this paper is devoted above all to consideration of a practical probabilistic method of prediction of the statistics of road traffic noise by use of a filtered Poisson process model with a simplified elementary time pattern.

The effectiveness of the proposed simple method is experimentally verified too, by applying it to the actual road traffic noise data observed in a large city.

1. Introduction

When the problem of statistical prediction of road traffic noise is theoretically considered, it is essentially important to pay our attention to the actual situation of road traffic flow and its surrounding sound propagation characteristic. The former characteristic can be grasped rather easily as several types of statistical traffic flow models, such as an exponentially distributed vehicle model, an Erlang or a gamma headway distribution type model, etc. [2, 4, 6, 7, 11]. On the other hand, it is very difficult to identify the actual system characteristic of the surrounding sound propagation environment with the sound diffraction and/or attenuation effects. In fact, in most of the previous papers, the sound propagation characteristic was restricted to an idealized case like a free sound field.

For purpose of generalizing these theoretical studies, several kinds of prediction approaches, applicable to an arbitrary sound propagation environment, have been proposed by introducing the well-known filtered Poisson process model and the Stratonovich's random point system model, based on the energy composition of component elementary time patterns [8, 9, 12]. It is essentially too difficult to predict the probability distribution of the road traffic noise fluctuation under an actual sound field, owing to the difficulty of identifying the surrounding sound propagation environment.

From the above practical points of view, in this paper, a practical method of prediction of the level probability distribution form of the road traffic noise is theoretically proposed by use of the filtered Poisson process model with a simplified elementary time pattern. The effectiveness of the present prediction theory is experimentally confirmed too, by applying it to the actual data of road traffic noise level fluctuation observed in a large city. The experimental results show fair agreement with the theory, in spite the of introduction of an extremely practical approximation of the elementary time pattern.

2. Theoretical considerations

2.1. Cumulant statistics of sound intensity fluctuation

In the problems of evaluation and/or regulation of road traffic noise, the statistics such as L_x sound levels (like median, L_5 and L_{10}), defined as a $(100-X)$ percentage point of the level probability distribution, as well as the lower order statistics like L_{eq}, are very often used. Accordingly, it is first fundamental to find an explicit expression for the noise level distribution function. In this section, let us consider the relationship between the elementary time pattern due to one vehicle passing and the various cumulant statistics of the total sound intensity fluctuation due to many vehicles passing.

Now, let us consider the road traffic noise shown in Fig. 1, and introduce the following assumptions [7]:

1) the road considered here has J lanes of an arbitrary length of straight or curved lines;

2) the traffic on the jth lane flows with a constant speed v_j;

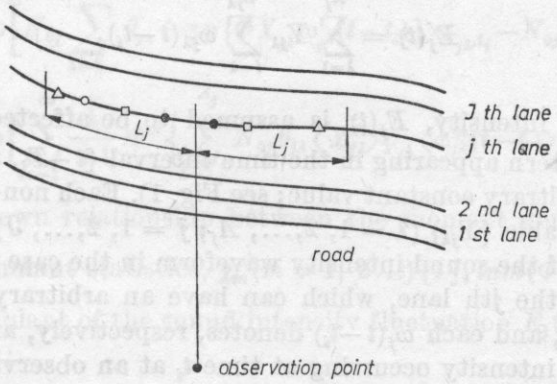

Fig. 1. Traffic flow of random point sources on a multi-lane road 0, •, □, △ – vehicle types

3) the traffic flowing on the jth lane is formed by Λ_j different types of vehicles;

4) the average number of vehicles flowing on the jth lane is N_j per unit time interval, where the number of the λth type of vehicles is $N_{j\lambda}(\lambda = 1, 2, \ldots, \Lambda_j)$;

5) n_j is a random variable expressing the number of vehicles in the arbitrary line segment $[-L_j, L_j]$ of the jth lane, and its probability function is of the usually used Poisson distribution type, i.e.

$$P(n_j) = \frac{1}{n_j!} \exp(-N_{0j}) N_{0j}^{n_j}, \quad \left(N_{0j} \triangleq N_j \frac{2L_j}{v_j}\right); \tag{1}$$

6) the probability that $n_{j\lambda}$ vehicles of the λth type appear in the above n_j vehicles is governed by the following multi-nomial distribution:

$$P(n_{j1}, n_{j2}, \ldots, n_{j\Lambda j} | n_j) = \frac{n_j}{n_{j1}!\, n_{j2}!\, n_{j\Lambda j}!} \theta_{j1}^{n_{j1}} \theta_{j2}^{n_{j2}} \ldots \theta_{j\Lambda_j}^{n_{j\Lambda_j}}$$
$$\left(\sum_{\lambda=1}^{\Lambda_j} n_j = n_j \text{ for all } j\right), \tag{2}$$

where $\theta_j = N_{j\lambda}/N_j \left(\sum_{\lambda=1}^{j} \theta_{j\lambda} = 1 \text{ for all } j\right)$ denotes the mixture ratio of the λth type of vehicles in the jth lane of road;

7) the sound intensity fluctuation emitted from each source is statistically uncorrelated with that from every other source.

Now, let us introduce the filtered Poisson process as one of the stochastic time series models for the sound intensity wave, $E_j(t)$, at an observation point, due to the traffic flowing only on the jth lane, as follows:

$$E_j(t) = \sum_{\lambda=1}^{\Lambda_j} Y_{j\lambda} \sum_{i=1}^{n_{j\lambda}} \omega_{j\lambda}(t-t_i), \tag{3}$$

where the sound intensity, $E_j(t)$, is assumed to be affected only by the elementary time pattern appearing in the time interval $[t-T_j, t+T_j]$ ($T_j \triangleq L_j/v_j$, where L_j is an arbitrary constant value; see Fig. 1). Each non-negative independent random variable $\{Y_{j\lambda}\}$ ($\lambda = 1, 2, \ldots, \Lambda_j$; $j = 1, 2, \ldots, J$), reflects the random peak value of the sound intensity waveform in the case when the λth type vehicle flows on the jth lane, which can have an arbitrary type probability distribution form, and each $\omega_j(t-t_i)$ denotes, respectively, an elementary time pattern of sound intensity occurring at time t_i at an observation point, which is standardized so that the maximum value of the elementary time pattern is equal to one. Furthermore, $\{t_i\}$ are mutually independent random time points with the uniform distribution function $P(t_i) = 1/2T_j$ (for all i).

The moment generating function of $E_j(t)$ is given as follows:

$$m_j(\Phi) \triangleq \langle \exp[\Phi E_j(t)] \rangle = \left\langle \left\langle \left\langle \exp\left\{ \Phi \sum_{\lambda=1}^{\Lambda_j} Y_{j\lambda} \sum_{i=1}^{n_{j\lambda}} \omega_{j\lambda}(t-t_i) \right\} \right\rangle_{Y_{j\lambda}, t_i | n_{j\lambda}, n_j} \right\rangle_{n_{j\lambda}|n_j} \right\rangle_{n_j}$$

$$= \left\langle \left\langle \sum_{\lambda=1}^{\Lambda_j} \langle \exp\{\Phi Y_{j\lambda} \omega_{j\lambda}(t-t_i)\} \rangle^{n_{j\lambda}}_{Y_{j\lambda}, t_i | n_{j\lambda}, n_j} \right\rangle_{n_{j\lambda}|n_j} \right\rangle_{n_j}, \tag{4}$$

where $\langle \cdot \rangle_u$ denotes an averaging operation with respect to its subindex, u, and $\langle \cdot \rangle_{u|v}$ a conditional averaging operation with respect to u when v is set at a constant value.

By using equation (2), the following expression can be easily derived:

$$\left\langle \left\langle \sum_{\lambda=1}^{\Lambda_j} \exp\{\Phi Y_{j\lambda} \omega_{j\lambda}(t-t_i)\} \right\rangle^{n_{j\lambda}}_{Y_{j\lambda}, t_i | n_{j\lambda}, n_j} \right\rangle_{n_{j\lambda}|n_j}$$

$$= \sum_{n_{j1}, n_{j2}, \ldots, n_{j\Lambda_j}} \frac{n_{j1}}{n_{j1}!\, n_{j2}! \ldots n_{j\Lambda_j}!} [\theta_{j1} \langle \exp\{\Phi Y_{j1} \omega_j(t-t_i)\} \rangle_{Y_{j1}, t_i | n_j}]^{n_{j1}} \times$$

$$\times [\theta_{j\Lambda_j} \langle \exp\{\Phi Y_{j\Lambda_j} \omega_{j\Lambda_j}(t-t_i)\} \rangle_{Y_{j\Lambda_j}, t_i | n_j}]^{n_{j\Lambda_j}}$$

$$= \left[\sum_{\lambda=1}^{\Lambda_j} \theta_{j\lambda} \langle \exp\{\Phi Y_{j\lambda} \omega_{j\lambda}(t-t_i)\} \rangle_{Y_{j\lambda}, t_i} \right]^{n_j}. \tag{5}$$

Thus, using equation (1), the moment generating function can be explicitly derived as follows:

$$m_j(\Phi) = \sum_{n_j=0} \frac{1}{n_j!} \exp(-N_{0j}) \left[N_{0j} \sum_{\lambda=1}^{\Lambda_j} \theta_{j\lambda} \langle \exp\{\Phi Y_{j\lambda} \omega_{j\lambda}(t-t_i)\} \rangle_{Y_{j\lambda}, t_i} \right]^{n_j}$$

$$= \exp\left[N_{0j} \sum_{\lambda=1}^{\Lambda_j} \theta_{j\lambda} \langle \exp\{\Phi Y_{j\lambda} \omega_{j^\lambda}(t-t_i)\} \rangle_{Y_{j\lambda}, t_i} - N_{0j} \right]$$

$$= \exp\left[\sum_{m=1}^{\infty} \frac{1}{m!} \Phi^m \left\{ \sum_{\lambda=1}^{\Lambda_j} N_{0j} \theta_{j\lambda} \langle Y_{j\lambda}^m \rangle_{Y_{j\lambda}} \langle \omega_{j\lambda}^m (t-t_i) \rangle_{t_i} \right\} \right]. \tag{6}$$

Using the well-known relationship between the moment generating function $m(\Phi)$, and the cumulant statistics, $\chi_m (m = 1, 2 \ldots)$ [1]; $lnm(\Phi) = \sum_{m=1}^{\infty} \Phi^m \chi_m / m!$, the mth order cumulant of the sound intensity fluctuation $E_j(t)$ can be directly derived as follows:

$$\chi_{mE_j} = \sum_{\lambda=1}^{\Lambda_j} N_{0j} \theta_{j\lambda} \langle Y_{j\lambda}^m \rangle \, Y_{j\lambda} \langle \omega_{j\lambda}^m (t - t_j) \rangle_{t_i}$$

$$= \sum_{\lambda=1}^{\Lambda_j} N_{0j} \theta_{j\lambda} \langle Y_{j\lambda}^m \rangle \, Y_{j\lambda} \frac{1}{2T_j} \int_{-T_j}^{T_j} \omega_{j\lambda}^m(\tau) \, d\tau. \tag{7}$$

Thus, the mth cumulant of the total sound intensity $E(t) = \sum_{j=i}^{J} E_j(t)$, due to the traffic flowing on a road having J lanes of infinite length ($L_j \to \infty$; for all j), can be easily obtained as:

$$\chi_{mE} = \sum_{j=1}^{J} \chi m E_j = \sum_{j=1}^{J} \sum_{\lambda=1}^{\Lambda_j} N_{j\lambda} \langle Y_{j\lambda}^m \rangle \int_{-\infty}^{\infty} \omega_{j\lambda}^m(\tau) \, d\tau, \tag{8}$$

where

$$N_{j\lambda} \triangleq \lim_{T_j \to \infty} \frac{1}{2T_j} N_{0j} \theta_{j\lambda} = N_j \theta_{j\lambda} \tag{9}$$

is the average number of the λth type vehicles flowing on the jth lane per unit time interval (see assumption (4) and equation (1)).

2.2 Cumulant statistics of sound level fluctuation

The moment generating function of the sound level fluctuation defined by

$$L = M \ln(E/E_0) \qquad \left(M \triangleq \frac{10}{\ln 10}, \quad E_0 = 10^{-12} W/\mathrm{m}^2 \right), \tag{10}$$

can be obtained as follows:

$$m_L(\Phi) \stackrel{\Delta}{=} \langle \exp(\Phi L) \rangle_L = \left\langle \left(\frac{E}{E_0} \right)^{\Phi M} \right\rangle_E . \tag{11}$$

Using the previous relationship between the moment generating function and the cumulant statistics, and letting $\Phi M = m$ in equation (11), the following equality can be obtained:

$$\sum_{i=1}^{\infty} \frac{1}{i!} \left(\frac{m}{M} \right)^i \chi_{iL} = \ln \langle E^m \rangle - m \ln E_0 \quad (m = 1, 2 \ldots), \tag{12}$$

here, χ_{iL} denotes the ith order cumulant of the sound level L.

Equation (12) can be concretely written as

(13)

$$\ln \langle E \rangle - \ln E_0 = \frac{1}{M} \chi_{1L} + \frac{1}{2!} \left(\frac{1}{M} \right)^2 \chi_{2L} + \frac{1}{3!} \left(\frac{1}{M} \right)^3 \chi_{3L} + \frac{1}{4!} \left(\frac{1}{M} \right)^4 \chi_{4L} + \ldots,$$

$$\ln \langle E^2 \rangle - 2 \ln E_0 = \frac{2}{M} \chi_{1L} + \frac{1}{2!} \left(\frac{2}{M} \right)^2 \chi_{2L} + \frac{1}{3!} \left(\frac{2}{M} \right)^3 \chi_{3L} + \frac{1}{4!} \left(\frac{2}{M} \right)^4 \chi_{4L} + \ldots,$$

$$\ln \langle E^3 \rangle - 3 \ln E_0 = \frac{3}{M} \chi_{1L} + \frac{1}{2!} \left(\frac{3}{M} \right)^2 \chi_{2L} + \frac{1}{3!} \left(\frac{3}{M} \right)^3 \chi_{3L} + \frac{1}{4!} \left(\frac{3}{M} \right)^4 \chi_{4L} + \ldots,$$

$$\ln \langle E^4 \rangle - 4 \ln E_0 = \frac{4}{M} \chi_{1L} + \frac{1}{2!} \left(\frac{4}{M} \right)^2 \chi_{2L} + \frac{1}{3!} \left(\frac{4}{M} \right)^3 \chi_{3L} + \frac{1}{4!} \left(\frac{4}{M} \right)^4 \chi_{4L} + \ldots.$$

By solving these linear simultaneous equations, the cumulant statistics $\chi_{nL} (n = 1, 2, \ldots)$ of sound level can be obtained from the statistical information $\langle E^n \rangle$ on the moment statistics of sound intensity. Furthermore, as is well-known, these moment statistics $\langle E^n \rangle$ of sound intensity can be easily calculated from the cumulant statistics χ_{nE} of sound intensity as follows:

$$\begin{gathered} \langle E \rangle = \chi_{1E}, \quad \langle E^2 \rangle = \chi_{2E} + \langle E \rangle^2, \quad \langle E^3 \rangle = \chi_{3E} + 3 \langle E \rangle \langle E^2 \rangle - 2 \langle E \rangle^3, \\ \langle E^4 \rangle = \chi_{4E} + 4 \langle E \rangle \langle E^3 \rangle + 3 \langle E^2 \rangle - 12 \langle E \rangle^2 \langle E^2 \rangle + 6 \langle E \rangle^4, \ldots. \end{gathered} \tag{14}$$

2.9. A simplified expression of sound level distribution for practical use

In this section, in view of the establishment of a practical evaluation method, a simplified expression of the probability distribution is first introduced, as follows (its theoretical background is shown in [10]):

$$P(L) = \frac{1}{\sqrt{2\pi \chi_{2L}}} \exp \left\{ - \frac{(L - \chi_{1L})^2}{2 \chi_{2L}} \right\} \text{(Gaussian distribution)}. \tag{15}$$

Accordingly, it is sufficient to solve only two lower order cumulants χ_{1L} and χ_{2L} in equation (13).

2.4. *A simplification of the elementary time pattern*

In the practical evaluation procedure, the following points must be noticed:

1) In order to calculate concretely $\chi_{mE}(m = 1, 2,\ldots)$ by use of equation (8), it is first necessary to obtain the statistical or deterministic information on $N_{j\lambda}$, $Y_{j\lambda}$ and $\omega_{j\lambda}$ ($\lambda = 1, 2,\ldots, \Lambda_j$; $j = 1, 2,\ldots, J$). As is mentioned in the introduction, the statistical properties of $N_{j\lambda}$ and $Y_{j\lambda}$ can be grasped rather easily from the usual theoretical and/or experimental considerations. On the contrary, it is not so easy to systematically evaluate $\omega_{j\lambda}(\tau)$ under an actual sound propagation environment.

2) It is not necessary to estimate $\omega_{j\lambda}(\tau)$ itself accurately, but it is quite enough to obtain only the whole value of the definite integral $\int_{-\infty}^{\infty} \omega_{j\lambda}^m(\tau)\,d\tau$, for the purpose of determining $\chi_{mE}(m = 1, 2,\ldots)$. Moreover, only the total sum for each cumulant statistics in each lane and vehicle type case is useful for the above probabilistic evaluation. That is, the values of the cumulant statistics of sound intensity, χ_{mE}, are not influenced sensitively by the instantaneous waveform itself of $\omega_{j\lambda}(\tau)$, owing to the above smoothing operation effect.

Thus, the probabilistic evaluation index like L_x for the sound level fluctuation, is not influenced sensitively by the instantaneous waveform of the individual time pattern $\omega_{j\lambda}(\tau)$. Based on this fundamental viewpoint, it is possible to find the reason why the elementary time pattern can be extremely simplified.

First, let us consider the standard case when the same type vehicles flow on a single lane road ($J = \Lambda = 1$) under a free sound field. At this time, χ_{mE} can be exactly expressed as follows (see equation (8)):

$$\chi_{mE} = N_{11}\langle Y_{11}^m\rangle \int_{-\infty}^{\infty} \omega_{11}^{mm}(\tau)\,d\tau = N_{11}\langle Y_{11}^m\rangle \int_{-\infty}^{\infty} \frac{1}{(1+\beta\tau^2)^m}\,d\tau$$

$$= N_{11}\langle Y_{11}^m\rangle \frac{\pi}{\sqrt{\beta}} A_m, \qquad (16)$$

with

$$A_m = \frac{(2m-3)!!}{(2m-2)!!}, \qquad (17)$$

where β is a certain constant value and $(*)!!$ is defined as

$$(2m)!! = 2m(2m-2)\ldots 4\cdot 2,$$
$$(2m-1)!! = (2m-1)(2m-3)\ldots 5\cdot 3\cdot 1,$$
$$0!! = (-1)!! = 1. \qquad (18)$$

Hereupon, let us consider an extremely simplified case when this original elementary waveform on dB scale is approximated by a triangular waveform, as shown in Fig. 2, under the condition of equivalence of the average sound intensity. That is, the mth order cumulant $\chi_{mE}(\Delta)$ of a triangular wave-

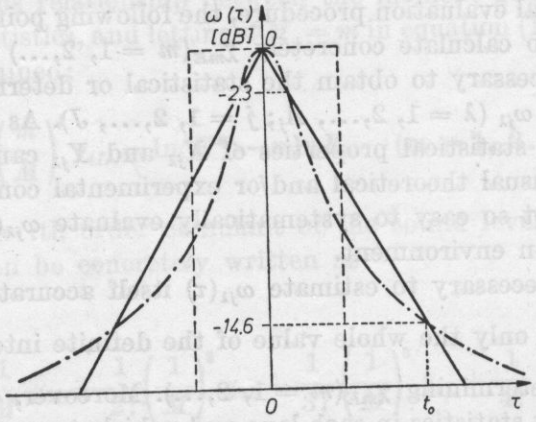

Fig. 2. Relationship between an original elementary waveform and its simplified triangular time pattern for sound level. Original waveform: ——·——, simplified triangular time pattern: ——

form corresponding to χ_{mE}, can be easily derived under the condition $\chi_{1E}(\Delta) = \chi_{1E}$, as follows:

$$\chi_{mE}(\Delta) = N_{11}\langle Y_{11}^m\rangle \int_{-\infty}^{\infty} \exp\left[-\mathrm{m}\frac{2}{\pi}\sqrt{\beta}\,|\tau|\right] d\tau$$

$$= N_{11}\langle Y_{11}^m\rangle \frac{\pi}{\sqrt{\beta}} B_m = \frac{B_m}{A_m}\chi_{mE}, \qquad (19)$$

with

$$B_m = \frac{1}{m}. \qquad (20)$$

If the original elementary waveform is approximated in trial by a square waveform, the corresponding $\chi_{mE}(\square)$ can be directly derived as follows:

$$\chi_{mE}(\square) = N_{11}\langle Y_{11}^m\rangle \int_{-\pi/2\sqrt{\beta}}^{\pi/2\sqrt{\beta}} 1\,d\tau = N_{11}\langle Y_{11}^m\rangle \frac{\pi}{\sqrt{\beta}} C_m, \quad C_m = 1. \qquad (21)$$

Table 1 shows a comparison between A_m and B_m for several values of m (of course, $\chi_{mE}(\Delta) \simeq_{mE}$ if $B_m \simeq A_m$). It is very interesting to note that the value

Table 1. A comparison between A_m and B_m for several values of m

m	A_m	B_m	C_m
1	1.000	1.000	1.0
2	0.500 (= 1/2)	0.500 (= 1/2)	1.0
3	0.375 (= 3/8)	0.333 (= 3/9)	1.0
4	0.313 (= 5/16)	0.250 (= 4/16)	1.0
5	0.273 (= 35/128)	0.200 (= 25/125)	1.0

of χ_{2E} (i.e. the variance of sound intensity) is equal to that of $\chi_{2E}(\Delta)$. From this table, it is obvious that $\chi_{mE}(m = 1\text{–}5)$ for an original waveform can be successfully approximated by $\chi_{mE}(\Delta)$ for a simplified triangular waveform and that it cannot be approximated by $\chi_{mE}(\square)$ for a simplified square waveform.

3. Experimental considerations

3.1 Outline of experiment

The actual location of the road, bank and two observation points is shown in Fig. 3. The road considered here has two lanes. The received random noise fluctuation waves at the two observation points O_1 and O_2 were coincidently put on record by use of a data recorder. Table 2 gives the observed values of road traffic flow in every observation time interval.

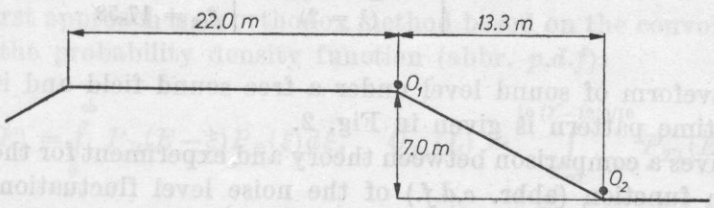

Fig. 3. Actual location of the road with a bank and the two observation points

Table 2. Observed values of road traffic flow (vehicles/10.5 min.)

Starting time point of observation	Up lane ($j = 1$)		Down lane ($j = 2$)	
	have vehicle ($\lambda = 1$)	light vehicle ($\lambda = 2$)	heavy vehicle ($\lambda = 1$)	light vehicle ($\lambda = 2$)
13.10 *PM*	16	21	12	9
13.30	13	13	13	11
14.00	7	13	12	8
14.30	8	16	12	7
15.00	12	8	8	12
Average	11.2	14.2	11.4	9.4

3.2. *Results of experiments*

a) Noise level probability distribution at the observation point O_1

The sound propagation environment between an individual vehicle on the road and the observation point O_1 can be regarded as a free sound field. At this time, the time pattern of sound intensity, $\omega_{j\lambda}(\tau)$, in equation (8) can be given as follows ($\lambda = 1, 2$; $j = 1, 2$; see Table 2):

$$\omega_{j\lambda}(\tau) = \frac{1}{1+\beta_{j\lambda}\tau^2}. \tag{22}$$

Table 3 shows concrete values of $\beta_{j\lambda}$ estimated experimentally by use of the actual time pattern observed on a level recorder. The relationship between the

Table 3. Estimated value of $\beta_{j\lambda}$ ($j = 1, 2$; $\lambda = 1, 2$)

Up lane ($j = 1$)	heavy vehicle ($\lambda = 1$)	$\beta_{11} = 1.55$
	light vehicle ($\lambda = 2$)	$\beta_{12} = 1.23$
Down lane ($j = 2$)	heavy vehicle ($\lambda = 1$)	$\beta_{21} = 18.40$
	light vehicle ($\lambda = 2$)	$\beta_{22} = 17.58$

original waveform of sound level under a free sound field and its simplified triangular time pattern is given in Fig. 2.

Fig. 4 gives a comparison between theory and experiment for the cumulative distribution function (abbr. *c.d.f.*) of the noise level fluctuation. Hereupon, dour lower order cumulants (χ_{1E}, χ_{2E}, χ_{3E} and χ_{4E}) were first calculated by introfucing simplified time patterns for every lane and vehicle type case, and then, only two parameters χ_{1L} and χ_{2L} in equation (15) were determined by solving the simultaneous equations (cf. equations (13)). Since the theoretical *c.d.f.* curve predicted from an original elementary waveform under a free sound field (cf. equation (22)) agrees with that from a simplified triangular waveform, this curve was omitted here. As is directly found in this figure, the effect of the background noise on the resultant traffic noise level distribution form cannot be neglected in a specific case with a light traffic flow (cf. Table 2). In order to increase the accuracy of prediction of the noise level probability distribution, the above background noise generated independently by the other different noise sources should be taken into consideration for the above noise evaluation method.

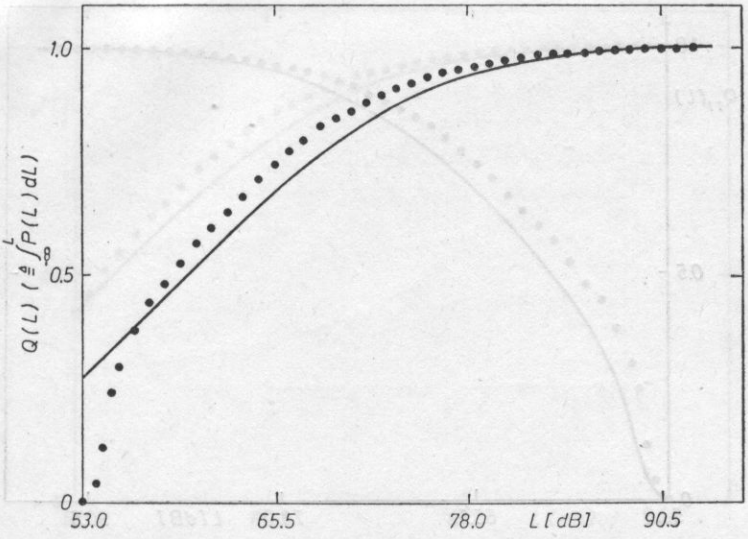

Fig. 4. A comparison between the theoretically predicted curve and the experimentally sampled points for the cumulative noise level distribution at the observation point O_1 (cf. Fig. 3). The experimentally sampled points are marked by · and the theoretically predicted curve is shown by ——

The following two approaches can be especially introduced as an attempt to improve the above evaluation procedure:

1) the first approach is an orthodox method based on the convolution of the ntegral of the probability density function (abbr. *p.d.f*):

$$P_{T1}(E) = \int_0^{\infty} P_R(E-\xi)P_B(\xi)d\xi, \quad Q_{T1}(L) = \int_{-\infty}^{10\,(L-120)/10} P_{T1}(E)dE. \qquad (23)$$

Here, $P_R(*)$, $P_B(*)$ and $P_{T1}(*)$ are, respectively, the *p.d.f.* of the road traffic noise intensity, that of the background noise intensity and that of the total noise intensity. The above equation is derived by using the additive property of two statistically independent sound intensities.

Fig. 5 shows a comparison between theory and experiment in the form of the sound level distribution. The theoretically predicted curve was calculated by using equation (23) (the lognormal distribution was employed as $P_R(*)$ in equation (23); see equation (15)). It is fairly troublesome to obtain the finite integral of equation (23), even if this method is quite orthodox.

2) the second approach is a practical method to avoid the above trouble of calculating the finite integral.

If the noise level probability distribution restricted only in the level range $[L_0, \infty]$ (L_0 — an arbitrary constant value) is considered, the following expres-

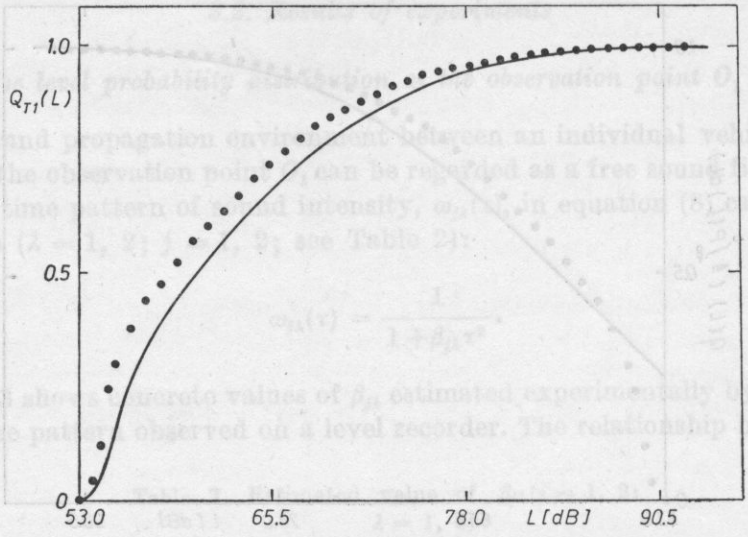

Fig. 5. A comparison between the theoretically predicted curve and the experimentally sampled points for the cumulative noise level distribution at the observation point O_1. The experimentally sampled points are marked by · and the theoretical curve predicted by use of equation (23) is shown by ——

sion derived on the basis of the fundamental property of a conditional probability must be employed:

$$Q_{T2}(L) = Q_{EX}(L_0) + [1 - Q_{EX}(L_0)] \frac{Q_T(L) - Q_T(L_0)}{1 - Q_T(L_0)} \quad (L \geqslant L_0). \tag{24}$$

Here, $Q_{EX}(L_0)$ denotes the experimental *c.d.f* at a level point L_0 and $Q_T(*)$ is defined as

$$Q_T(*) = \int_{-\infty}^{*} P(L)dL \quad (* = L \text{ or } L_0). \tag{25}$$

The *c.d.f.* curve predicted theoretically by use of equations (24), (15) and (25) and the experimentally sampled points are compared in Fig. 6.

From Figs. 5 and 6, it is obvious that the above two evaluation methods show a fairly good agreement with the experimental results.

b) Noise level probability distribution at the observation point O_2

The elementary time pattern of sound intensity, $\omega_{j\lambda}(\tau)$, at the observation point O_2 can be approximated as follows:

$$\omega_{j\lambda}(\tau) = \frac{1}{1+\beta_{j\lambda}\tau^2} \frac{a_j^2 + (v_j\tau)^2}{b_j^2 + (v_j\tau)^2} 10^{-\Delta L_j(\tau;f_0)}, \tag{26}$$

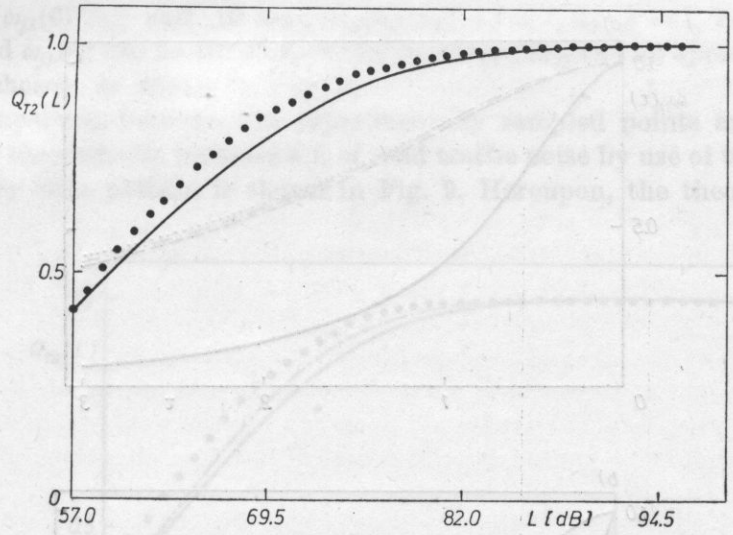

Fig. 6. A comparison between the theoretically predicted curve and the experimentally sampled points for the cumulative noise level distribution at the observation point O_1. The experimentally sampled points are marked by · and the theoretical curve predicted by use of equations (24) and (15) is shown by ——

where the values of $\beta_{j\lambda}(j = 1, 2; \lambda = 1, 2)$ are given in Table 3. Furthermore, a_j and b_j are the shortest distances between the jth lane in the road and the observation points O_1 and O_2 respectively (see Fig. 7), and $\Delta L_j(\tau; f_0)$ denotes the sound attenuation which can be easily calculated by use of an acoustical evaluation chart of the barrier, based on a value of the Fresnel number $N_j(\tau; f_0)$ [3, 5]:

$$N_j(\tau; f_0) = 2\delta_j(\tau) f_0/c. \tag{27}$$

Here, f_0 denotes the representative frequency in the power spectrum of an actual road traffic noise and c is the speed of sound. Furthermore, $\delta_j(\tau)$ is the difference $((\overline{SP}+\overline{PO_2})-\overline{SO_2})$ of the sound propagation path length which can be determined by using the location of a vehicle on the jth lane at the time τ and the observation point O_2. Fig. 8 shows the normalized elementary time

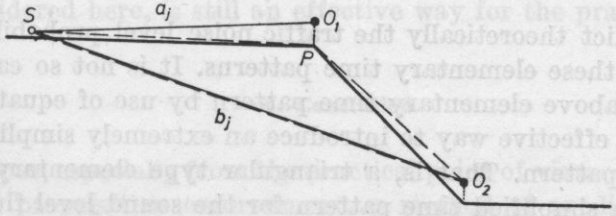

Fig. 7. Location of the jth lane and the two observation points O_1 and O_2

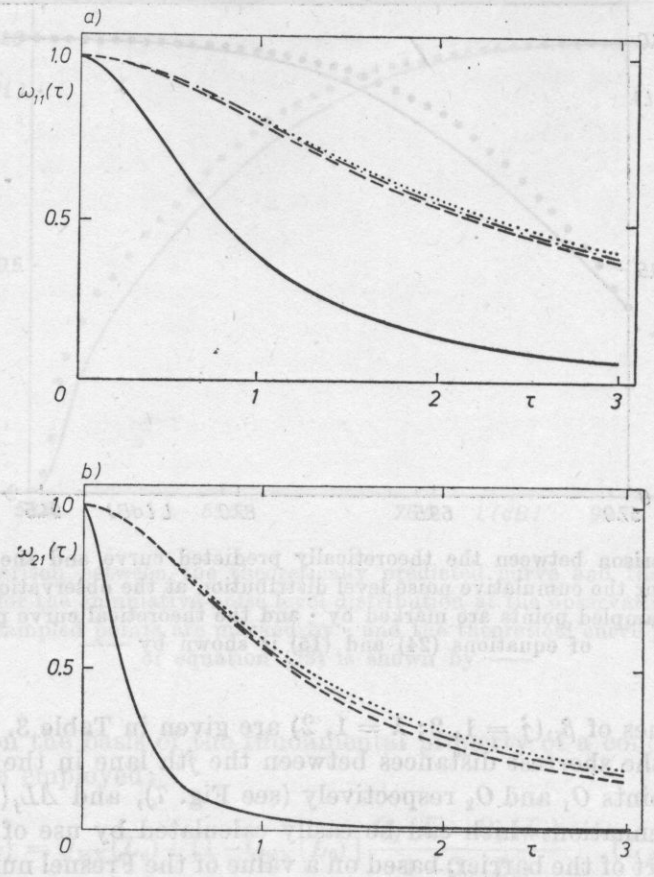

Fig. 8. Normalized time patterns $\omega_{j1}(\tau)$ $(j = 1, 2)$ at the representative frequency point $f_0 = 500$, 700 and 1000 Hz. The respective time patterns are shown by: — — — — $f_0 = 500$, ——·—— $f_0 = 700$, ... $f_0 = 1000$, and a typical elementary time pattern in the idealized case with a free sound field is simultaneously shown by ——. *a)* $\omega_{11}(\tau)$ $(j = 1, \lambda = 1)$; *b)* $\omega_{21}(\tau)$ $(j = 2, \lambda = 1)$

patterns $\omega_{j1}(\tau)$ $(j = 1, 2$; i.e. heavy vehicle) at $f_0 = 500$, 700 and 1000 Hz, calculated from equation (26). The normalized elementary time pattern in an idealized case with free sound field (cf. equation (22)) is simultaneously shown in this figure.

Let us predict theoretically the traffic noise level probability distribution form by using these elementary time patterns. It is not so easy, however, to determine the above elementary time pattern by use of equation (26). Accordingly, it is an effective way to introduce an extremely simplified type of elementary time pattern. That is, a triangular type elementary waveform was introduced as a simplified time pattern for the sound level fluctuation at the observation point O_2, which was determined especially by using two values;

$10 \log_{10}[\omega_{j\lambda}(0)/E_0]$ and $10 \log_{10}[\omega_{j\lambda}(t_0)/E_0]$ $(j = 1, 2;\ \lambda = 1, 2)$. Hereupon, $\omega_{j\lambda}(0)$ and $\omega_{j\lambda}(t_0)$ can be calculated from equation (26), and an appropriate value of t_0 is chosen, as shown in Fig. 2.

A comparison between the experimentally sampled points and the curve predicted theoretically for the *c.d.f.* of road traffic noise by use of this simplified elementary time pattern is shown in Fig. 9. Hereupon, the theoretical curve

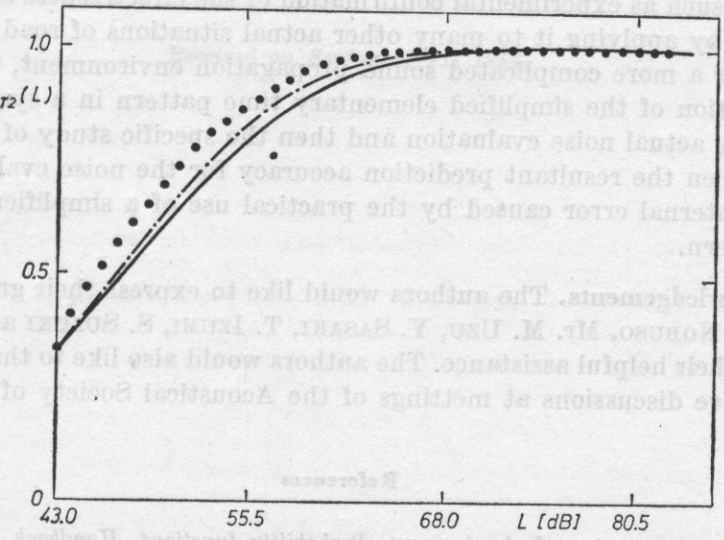

Fig. 9. A comparison between the theoretically predicted curve and the experimentally sampled points for the cumulative noise level distribution at the observation point O_2 (cf. Fig. 3). The experimentally sampled points are marked by ·. The theoretical curve predicted by use of a simplified triangular type of elementary time pattern is shown by —— · —— and that predicted by use of an accurate elementary time pattern (see equation (26)) is shown by ——

was calculated from equations (15) and (24) ($L_0 = 43$ dB). The theoretical curve calculated by using equation (26) is simultaneously shown in this figure. From this figure, it is obvious that its prediction accuracy can be hopefully increased by improving the degree of the approximation of the elementary time pattern. But the prediction method based on a simplified triangular type elementary time pattern, considered here, is still an effective way for the practical usage.

4. Conclusion

In this paper, especially from the practical point of view of evaluation of the actual sound propagation environment, a method of prediction of the level *p.d.f.* for the actual road traffic noise fluctuation was first proposed in a hybrid form

of theory and experiment by use of a filtered Poisson process model with a simplified elementary time pattern of triangular type. Then, the effectiveness of the proposed evaluation method was experimentally confirmed by applying it to the actual road traffic noise data observed in a large city. Such a practical prediction method based on a simplified triangular type elementary time pattern is still at an early stage of study. Therefore, the present study was mainly focussed on its methodological viewpoint. There still remain many types of future problems, such as experimental confirmation of the effectiveness of the method proposed, by applying it to many other actual situations of road traffic noise data under a more complicated sound propagation environment, the optimum determination of the simplified elementary time pattern in a systematic relation to the actual noise evaluation and then the specific study of the relationship between the resultant prediction accuracy for the noise evaluation index and the internal error caused by the practical use of a simplified elementary time pattern.

Acknowledgements. The authors would like to express their grateful thanks to Dr. M. NOBUSO, Mr. M. UZU, Y. SASAKI, T. IZUMI, S. SUZUKI and N. NAKASAKO for their helpful assistance. The authors would also like to thank for many constructive discussions at mettings of the Acoustical Society of Japan.

References

[1] M. ABRAMOWITZ, I. A. ATEGUN, *Probability functions. Handbook of mathematical functions with formulas, graphs, and mathematical tables*, National Bureau of Standards U.S. Government Printing Office, Washington 1964, p. 928.

[2] D. E. BLUMENFELD, G. H. WEISS, *Effects of headway distributions on second order properties of traffic noise*, Journal of Sound and Vibration, **41**, 1, 93–102 (1975).

[3] C. M. HARRIS, *Sound propagation in the open air. Handbook of noise control*, McGraw Hill, New York, 1979, p. 3.

[4] U. J. KURZE, *Statistics of road traffic noise*, Journal of Sound and Vibration, **18**, 2, 171–195 (1971).

[5] Z. MAEKAWA, *Sound insulation and vibration control, Architectural acoustics*, Kyoritsu Syuppan, Tokyo, 1968, p. 103.

[6] M. OHTA, S. YAMAGUCHI, S. HIROMITSU, *A unified study on the prediction problem of road traffic noise with various types of vehicles and multi-lanes on a road of arbitrary length (theory and simulation experiment)*, Journal of the Acoustical Society of Japan, **32**, 7, 403–412 (1976).

[7] M. OHTA, S. YAMAGUCHI, H. IWASHIGE, *A statistical theory for road traffic noise based on the composition of component response wave and its experimental confirmation*, Journal of Sound and Vibration, **52**, 4, 587–601 (1977).

[8] M. OHTA, S. YAMAGUCHI, S. HIROMITSU, *A new systematical trial to unified statistical treatment of road traffic noise under the arbitrary sound propagation environment*, Journal of the Acoustical Society of Japan, **33**, 12, 672–675 (1977).

[9] M. OHTA, S. YAMAGUCHI, A. IKUTA, *Statistical estimation of road traffic noise in an arbitrary sound propagation environment by use Stratonovich's theory for a random points system*, Journal of Sound and Vibration, **69**, 2, 275–283 (1980).

[10] M. Ohta, S. Yamaguchi, Y. Mitani, *A simplified probabilistic evaluation method for the sound insulation effect of barriers*, Bulletin of the Australian Acoustical Society, **11**, 3, 97–103 (1983).

[11] K. Takagi, K. Hiramatsu, T. Yamamoto, K. Hashimoto, *Investigations on road traffic noise based on an exponentially distributed vehicles model-single line flow of vehicles with same acoustic power*, Journal of Sound and Vibration, **36**, 3, 417–431 (1974).

[12] M. Uzu, Y. Sasaki, M. Nobuso, M. Ohta, *A practical hybrid method for prediction of road traffic noise from a viewpoint of filtered Poisson process model*, Journal of the Acoustical Society of Japan, **39**, 12, 791–797 (1983).

Received on September 11, 1984.

IX CONFERENCE ON THE UTILIZATION OF ULTRASONIC METHODS FOR STUDYING THE PROPERTIES OF CONDENSED MATTER

Žilina (Czechoslovakia), 23-25 August, 1984

The Ninth Conference on the Utilization of Ultrasonic Methods for Studying the Properties of Condensed Matter was held on 23–25 August, 1984 in Žilina (Czechoslovakia). The Conference was sponsored by the Physics Section of the Slovak Mathematicians and Physicists Association, the Acoustic Committee (Ultrasonics Subcommision) of the Czechoslovak Academy of Sciences, and organized by the Physics Department of the Technical University of Advanced Transport and Communication Engineering in Žilina, and the Physics Institute of the Slovak Academy of Sciences in Bratislava. RNDr. S. Kolník, CSc. was the chairman of the Organizing Committee of the Conference.

Three general lectures were delivered:

W. Arnold, *The generation of ultrasound by short laser pulses and its applications in physics and NDT.*

H. J. Frőhlich, *Surface acoustic waves in lithium niobate-physical properties and technical applications.*

G. Sorge, U. Straube, *Ultrasonic investigation of structural phase transitions.*

The following communications were delivered:

P. Sladký, *Acoustooptic and optoacoustic effects in solids.*

W. Arnold, P. Doussineau, A. Levelut, S. Ziolkiewicz, *Elastic low-energy excitations in $LiTaO_3$.*

P. Koštial, *Study of the stability of electrographic layers by using of SAW.*

J. Lewandowski, *Determination of metal texture from acoustic wave measurements.*

J. Lewandowski, *Velocity of propagation and attenuation of acoustic waves in heterogeneous viscoelastic bodies.*

P. Koštial, J. Ďurček, *Ultrasonic investigation of Se-Te alloys.*

H. Gawda, *Determination of fibres crystalline of plants from ultrasonic measurements.*

V. N. Hudaiberdyev, P. K. Habibullaev, S. A. Burhonov, E. K. Reznik, I. I. Shinder, *Investigation of particularities found out in intermolecular interaction for glycerine ethers and esters by acoustic methods.*

S. Ernst, K. Bebek, E. Zorębski, E. Soczkiewicz, *Rheological and volume effects in highly viscous polyhydroxyalcohols.*

J. Dominec, *Ultrasonic attenuation in semiconductive Bi-Sb alloys.*

J. Slabeycius, P. Koštial, *The investigation of the relaxation spectrum of amorphous layers by ultrasonic methods.*

M. Košek, J. Zelenka, *DC electric field influence on SAW propagation at piezoelectric media.*

H. J. Frőhlich, *SAW propagation in $LiNbO_3$ in biasing electric field.*

K. Čápová, I. Čáp, *The optical investigation of the 50-MHz SAW field.*

D. Čiplys, A. Domarkas, I. Kraujalineė, R. Rimeika, *Acoustic investigation of Ti-diffused $LiNbO_3$ surface.*

M. Košek, *The interdigital SAW transducers analysis with use of a computer.*

M. Weinacht, R. Wobst, *SAW properties of layered systems.*

G. Sorge, J. Janich, *Ultrasonic and elastic resonance methods for investigation of phase transitions in $NaH_3(SeO_3)_2$.*

D. Vajda, J. Kovár, J. Kejst, B. Březina, *Attenuation of elasitc waves in TGS crystals dopped by α-alanine near the Curie point.*

V. Petnikov, *The possibilities of active nonlinear spectroscopy of inhomogeneous condensed media.*

P. Hegedüš, C. Musil, S. Kolník, I. Čáp, *Velocity of ultrasonic waves in alkaline earth floride and rare earth floride mixture crystal system.*

Ya. M. Soifer, *The photodamping of dislocations in KCl single crystals.*

V. I. Mirgorodski, *Propagation of acoustic solitari impulses at acoustoelectric interaction.*

S. E. Esipov, *Nonlinear hysteresiable characteristics of hot electron system due to electron-optical phonon and electron-electron interactions in semiconductors.*

J. Štelina, J. Braciník, *Electric field in the sample with the amplified acoustic flux.*

These papers will be published in Acta Physica Slovaca.

Eugeniusz Soczkiewicz
(Gliwice)